ENERGY EFFICIENT COOPERATIVE WIRELESS COMMUNICATIONS

A thesis submitted to the University of Manchester
for the degree of Doctor of Philosophy
in the Faculty of Engineering and Physical Sciences

2010

Sarmad Sohaib

School of Electrical and Electronic Engineering

Contents

List of Tables

List of Figures

Abstract

Cooperative diversity exploits the broadcast nature of wireless channels and uses relays to improve link reliability. Most cooperative communication protocols are assumed to be synchronous in nature, which is not always possible in wireless communication. Also the relay nodes are assumed to be half duplex which in turn reduces the spectral efficiency. In this thesis, we first present a novel asynchronous cooperative communication protocol exploiting polarization diversity, which does not require synchronization at the relay node. Dual polarized antennas are employed at the relay node to achieve full duplex amplify-and-forward (ANF) communication. Hence the transmission duration is reduced which results into an increased throughput rate. Capacity analysis of the proposed scheme ascertains the high data rate as compared to conventional ANF. Bit error rate (BER) simulation also shows that the proposed scheme significantly outperforms both the non-cooperative single-input single-output and the conventional ANF schemes. Considering channel path loss, the proposed scheme consume less total transmission energy as compared to ANF and non-cooperative scheme in more practical distance range. Thus the proposed scheme is suitable for high rate and energy efficient relay-enabled communication.

In addition to that, we also present a novel power allocation scheme for multiple relay nodes that results in efficient cooperative multiple-input multiple-output (MIMO) communication. Considering channel path loss, the total transmission energy is distributed between the source and the relay nodes. The energy distribution ratio between the relay and direct link is optimized such that the quality of received signal is maintained with minimum total transmission energy consumption. We calculate the energy distribution ratio analytically and verified it through computer simulation. With the new power allocation scheme, the system also obtains an increased channel capacity as compared to cooperative scheme with conventional equal power allocation and non-cooperative scheme. Optimal relay positioning with proposed energy allocation scheme is also explored to maximize the capacity.

Declaration

No portion of the work referred to in this thesis has been submitted in support of an application for another degree or qualification of this or any other university or other institution of learning.

Copyright Statement

i The author of this thesis (including any appendices and/or schedules to this thesis) owns any copyright in it (the Copyright) and he has given The University of Manchester the right to use such Copyright for any administrative, promotional, educational and/or teaching purposes.

ii Copies of this thesis, either in full or in extracts, may be made only in accordance with the regulations of the John Rylands University Library of Manchester. Details of these regulations may be obtained from the Librarian. This page must form part of any such copies made.

iii The ownership of any patents, designs, trade marks and any and all other intellectual property rights except for the Copyright (the "Intellectual Property Rights") and any reproductions of copyright works, for example graphs and tables ("Reproductions"), which may be described in this thesis, may not be owned by the author and may be owned by third parties. Such Intellectual Property Rights and Reproductions cannot and must not be made available for use without the prior written permission of the owner(s) of the relevant Intellectual Property Rights and/or Reproductions.

iv Further information on the conditions under which disclosure, publication and exploitation of this thesis, the Copyright and any Intellectual Property Rights and/or Reproductions described in it may take place is available from the Head of School of Electrical and Electronic Engineering.

Acknowledgements

I would like to express my gratitude to supervisor Dr. Daniel K. C. So for his continual advice and encouragement throughout the project. University of Engineering and Technology, Taxila, Pakistan and Higher Education Commission, Pakistan are acknowledged for their support and funding for this project.

I wish to express my thanks to all my postgraduate colleagues especially, Mr. Omair Shahid, Mr. Junaid Ahmed, Mr. Hassan Khan, Dr Ulises Pineda Rico, and Dr Di Lu for their support, motivation and fruitful discussions.

Finally, I am forever indebted to my parents and my sisters for their understanding, patience and encouragement when it was most required.

Dedication

To my lovely parents.

List of Abbreviations

ADC	Analog-to-digital converter
ANF	Amplify-and-forward
ARQ	Automatic repeat-request
AWGN	Additive white Gaussian noise
BER	Bit error rate
CDMA	Code division multiple access
CP	Cyclic prefix
CRC	Cyclic redundancy check
CSI	Channel state information
DAC	Digital-to-analog converter
D-BLAST	Diagonal-Bell Laboratories Layered Space-Time
DFE	Decision feedback equalizer
DFT	Discrete Fourier transform
DNF	Decode-and-forward
EGC	Equal gain combiner
EMT	Electro magnetic transmission
FBF	Feedback filter
FFF	Feed forward filter
FIR	Finite impulse response
IDFT	Inverse discrete Fourier transform
ISI	Inter symbol interference
LOS	Line of sight
MIMO	Multiple-input multiple-output
MISO	Multiple-input single-output

MLSE	Maximum likelihood sequence estimation
MMSE	Minimum mean square error
MRC	Maximal ratio combiner
MSE	Mean squared error
OSIC	Ordered Successive interference cancellation
pdf	Probability density function
PSD	Power spectral density
QPSK	Quadratic phase shift keying
RCPC	Rate punctured convolutional code
RF	Radio front end
RMS	Root mean square
SC	Selection combiner
SER	Symbol error rate
SIMO	Single-input multiple-output
SISO	Single-input single-output
SNR	Signal to noise ratio
STBC	Space-time block code
STC	Space-time code
STTC	Space-time trellis code
V-BLAST	Vertical-Bell Laboratories Layered Space-Time
XPC	Cross-polarization coupling
XPD	Cross-polarization discrimination
ZF	Zero forcing

List of Variables

A	Peak amplitude of LOS
a	Amplitude of a multipath component
B_C	Coherence bandwidth
B_D	Measure of spectral broadening
B_S	Bandwidth of transmitted signal
C	Channel Capacity
d	Distance for path loss
d_o	Reference distance for path loss
E^s	Transmitted signal energy
f_D	Doppler frequency
G_r	Receive antenna gain
G_t	Transmit antenna gain
$\mathbf{H}$	Channel matrix
$I\,(;)$	Mutual information
I_0	Modified Bessel function of the first kind and zero order
K	Ricean factor
M_r	Number of receive antennas
M_t	Number of transmit antennas
$\mathbf{N}$	Noise matrix
N_o	Power spectral density of AWGN
$p(x)$	probability density function
PL	Path loss
PL_o	Path loss at reference distance d_o
P_r	Received power

P_t	Transmit power
T_C	Coherence time
T_S	Symbol period
T	Frame duration
$\mathbf{W}$	Filter matrix
$\mathbf{X}$	Transmitted data matrix
X_σ	Standard deviation of the log-normal shadowing effect
$\hat{\mathbf{x}}$	Estimated signal
$\mathbf{Y}$	Received data matrix
α	Path loss exponent
δ	Kronecker delta function
γ	Signal-to-noise ratio
λ	Wavelength
σ_T	RMS delay spread
θ	Phase
χ	Cross polarization discrimination
ρ_r	Receive correlation coefficient
δ	Symbol delay
χ	Cross polarization channel power
k_r	Relay amplification factor

List of Mathematical Notations

$(\cdot)^H$	matrix Hermitian
$(\cdot)^\dagger$	matrix pseudo-inverse
$(\cdot)^*$	complex conjugate
$\det(\cdot)$	determinant of a matrix
$\mathbb{E}(\cdot)$	expectation operator of a random variable
$\mathrm{diag}(\cdot)$	a vector that contains all diagonal elements of a matrix
$\log_2(\cdot)$	base-2 logarithm
$\lvert\cdot\rvert$	amplitude of a scalar
$\lVert\cdot\rVert$	norm of a vector
$\lVert\cdot\rVert_F$	Frobenius norm of a matrix
$\mathbf{I}_M$	$M \times M$ Identity matrix
$\approx$	approximately equal to
$\mathcal{R}$	real field
$\otimes$	circular convolution
$\triangleq$	defined to be

Chapter 1

Introduction

1.1 History of Wireless Communication Systems

The wireless communication industry has seen remarkable growth in the past decade. Each new generation of wireless systems has brought notable improvement in terms of data rates, link reliability, and battery life. The first mobile communication systems were analog, which are known as first generation (1G) systems. With the advent of digital communication, second generation (2G) systems emerged. In Europe, the most popular 2G system was Global System for Mobile communication (GSM), which supported the data rate of 9.6kbps [1]. The demand for higher data rates led to the development of third generation (3G) system known as Universal Mobile Telecommunication System (UMTS). UMTS standards are based on code division multiple access (CDMA) technology that is able to provide at least 384kbps for outdoor and 2Mbps for indoor environment [2]. However, there is a demand for an even higher data rate in limited available radio frequency spectrum and multipath fading environment. In 3GPP Long Term Evolution (LTE) the use of multiple antennas at both the transmitter and the receiver is the key to meeting such a demand. LTE is a step towards fourth generation (4G) systems that provide high spectral efficiency due

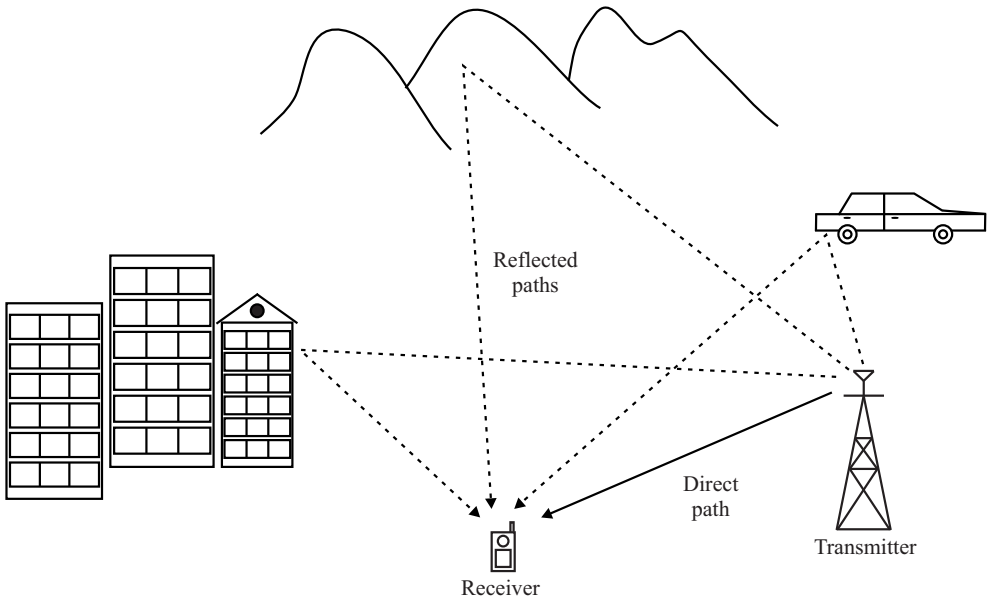

Figure 1.1: Multipath fading environment.

to the use of multiple antennas, also known as multiple-input multiple-output (MIMO) systems. The use of four transmit and receive antennas can provide a peak downlink data rate of 326.4Mbps [3].

1.2 Multi-antenna Systems

Many communication systems have been designed to enhance the performance in terms of link reliability, data rates, and battery life and interference reduction. The major technical challenge in wireless communication is multipath fading that arises between the transmitter and receiver due to the scattering environment as can be seen in Fig. 1.1. This multipath effect induces severe channel impairments but can also be carefully exploited to improve the link quality. By using multiple antennas at the transmitter and receiver, the receiver will be provided with multiple versions of an information bearing signal. Thus the multiple spatial channels can be utilised to provide diversity and/or multiplexing gain [4, 5].

The achievable capacity of a MIMO system increases with the increase in

minimum number of transmit and receive antennas. Also, by using multiple antennas, spatial channels can be exploited to provide spatial diversity gain which is not present in the single antenna systems. Based on providing higher capacity or diversity gain, the MIMO technologies are broadly categorized into spatial multiplexing and spatial diversity [6]. These categories will be discussed later in the thesis.

1.3 Cooperative MIMO Communications

In conventional point-to-point communication, transmission channels can be highly uncertain due to multipath fading. Therefore, reliable communication between each pair of transmitter and receiver can not be ensured. Cooperative communication has emerged as a new communication paradigm for wireless networks such as wireless ad hoc networks, sensor networks, and cellular networks to exploit the spatial diversity gain inherent in multiuser wireless systems. It mimics the performance advantages of MIMO systems and is achieved by transmission through additional relay nodes [4, 7–13].

Fig 1.2 illustrates the ideas behind cooperative communication. It shows

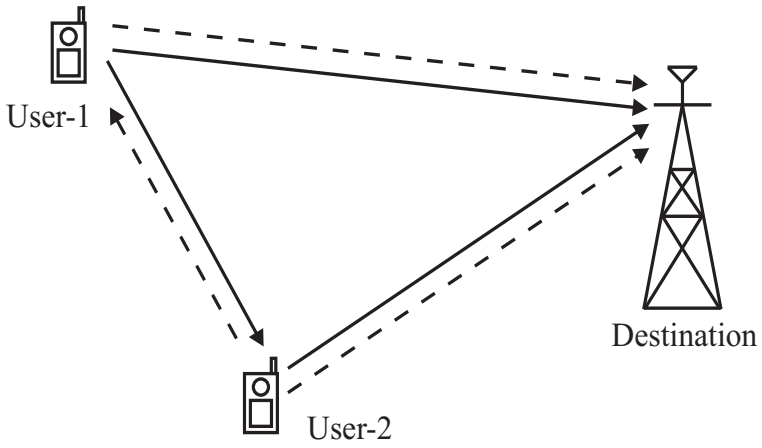

Figure 1.2: Cooperative communication network.

two mobile nodes communicating with the same receiver. The mobile nodes can overhear each other's information in which case they can transmit the overheard information along with their own data. As the fading links from the two mobiles are statistically independent, this generates spatial diversity.

1.4 Motivations

Most cooperative communication protocols [7, 8, 10, 14] assume frame or symbol level synchronization between the cooperating nodes. Practically this assumption is difficult to maintain in distributed wireless networks. The lack of synchronization results in inter-symbol interference (ISI) and degrades the system performance. In [15] and [16], asynchronous cooperative protocols are proposed to tackle this problem. Although the schemes [15, 16] can mitigate the synchronization problem, they used half duplex relay nodes just like most of the other existing schemes [7, 8, 10, 14]. The assumption of half duplex relay nodes reduces spectral efficiency due to bandwidth expansion or extended time duration.

Another issue with cooperative communication networks is the energy consumption of the nodes. As with most energy constrained networks, multi-relay nodes cooperative wireless sensor networks are usually powered by batteries which have limited energy and are mostly difficult to change or recharge [17]. Therefore, minimizing the energy consumption to maximize the life-time of cooperative networks is an important factor in network design. Energy efficient protocols must be derived and used for data transfer to increase network life. In [18], the power allocation expression is derived to maximize the channel capacity in fading environment. In [19], symbol error rate is minimized for optimal power allocation. However, these works ignore the channel path loss which is inevitable in practical implementations.

1.5 Contributions

The first contribution of this thesis is the novel asynchronous polarized cooperative MIMO communication scheme which does not require a centralized unit. Unlike most of the existing cooperative schemes, [7, 8, 10, 14] the new protocol does not require frame or symbol level synchronization at the relay node. The relay node in the proposed scheme employs dual-polarized antennas with separate radio frequency (RF) chains. This enables the relay to transmit and receive at the same time and the same frequency band which increases the transmission data rates and improves the link reliability. The installation of co-polarized multiple antennas at the relay node in place of dual-polarized antennas is not feasible because the transmitted signal from the transmit antenna will fully overwhelm its receive antenna. Thus, the received signal cannot be retrieved. However, with the employment of polarized antennas, the transmitted signal at one polarization is orthogonal to the received signal at another polarization. Hence, full duplex communication can be achieved. The effect of cross-polarization is considered in the analysis because it is not possible to maintain the polarization between the transmitter and the receiver due to the complex propagation environment in terrestrial wireless communications. For a more realistic scenario, path loss is also included in the investigation which is usually ignored in the existing literature. A frequency domain receiver for this system is presented and the capacity is also analyzed. As multiple RF chains are used in this scheme, energy consumption analysis is also performed to ensure a fair comparison with conventional relaying scheme.

Another contribution in this thesis is the novel power allocation scheme for multi-relay nodes cooperative network. The scheme aims to minimize the total transmission energy consumption without affecting the link quality thereby increasing the network life time. The power ratio between the direct and relayed

links is optimized to achieve this aim. This power ratio is evaluated analytically and is compared with simulation results. The channel capacity with the new power allocation scheme is also compared with conventional equal power cooperative scheme and non-cooperative SISO. The relay nodes positioning that maximizes the capacity using the proposed power allocation scheme is also discussed.

1.6 Thesis Organization

This thesis consists of seven chapters. This first chapter begins with the overview of history and current trends in wireless communications. It explains the motivation of this research work and the contributions made.

In chapter 2, an overview of the wireless communication channel and its characteristics are given. The chapter begins with an overview of different types of fading channels. Next, depending on the relationship between the signal parameters and channel parameters, different types of small-scale fading are discussed. Equalization techniques are also discussed in the chapter.

In chapter 3, multi-antenna systems are reviewed. This chapter covers the underlying principles of spatial diversity and discusses on different diversity combining techniques at the receiver. We give an overview of MIMO channel model and study how multiple antennas can enhance channel capacity and in particular how MIMO systems can provide a linear increase in capacity making it attractive for practical systems. We also discuss how multiple antennas can offer diversity. The architectures of different MIMO transmission schemes such as Bell Laboratories Layered Space-Time (BLAST), and Space time coding (STC) are also provided.

Existing literature that contribute to cooperative communication are presented in chapter 4. The basic relay model is discussed along with various cooperative signaling methods. The performance analysis of amplify-and-forward is discussed in detail as it is the main focus of our work.

The novel energy efficient asynchronous polarized cooperative scheme is presented in chapter 5. To evaluate the performance of this scheme, extensive computer simulations are performed and the results for BER, energy and capacity analysis are presented.

Chapter 6 details the new power allocation scheme for efficient cooperative communication. The energy is distributed between the relay and direct link to minimize the total transmission energy consumption. We calculate the energy distribution ratio analytically and verify it through computer simulation.

Finally, chapter 7 concludes the thesis and discusses future work.

1.7 List of Publications

Journal Publications

1. Sarmad Sohaib and Daniel K. C. So., Energy Efficient Asynchronous Polarized Cooperative Protocol, *IEEE Transaction on Vehicular Technology (in preparation)*

2. Sarmad Sohaib and Daniel K. C. So., Power Allocation for Efficient Cooperative Communication, *IEEE Transaction on Signal Processing (in preparation)*

Conference Publications

1. Sarmad Sohaib and Daniel K. C. So, Energy Analysis of Asynchronous Polarized Cooperative MIMO Protocol, in *IEEE Intl Symposium on Personal,*

Indoor and Mobile Comms (PIMRC). 2010

2. Sarmad Sohaib, Daniel K. C. So, and Junaid Ahmed, Power Allocation for Efficient Cooperative Communication, in *Proc. IEEE Intl Symposium on Personal, Indoor and Mobile Comms (PIMRC)*. 2009

3. Sarmad Sohaib and Daniel K. C. So., Asynchronous Polarized Cooperative MIMO Communication, in *Proc. IEEE Vehicular Technology Conference (VTC)- Spring*. 2009

4. Sarmad Sohaib and Daniel K. C. So, Cooperative MIMO Communications, in *EEE PGR Conference, The University of Manchester, UK*. 2008

Chapter 2

Wireless Channel and Equalization

2.1 Introduction

In wireless communication, information bearing signal is transmitted through the channel to the receiver by means of electromagnetic waves. The received signal is distorted by the propagation channel and noise. Therefore, in order to design a high-quality wireless system, these factors need to be analyzed.

In this chapter, we will present some background knowledge of wireless channels. The characteristics and model of wireless communication channel are described in section 2.2 - 2.4. In section 2.5, different types of small scale fading are discussed. Multipath fading models are reviewed in section 2.6. Equalizers, used to mitigate the inter symbol interference (ISI) problem are then discussed in section 2.7.

2.2 Characteristics of Wireless Communication Channel

In wireless communications, the transmission path may vary from line of sight (LOS) to one that is severely obstructed by structures such as mountains, and buildings. The signal propagates in wireless channel through reflection, scattering and diffraction. The receiver receives signals from transmitter through different path with different travel time and hence, different phase. These signals are combined either constructively or destructively which results in rapid fluctuation in the received signal strength. The received signal strength also reduces slowly as the distance between transmitter and receiver increases. The modeling of such a radio channel is important for mobile radio system design as this can enable us to use the channel in the best of our interest. On the basis of transmitter-receiver (T-R) separation, fading models can be broadly categorized as

- Large-scale model
- Small-scale model

2.3 Large-Scale Path Loss and Shadowing Model

Large scale path loss is the attenuation of the average signal power along the path of transmission that depends upon the distance from the transmitter. This is also known as macroscopic fading which increases exponentially as the distance increases. It shows the gradual decay of the received signal power in a range of hundreds or thousands of meters.

Large scale fading can be characterized by path loss that is defined as the attenuation in power density of an electromagnetic wave as it propagates through

space. The general propagation model for path loss is given by [20]

$$\frac{P_r}{P_t} = \frac{PL_0}{d^\alpha} \tag{2.1}$$

where α is the path loss exponent that typically ranges from 2 to 5 depending upon the propagation environment, P_r and P_t are the received and transmitted powers respectively. PL_0 is the path loss at a reference distance d_0 that is related to the frequency, antenna gains, and other factors by

$$PL_0 = \frac{\lambda^2 G_t G_r}{(4\pi)^2} \tag{2.2}$$

where λ is the wavelength, G_t and G_r are the transmitter and receiver antenna gains respectively.

Apart from the path loss, the variation of terrain and presence of obstacles will cause shadowing which is modeled as log-normal distribution. It demonstrates the variation of the received signal power in different locations at a fixed distance. The effect of shadowing can be mathematically expressed as

$$PL\,(d) = PL_0 + 10\alpha \log_{10}\left(\frac{d}{d_0}\right) + X_\sigma \tag{2.3}$$

where the first two terms accounts for the path loss at distance d, and X_σ represents log-normal shadowing effect and is a zero mean Gaussian distributed random variable in logarithm scale.

2.4 Small-Scale Fading

In mobile communication, the rapid fluctuation of the received signal's amplitude or phase over a very short period of time or distance is called small-scale fading or microscopic fading. This variation of the signal is in tens of wavelengths or a

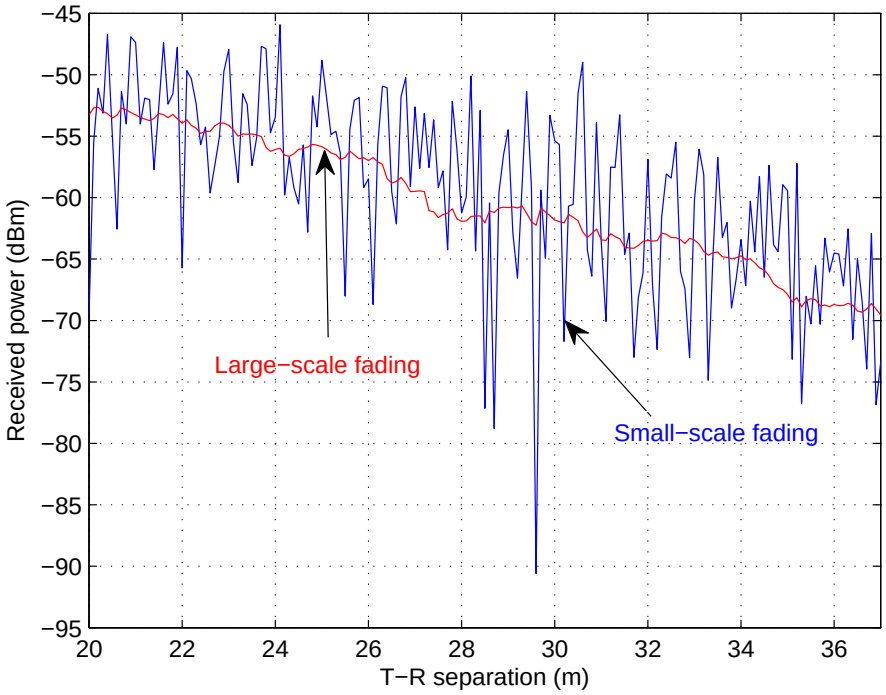

Figure 2.1: Large-scale and small-scale fading.

very short period of time (in the order of seconds), while the large-scale average path loss is kept at a constant level. The factors influencing small-scale fading are multipath propagation, speed of the mobile and surrounding objects, and the transmission bandwidth of the signal. Fig. 2.1 illustrates the combined effect of large-scale and small-scale fading.

2.4.1 Multipath Fading

Multipath fading is the phenomenon which occurs when a signal arrives at the receiver via multiple propagation paths. These replicas of the transmitted signal that arrives at the receiver through different paths possess different phase and amplitude which results in rapid variations in the amplitude. Mathematically, it

can be modeled as [20]

$$h(t,\tau) = \sum_{i=0}^{N-1} a_i\left(t,\tau\right) e^{j\theta_i(t,\tau)} \delta\left(\tau - \tau_i\left(t\right)\right) \tag{2.4}$$

where $a_i(t,\tau), \tau_i\left(t\right)$ and θ_i are the amplitude, excess delay, and phase of the i-th multipath component at time t respectively. τ_i is the time delay of the i-th impulse. Excess delay is the relative delay of the i-th component compared to the first arriving component. There are N number of multipath components, each with respective amplitude, excess delay, and phase.

2.4.2 Doppler Shift

Small-scale fading is also influenced by the relative motion of transmitter and receiver referred as Doppler shift. It is the shift in the received signal frequency due to motion. The amount of frequency shift is subject to the mobile velocity and the wave incident angle. The shift f_D can be expressed as [21]

$$f_D = \frac{v}{\lambda} \cos\psi \tag{2.5}$$

where v is the speed of movement, λ is the wavelength and ψ is the angle between the direction of motion and the wave propagation. It can be observed from (2.5) that the Doppler shift is positive if the mobile is moving towards the direction of arrival of the wave i.e. the apparent received frequency is increased. On the other hand, the Doppler shift is negative if the mobile is moving away from the direction of arrival of the wave i.e. the apparent received frequency decreases [21].

2.5 Types of Small-Scale Fading

Fading experienced by signal propagation through the channel depends on the nature of transmitted signal with respect to the channel characteristics [21]. Depending on the relationship between the signal parameters (such as bandwidth, and symbol period) and channel parameters (such as Doppler spread, and rms dealy spread), the transmitted signal will experience different types of fading. Time dispersion and frequency dispersion leads to four types of fading that are explained in the following subsections.

2.5.1 Fading Effects Due to Multipath Time Delay Spread

The time dispersion due to multipath causes the transmitted signal to undergo either flat or frequency selective fading.

Flat Fading

If the mobile radio channel possesses a constant gain and linear phase response over a bandwidth which is greater than the transmitted signal bandwidth, the received signal will undergo flat fading [21]. In this type of fading, the spectral characteristics of the transmitted signal are preserved at the receiver. However, the strength of the received signal changes with time due to fluctuations in the gain of the channel caused by multipath.

Flat fading can be mathematically summarized as [21]

$$B_S \ll B_C \tag{2.6}$$

and

$$T_S \gg \sigma_\tau \tag{2.7}$$

where B_S is the bandwidth of the transmitted signal, T_S is the symbol period,

and B_C and σ_τ are the coherence bandwidth and the rms delay spread of the channel respectively. Coherence bandwidth is a statistical measurement of the range of frequencies over which the channel amplitude is correlated. RMS delay spread is the standard deviation for all excess delays [21]. Flat faded channels are also called amplitude varying and narrowband channels, because the bandwidth of the applied signal is narrow as compared to the channel bandwidth.

Frequency Selective Fading

If the radio channel has a constant gain and linear phase response over a bandwidth that is smaller than the transmitted signal bandwidth, then the received signal will undergo frequency selective fading. In terms of time domain, the symbol period is much less than delay spread. After one symbol is transmitted, the delayed component of this signal will remain in the channel along with the subsequent transmitted signal, thereby, creating a distortion called ISI.

Frequency selective fading can be mathematically summarized as [21]

$$B_S > B_C \tag{2.8}$$

and

$$T_S < \sigma_\tau. \tag{2.9}$$

Equalization techniques are needed to retrieve the original transmitted single in frequency selective channel, which will be discussed in section 2.7.

2.5.2 Fading Effects Due to Doppler Spread

This type of fading only deals with the rate of change of the channel due to motion. Depending on how rapidly the transmitted baseband signal changes as compared to the rate of change of channel, a channel can be classified as either

fast fading or slow fading.

Fast Fading

In this type of fading, the channel impulse response changes rapidly within the symbol duration i.e. the coherence time of the channel is smaller than the symbol period. This type of fading causes frequency dispersion due to Doppler spreading, that leads to signals distortion and is also called time selective fading [21]. Mathematically, we can summarize it as

$$T_S > T_C \tag{2.10}$$

and

$$B_S < B_D \tag{2.11}$$

where, T_C is the coherence time and B_D is the Doppler spread. Coherence time is a statistical measure of the period over which channel fading process is correlated. Doppler spread is measure of the spectral broadening caused by the time variation of the channel and is defined as the range of frequencies over which the received Doppler spectrum is essentially non-zero.

Slow Fading

In this type of fading, the channel impulse response changes at a rate much slower than the transmitted signal [22]. These channels may be assumed static over one or several time periods. In frequency domain, this implies that the Doppler spread of the channel is much less than the bandwidth of the baseband signal. Mathematically, we can summarize it as

$$T_S \ll T_C \tag{2.12}$$

$$B_S \gg B_D. \tag{2.13}$$

2.6 Common Multipath Fading Models

In this section we present two common multipath fading models - Rayleigh and Ricean fading.

2.6.1 Rayleigh Fading

Rayleigh fading is caused by the superposition of a large number of independent scattered components with similar power. The in-phase and quadratic components of the received signal are assumed to be an uncorrelated zero mean complex valued Gaussian process [23]. The envelope of the received signal has a Rayleigh distribution with the probability density function (pdf) given by

$$p(x) = \frac{x}{\sigma_x^2}\, e^{-x^2/2\sigma_x^2}\, u(x), \tag{2.14}$$

where $\mathbb{E}\left[x^2\right] = 2\sigma_x^2$, and $u(x)$ is the unit step function given by

$$u(x) = \begin{cases} 1 & \text{if } x \geq 0,\ x \in \mathcal{R} \\ 0 & \text{if } x < 0,\ x \in \mathcal{R}. \end{cases} \tag{2.15}$$

The Rayleigh fading model is commonly used in the case where there is no LOS between the transmitter and the receiver, such as urban city centre.

2.6.2 Ricean Fading

When the LOS is present between the transmitter and receiver, the envelope of the received signal can be modeled by Ricean distribution with pdf given by

$$p\left(x\right) = \frac{x}{\sigma_x^2}\, e^{-\frac{(x^2+A^2)}{2\sigma_x^2}}\, I_o\left(\frac{Ax}{\sigma_x^2}\right)\, u(x) \tag{2.16}$$

where A is the peak amplitude of the dominant signal (LOS) and $I_o(x)$ is the modified Bessel function of the first kind and zero order defined as

$$I_o\left(x\right) = \frac{1}{2\pi}\int_0^{2\pi} e^{-x\cos\theta} d\theta. \tag{2.17}$$

In this type of multipath fading, the random multipath components arriving at different angles are superimposed on a stationary dominant signal. At the output of an envelope detector, this has the effect of adding a DC component to the random multipath [21].

The Ricean distribution is often defined in terms of factor K called *Ricean Factor*, which is the power ratio between LOS component and the scattered components i.e.

$$K = \frac{A^2}{2\sigma_x^2}. \tag{2.18}$$

As $A \to 0, K \to -\infty$ dB, and as the dominant path decreases in amplitude, the Ricean distribution degenerates to a Rayleigh distribution as can be seen from Fig. 2.2.

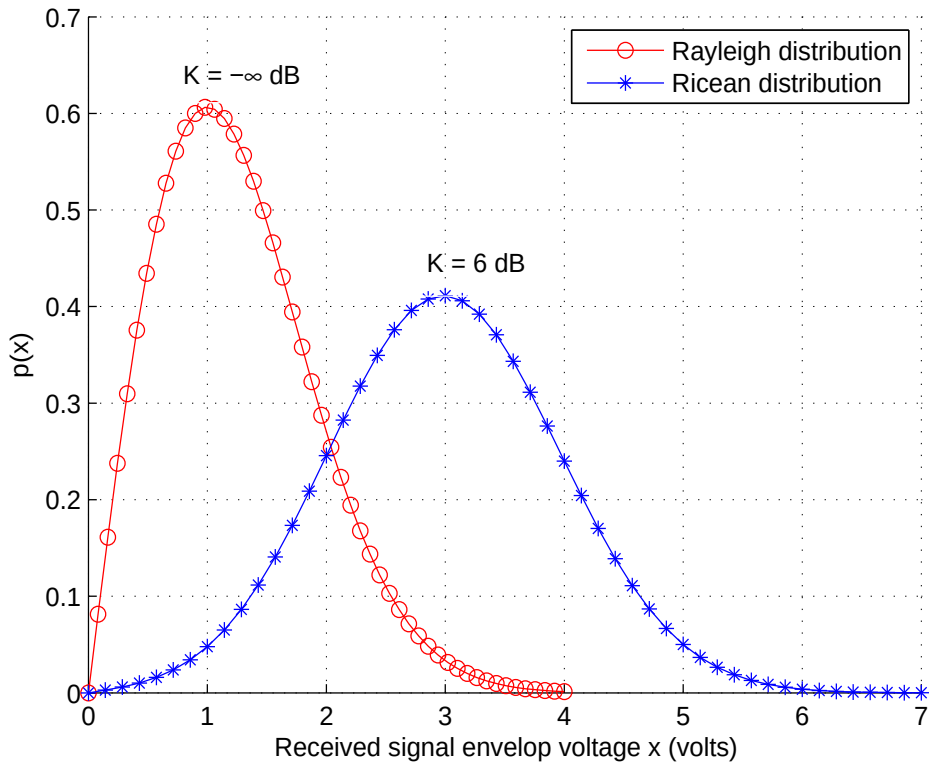

Figure 2.2: Probability density function of Ricean distribution: $K = -\infty$ dB (Rayleigh) and $K = 6$dB.

2.7 Equalization

In time dispersive channels, the symbol duration is much less than the rms delay spread which leads to ISI and can cause an irreducible error floor. Equalization is a signal processing technique used at the receiver to eliminate ISI [24]. It can be categorized into time or frequency domain approaches, and further subdivided into linear and non-linear techniques.

The time-domain linear equalizers are simple linear finite impulse response (FIR) filters that invert the channel in the sense that the product of the transfer function of the channel and equalizer fulfils a certain criterion [25]. This criterion can either be achieving a completely flat transfer function of the channel-filter concatenation, or minimizing the mean-squared error (MSE) at the filter output.

The non-linear equalizers are used in situations where the channel distortion is too severe for a linear equalizer to handle [26]. Decision Feedback Equalizer (DFE) and Maximum Likelihood Sequence Estimation (MLSE) equalizer are two very effective non-linear methods that offer improvements over linear equalization techniques and are used in most 2G and 3G systems.

Frequency domain equalization exploits the Fourier transform property, in which cyclic convolution in the time domain can become simple multiplication in the frequency domain. In the following subsection we present the linear frequency domain equalizer (FDE) as it is related to our work.

2.7.1 Frequency Domain Equalization

In the time domain the transmitted symbols are linearly convolved with the channel. Consider vector form with K symbols and L channel taps, the received signal in time domain is given by

$$\mathbf{y} = \mathbf{h} \otimes \mathbf{x} + \mathbf{n} \tag{2.19}$$

where $\otimes$ denotes the cyclic convolution operation. The cyclic convolution can be attained when the cyclic prefix is inserted to the beginning of the frame. This cyclic prefix contains the last symbols of the frame.

In frequency domain, the frequency domain of the symbols is multiplied with the frequency domain of the channel. Therefore, taking a K-point Fourier transform on $\mathbf{y}$ we obtain

$$\mathbf{Y} = \mathbf{HX} + \mathbf{N} \tag{2.20}$$

where $\mathbf{Y}$, $\mathbf{H}$, $\mathbf{X}$ and $\mathbf{N}$ are frequency domain representation of $\mathbf{y}$, $\mathbf{h}$, $\mathbf{x}$, and $\mathbf{n}$ respectively.

The k-th frequency bin of (2.20) can be expressed as

$$Y(k) = H(k)X(k) + N(k) \tag{2.21}$$

To equalize $Y(k)$, a filter coefficient $W(k)$ is multiplied. The signal after equalization can be expressed as

$$\hat{X}(k) = W(k)Y(k) \tag{2.22}$$

where $\hat{X}(k)$ is the equalized frequency domain symbol.

In the following we discuss two types of FDE: Zero Forcing (ZF) and Minimum Mean-Square Error (MMSE) equalizers. For the ease of notation and without loss of generality, we drop the index k in the following subsections.

A. Zero Forcing Equalizer

In the frequency domain, the ZF equalizer can be interpreted as enforcing a completely flat transfer function of the channel-filter concatenation by dividing Y by H for all frequency bins. Therefore the filter coefficient can be expressed as

$$W_{ZF} = 1/H. \tag{2.23}$$

The ZF equalizer has a disadvantage that this channel inversion may excessively amplify the noise at frequencies where the channel spectrum has deep nulls. The ZF equalizer neglects the effect of noise altogether and hence is not often used for wireless communication [21].

B. Minimum Mean-Square Error Equalizer

An MMSE equalizer is more robust as compared to the ZF equalizer where the criterion used is the minimization of the MSE between the transmitted symbol and the estimated one. Mathematically, it can be expressed as

$$W_{MMSE} = \arg\min_{W} \mathbb{E}\left[\left|X - \hat{X}_{MMSE}\right|^2\right]. \tag{2.24}$$

Substituting the value of $\hat{X}_{MMSE}$ into the objective function of Eq. (2.24)

$$\begin{aligned} J =& \mathbb{E}\left[|X - WY|^2\right] \\ =& \mathbb{E}\left[|X - W(HX + N)|^2\right]. \end{aligned} \tag{2.25}$$

Solving the above equation for minimum value of W, we take the derivate of J w.r.t. W and set it to 0, i.e. $\frac{dJ}{dW} = 0$

$$\begin{aligned} &\Rightarrow HH^*W^* - H + N_oW^* = 0 \\ &\Rightarrow (HH^* + N_oI_{M_t})W^* = H. \end{aligned} \tag{2.26}$$

Rearranging Eq. (2.26) we obtain,

$$W^* = H(HH^* + N_oI_{M_t})^{-1}. \tag{2.27}$$

Taking the Hermitian transpose on both sides, we thus obtain the final form

$$W_{MMSE} = (H^*H + N_oI_{M_t})^{-1}H^*. \tag{2.28}$$

Fig. 2.3 shows the BER performance comparison between ZF and MMSE equalizers. The wireless channel is assumed to be 3-taps Rayleigh frequency selective faded. The power delay profile is taken to be uniform. Zero mean

circular-symmetric complex Gaussian noise is considered. QPSK is used as the modulation scheme. From the results, MMSE equalizer has better BER performance than ZF equalizer. This is because ZF equalizer cancels all ISI, but can lead to considerable noise enhancement, whereas MMSE equalizer minimizes the expected mean squared error between the transmitted and detected symbol at the equalizer output. It provides a better balance between ISI mitigation and noise enhancement.

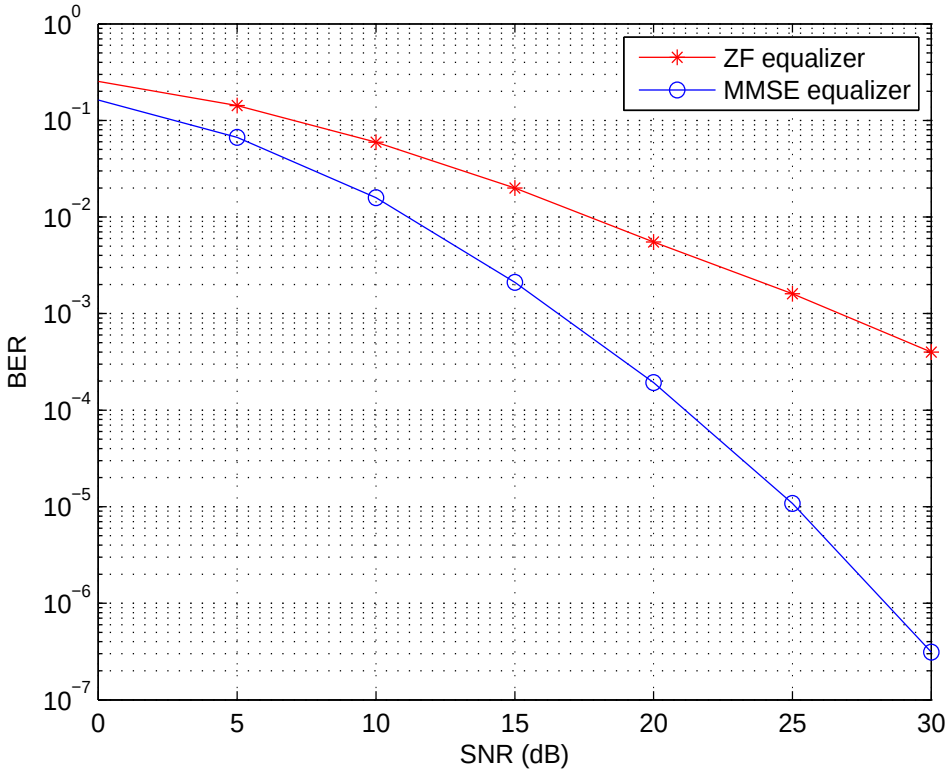

Figure 2.3: BER performance of ZF and MMSE equalizers.

Chapter 3

Multi-antennas Wireless Communications

3.1 Introduction

In this chapter, we start with an explanation of the multi-antenna systems in section 3.2. Various types of diversity and receiver combining techniques are presented in section 3.3 and 3.4 respectively. The system model and capacity of MIMO systems are then discussed in section 3.5 and 3.6 respectively. Several MIMO transmission schemes are presented in section 3.7 and 3.8.

3.2 Multi-antennas Systems

Wireless communication with multiple antennas has emerged as one of the major breakthroughs in modern communications that promises significant improvement in terms of both spectral efficiency and link reliability [27]. The idea behind the multiple antennas system is that the signals at transmit and receive antennas are combined in such a way that both the quality and data rate of the communication is improved.

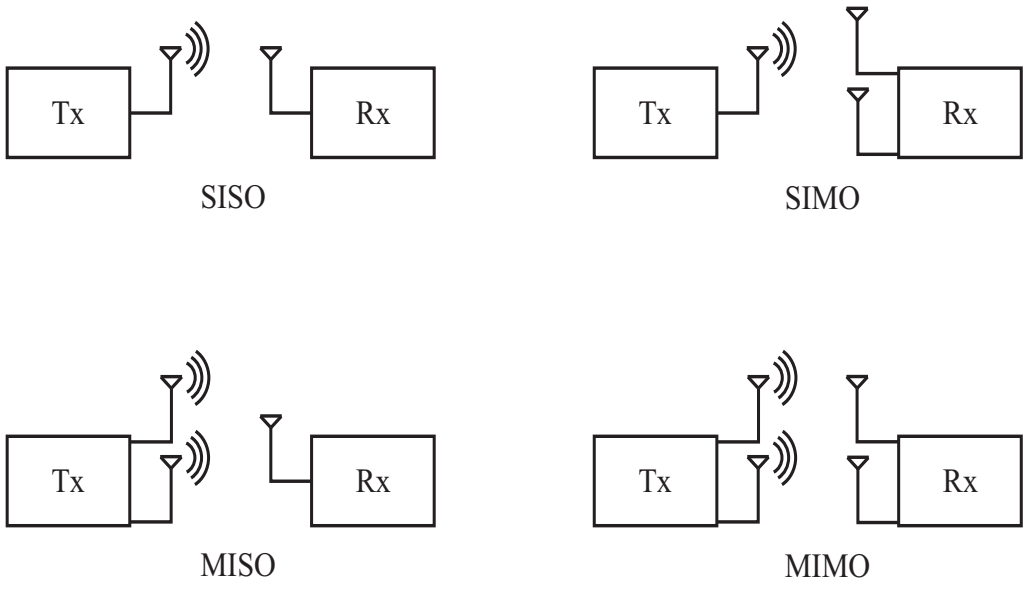

Figure 3.1: Different antenna configurations in space-time systems.

Fig. 3.1 illustrates the different antennas configurations used in radio communications. The most well know configuration is single-input single-output (SISO) that consists of a single antenna at both the transmitter and receiver. Single-input multiple-output (SIMO) uses a single transmit antenna and multiple receive antennas; multiple-input single-output (MISO) has multiple transmitting antennas and a single receiving antenna; multiple-input multiple-output (MIMO) has multiple transmit antennas and multiple receive antennas.

3.3 Diversity Techniques

Diversity refers to a method to reduce the effects of multipath fading and improve the reliability of a message signal by using two or more communication channels with different characteristics. It is based upon the fact that individual channels experience independent fading. Multiple versions of the same signal will fade in an uncorrelated manner and the probability that all versions are below a certain threshold level is much lower than the probability of any individual signal being

below that particular threshold. These multiple versions of the signals are combined at the receiver, and correspondingly, improve reliability of transmission.

In wireless communication, diversity techniques are classified as following:

- Temporal Diversity
- Frequency Diversity
- Spatial Diversity

3.3.1 Temporal Diversity

In this type of diversity, replicas of the signal are transmitted in multiple time slots separated at least by the coherence time of the channel. The coherence time is a statistical measure of the period over which channel fading process is correlated. Typically, the channel coherence time is of the order of tens to hundreds of symbols and therefore the channel is highly correlated across consecutive symbols [22]. Therefore the codewords are interleaved to obtain the independent or nearly independent fading gains at the input of the decoder. Since time interleaving results in decoding delays, this technique is usually effective for fast fading environments where the coherence time of the channel is small. For slow fading channels, a large interleaver can lead to a significant delay which is intolerable for delay sensitive applications such as voice transmission [28]. Therefore, time diversity is not suitable for mobile radio communication. Another disadvantage of this scheme is the loss of bandwidth efficiency due to the redundancy introduced in the time domain.

3.3.2 Frequency Diversity

Frequency diversity can be achieved by transmitting the same signal on more than one carrier frequencies. The frequencies need to be separated by more

than the coherence bandwidth of the channel, where the coherence bandwidth is a statistical measurement of the range of frequencies over which the channel amplitude is correlated. This separation ensures frequencies are not correlated and will not experience the same fade [29].

3.3.3 Spatial Diversity

This type of diversity is also referred as antenna diversity because multiple antennas are used for transmission and/or reception. In this type of diversity, replicas of the same signal are transmitted by physically separated antennas. These antennas are separated enough so that the fading associated with the different antennas is uncorrelated i.e. antenna spacing is larger than the coherence distance; where coherence distance is the minimum spatial separation of antennas for independent fading [28]. Unlike time diversity, the space diversity is bandwidth efficient and thus, an attractive diversity option for high data rate wireless communications. The spatial diversity can be subdivided into following three types.

- *Receive Diversity*: In this type of spatial diversity, multiple antennas are deployed at the receiver. Received signals from the antennas are combined using different combining techniques, thus mitigating multipath fading and improve the received signal quality. As multi-antennas are installed at the receiver, this adds to the cost and the complexity of the receiver. This is one of the main reasons that transmit diversity is preferred over the receive diversity.

- *Transmit Diversity*: In this type of spatial diversity, controlled redundancy is introduced at the transmitter, which can then be exploited by appropriate signal processing techniques at the receiver. This technique usually needs complete channel state information (CSI) at the transmitter to make this possible. However, with the advent of space time coding techniques

like Alamouti's scheme [30], it is possible to implement transmit diversity without channel knowledge at the transmitter [31].

- *Polarization Diversity*: Another type of antenna diversity is polarization diversity, where horizontal and vertical polarized signals are transmitted by two different polarized antennas and are received by two different polarized antennas. As two signals are uncorrelated by different polarization, the two antennas do not have to be installed far apart.

3.4 Diversity Combining Techniques

In the previous section, we have presented different forms of diversities. By using diversity techniques, we create a corresponding set of fading channels that are essentially different. The outputs of these statistically independent fading channels need to be combined in accordance with a criterion that will provide improved receive performance. This section will discuss some of the major diversity combining techniques based on receive diversity [32]. Nonetheless these techniques can also be used for other diversity types.

3.4.1 Selection Combining (SC)

This is the simplest combining method that involves M_r linear receivers and a logic circuit. Fig. 3.2 illustrates the structure of SC technique. In this scheme, the logic circuit selects the received signal with the highest instantaneous SNR and ignores the observations from other antennas.

Let us suppose $x(t)$ defines the complex envelop of the modulated signal transmitted. The complex envelop of the received signal of the k-th diversity branch is defined by

$$y_k(t) = h_k x(t) + n_k(t), \qquad k = 1, 2, \ldots, M_r \tag{3.1}$$

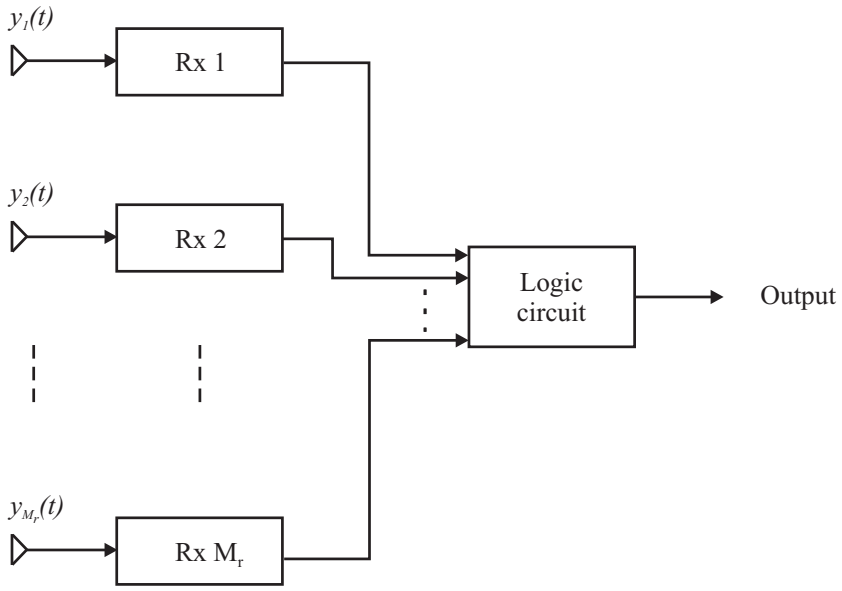

Figure 3.2: Block diagram of selection combining.

where $n_k(t)$ is the AWGN and h_k is the slow varying fading channel of the k-th branch.

The average SNR at the output of the k-th receiver is defined by

$$(SNR)_k = \left(\frac{\mathbb{E}\left[|h_k x(t)|^2\right]}{\mathbb{E}\left[|n_k(t)|^2\right]} \right) = \frac{\mathbb{E}\left[|x(t)|^2\right]}{\mathbb{E}\left[|n_k(t)|^2\right]} \mathbb{E}\left[|h_k|^2\right] \tag{3.2}$$

$$= \frac{E_s}{N_o} \mathbb{E}\left[|h_k|^2\right], \qquad k = 1, 2, \ldots, M_r \tag{3.3}$$

where E_s is the transmitted symbol energy and N_o is the noise spectral density. Now, the instantaneous output SNR of the k-th receiver is given by

$$\gamma_k = \frac{E_s}{N_o} |h_k|^2, \qquad k = 1, 2, \ldots, M_r. \tag{3.4}$$

The instantaneous SNR of the output signal of the SC is given by

$$\gamma_{sc} = \max\left\{\gamma_1, \gamma_2, \ldots, \gamma_{M_r}\right\}. \tag{3.5}$$

The advantage of this method is that it only requires one radio frequency (RF) receiver chain which keeps the cost down. It is not optimal as it ignores the information from all diversity branches except the one with the largest SNR [20].

3.4.2 Equal Gain Combining (EGC)

EGC is a suboptimal but simple linear combining method. In this type of receive combining technique, all the received signals are co-phased and then summed together with equal gain. The received signal is equalized by dividing the received symbol with the channel phase. In polar form, the channel is represented as $h_k = |h_k| e^{j\theta_k}$. The output of the EGC can be expressed as

$$y_{egc} = \sum_{k=1}^{M_r} y_k e^{-j\theta_k} = \sum_{k=1}^{M_r} |h_k| \ x + n_k e^{-j\theta_k}. \tag{3.6}$$

3.4.3 Maximal-Ratio Combining (MRC)

This type of diversity combining technique involves the use of linear receivers where the signals from all M_r branches are scaled according to their individual SNR. The received signals from M_r branches are phase aligned and summed. Fig. 3.3 shows the block diagram of MRC. The output signal is a linear combination of a weighted replica of all the received signals. It is given by

$$y_{mrc}(t) = \sum_{k=1}^{M_r} G_k y_k(t) \tag{3.7}$$

where y_k is the received signal at the receive antenna k, and G_k is the weighting factor for receive antenna k.

Substituting (3.1) into (3.7), we obtain

$$y_{mrc}(t) = x(t) \sum_{k=1}^{M_r} G_k h_k + \sum_{k=1}^{M_r} G_k n_k(t). \tag{3.8}$$

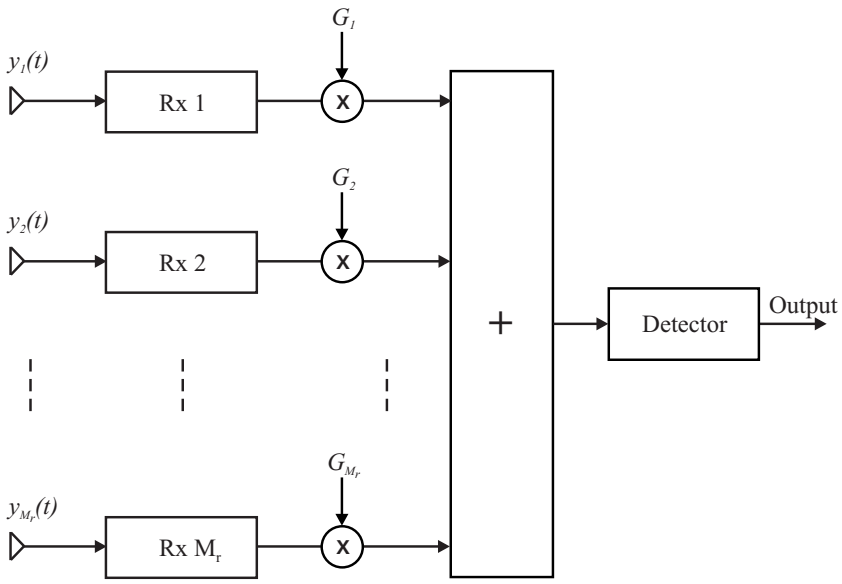

Figure 3.3: Block diagram of MRC.

Assuming that noise $n_k(t)$ from all branches $(k = 1, 2, \ldots, M_r)$ to be statistically independent, the output SNR is given by

$$SNR = \frac{\mathbb{E}\left[\left|x(t)\sum_{k=1}^{M_r} G_k h_k\right|^2\right]}{\mathbb{E}\left[\left|\sum_{k=1}^{M_r} G_k n_k(t)\right|^2\right]} \tag{3.9}$$

$$= \frac{\mathbb{E}\left[|x(t)|^2\right]}{\mathbb{E}\left[|n_k(t)|^2\right]} \frac{\mathbb{E}\left[\left|\sum_{k=1}^{M_r} G_k h_k\right|^2\right]}{\mathbb{E}\left[\sum_{k=1}^{M_r} |G_k|^2\right]} \tag{3.10}$$

$$= \frac{E_s}{N_o} \frac{\mathbb{E}\left[\left|\sum_{k=1}^{M_r} G_k h_k\right|^2\right]}{\mathbb{E}\left[\sum_{k=1}^{M_r} |G_k|^2\right]}. \tag{3.11}$$

Let γ_{MRC} be the instantaneous output SNR of the linear combiner, (3.11) becomes

$$\gamma_{MRC} = \frac{E_s}{N_o} \frac{\left|\sum_{k=1}^{M_r} G_k h_k\right|^2}{\sum_{k=1}^{M_r} |G_k|^2}. \tag{3.12}$$

From the Cauchy-Schwartz inequality for complex numbers [20], we have

$$\left|\sum_{k=1}^{M_r} G_k h_k\right|^2 \leq \sum_{k=1}^{M_r} |G_k|^2 \sum_{k=1}^{M_r} |h_k|^2 \tag{3.13}$$

where the equality holds when $G_k = h_k^*$, and leads to

$$\gamma_{MRC} = \frac{E_s}{N_o} \sum_{k=1}^{M_r} |h_k|^2 . \tag{3.14}$$

This method performs optimal combining since it can maximize the output SNR. As can be seen from (3.14), the maximum output SNR equals to sum of the instantaneous SNRs of the individual signals [20].

Fig. 3.4 shows the BER performance comparison among no diverstiy, SC, MRC and EGC. Single transmit and two receive antennas are used for SC, MRC and EGC. QPSK is used as modulation scheme. The channel is taken to be Rayleigh flat faded. AWGN is assumed. We can see that the EGC offers approximately a 1dB improvement over SC. In addition, MRC outperforms both SC and EGC as it sums the SNR from both branches.

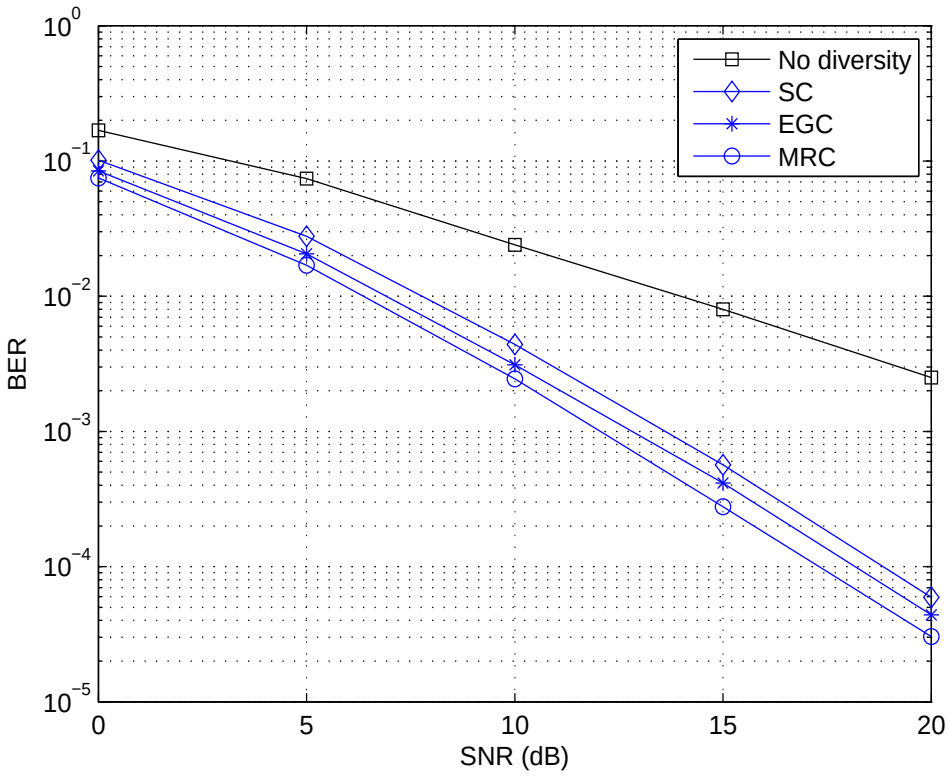

Figure 3.4: BER performance comparison among SC, MRC and EGC.

3.5 MIMO System Models

The MIMO system employs multiple antennas at the transmitter and the receiver to improve communication performance. It offers considerable increases in data throughput and link range without additional transmit power or bandwidth. This is achieved by higher spectral efficiency and diversity. In this section, we present the MIMO system model and it's associated polarized MIMO system model.

3.5.1 Conventional MIMO System Model

Consider a MIMO system with M_t transmit antennas and M_r receive antennas. The system block diagram is illustrated in Fig. 3.5. For a flat fading, and therefore memory-less channel, the MIMO channel is given by $M_r \times M_t$ matrix

$\mathbf{H}(t)$ with

$$\mathbf{H}(t) = \begin{bmatrix} h_{1,1} & h_{1,2} & \cdots & h_{1,M_t} \\ h_{2,1} & h_{2,2} & \cdots & h_{2,M_t} \\ \vdots & \vdots & \ddots & \vdots \\ h_{M_r,1} & h_{M_r,2} & \cdots & h_{M_r,M_t} \end{bmatrix}. \tag{3.15}$$

In rich scattering environment, there are enough multipaths between the transmitter and receiver. Therefore, it is reasonable to assume the channel coefficient h_{ij} to be independent and identically distributed (i.i.d.). Throughout this thesis, it is assumed that there is no dominant propagation path and $\mathbf{H}$ is a complex Gaussian distributed matrix with each entry h_{ij} be a complex Gaussian random variable with zero mean and 1/2 variance in each complex dimension.

Assuming signal x_j is launched from the j-th transmit antenna, the signal received at the i-th receive antenna, $y_i(t)$, is given by

$$y_i(t) = \sum_{j=1}^{M_t} h_{i,j}(t)\, x_j(t) + n_i(t), \qquad i = 1, 2, \ldots, M_r \tag{3.16}$$

where $n_i(t)$ is the AWGN. The input-output relationship for MIMO in (3.16) can

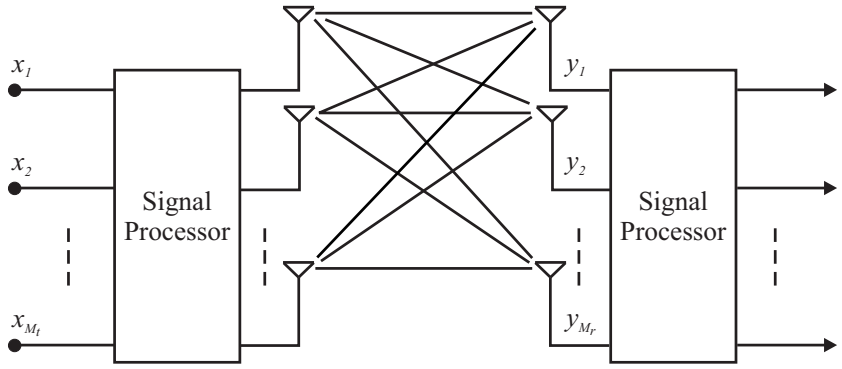

Figure 3.5: Block diagram of a MIMO system.

be rewritten in the compact matrix form as

$$\mathbf{y}(t) = \mathbf{H}(t)\,\mathbf{x}(t) + \mathbf{n}(t) \tag{3.17}$$

where $\mathbf{x}(t) = [x_1(t)\ x_2(t)\ \ldots\ x_{M_t}(t)]^T$ is a vector of dimension $M_t \times 1$ at time t with $\mathbb{E}\left[\mathbf{x}(t)\mathbf{x}(t)^H\right] = \mathbf{I}_{M_t} E_s$, $\mathbf{y}(t) = [y_1(t)\ y_2(t)\ \ldots\ y_{M_r}(t)]^T$ is an $M_r \times 1$ vector and $\mathbf{n}(t) = [n_1(t)\ n_2(t)\ \ldots\ n_{M_r}(t)]^T$ describes a noise vector of dimension $M_r \times 1$ vector with zero mean and variance matrix $N_o\mathbf{I}_{M_r}$.

3.5.2 Polarized MIMO Channel Model

Most channel models assume that the antenna transmit and receive with identical polarization. The use of antennas with different polarizations at the transmitter and receiver provides a polarization gain, which improves the system performance. In practice two polarization classifications are normally used: horizontal/vertical polarization ($0^o/90^o$) or slanted ($\pm 45^o$) [33]. In this thesis we assume same polarization at both the transmitter and receiver, i.e. both of them employ either ($0^o/90^o$) or ($\pm 45^o$). Fig. 3.6 shows the transmitter and receiver using horizontal/vertical polarization. The solid lines represent co-polarization i.e. transmission and reception on the same polarization, and the dotted lines represent cross-polarization i.e. transmission and reception on orthogonal polarizations. Assuming flat fading, the 2×2 MIMO channel matrix $\mathbf{H}$ also known as channel transfer matrix or polarization matrix is given as

$$\mathbf{H} = \begin{bmatrix} h_{sd}^{v} & h_{rd}^{v} \\ h_{sd}^{h} & h_{rd}^{h} \end{bmatrix}. \tag{3.18}$$

The diagonal elements of $\mathbf{H}$ correspond to co-polarization, while the off-diagonal elements correspond to cross-polarization. The power of the individual

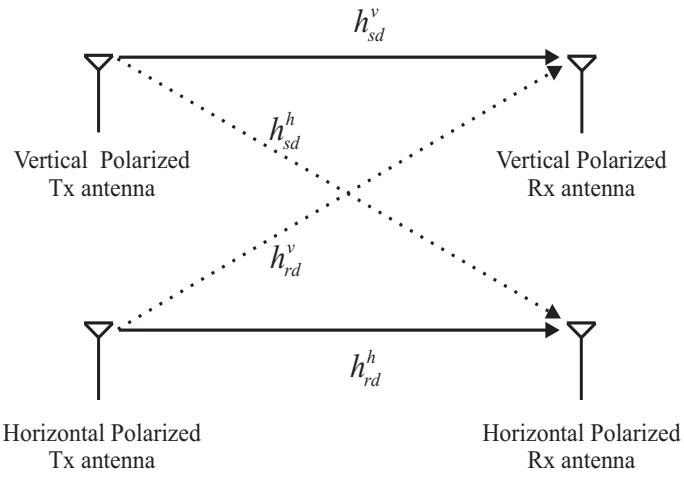

Figure 3.6: Dual-polarized transmitter and receiver with cross-polarization.

channel elements is assumed to be

$$\mathbb{E}\left[|h^v_{sd}|^2\right] = \mathbb{E}\left[\left|h^h_{rd}\right|^2\right] = 1 \tag{3.19}$$

$$\mathbb{E}\left[\left|h^h_{sd}\right|^2\right] = \mathbb{E}\left[|h^v_{rd}|^2\right] = \chi \tag{3.20}$$

where χ reflects the level of cross-polarization discrimination (XPD) of antenna [34] and is bounded as $0 \leq \chi \leq 1$. The cross-polarization can be viewed as a "leakage" from one signal to another that is caused due to the rich scattering nature of the environment [31, 35].

The XPD tells us how well one antenna discriminates its polarization from the other polarization. When χ is 1, it implies no XPD, which means that the antennas cannot discriminate at all between each other's signals. It was found that, typically, at the distances of 2.6km and above, $\chi = 1$, due to the rich scattering nature of the environment [31, 36].

3.6 MIMO System Capacity

The capacity of wireless communication channel is the maximum asymptotic error-free transmission rate that it can support [37]. It is the mutual information of the channel maximized over all possible input distributions [38]. Assuming channel knowledge is only available at the receiver and not at the transmitter, the capacity of the MIMO channels is defined as [39, 40]

$$C = \max_{p(x)} \; I(\mathbf{x}; \mathbf{y}) \tag{3.21}$$

where $p(x)$ is the pdf of the vector $\mathbf{x}$, and $I(\mathbf{x}; \mathbf{y})$ is the mutual information between vectors $\mathbf{x}$ and $\mathbf{y}$.

Solving (3.21), the capacity of the MIMO channel $\mathbf{H}$ is given by [41, 42]

$$C = \max_{p(x)} \; \log_2 \det \left(\mathbf{I}_{M_r} + \frac{E_s}{M_t N_o} \mathbf{H}\mathbf{H}^H \right). \tag{3.22}$$

The capacity C in (3.22) is also known as error-free spectral efficiency or data rate per unit bandwidth that can be sustained reliably over the MIMO link. Thus, if our bandwidth is W Hz, the maximum achievable data rate over this bandwidth using MIMO techniques is WC bit/s [6, 31].

Using single value decomposition (SVD), (3.22) can be further decomposed into

$$C = \sum_{i=1}^{M_r} \log_2 \left(1 + \frac{E_s}{M_t N_o} \lambda_i \right) \tag{3.23}$$

where λ_i is the eigenvalues of $\mathbf{H}\mathbf{H}^H$. Eq. (3.23) shows that the capacity of MIMO channel is the sum of the capacities of M_r SISO channels, each having power gain $\lambda_i, i = \{1, 2, \ldots, M_r\}$ and transmit power E_s/M_t.

The capacity in (3.23) is defined as a random variable. In analyzing the

capacity of fading channels, two commonly used statistics are the ergodic capacity and the outage capacity [6].

3.6.1 Ergodic Capacity

The ergodic capacity is the maximum mutual information averaged over all channel states. In statistical channels like a fading channel, when capacity is computed, it depends upon the statistics of the channel. As it is a random variable, the expected value of the capacity is computed to get the mean information rate. When the channel is unknown to the transmitter, the ergodic capacity $\bar{C}$ is given by

$$\bar{C} = \mathbb{E}\left[\sum_{i=1}^{M_r} \log_2\left(1 + \frac{E_s}{M_t N_o}\lambda_i\right)\right]. \tag{3.24}$$

Fig. 3.7 shows the ergodic capacity of different antenna configurations as a function of SNR. As expected, the ergodic capacity increases with the increase in SNR and also with M_t and M_r. We also observe that SIMO channel has a higher ergodic capacity than the MISO channel because the total transmit power is held constant, independent of the number of M_t transmit antennas.

3.6.2 Outage Capacity

Outage analysis quantifies the level of performance that is guaranteed with certain level of reliability. The $p\%$ outage capacity $C_{out,p}$ is defined as the transmission rate that can be guaranteed for $(100 - p)\%$ of the channel realizations. In other words, the outage capacity can be defined as $P\left(C \leq C_{out,p}\right)$. Fig. 3.8 compares the 10% outage capacity for several MIMO configurations as a function of SNR when the channel is unknown to the transmitter. As in the case of ergodic capacity, the outage capacity also increases with the increase in SNR and is higher with larger number of antennas.

The capacity with outage applies to slowly varying channels, where the instantaneous SNR is constant over the entire duration of the transmitted frame and then changes to a new value based on the fading distribution.

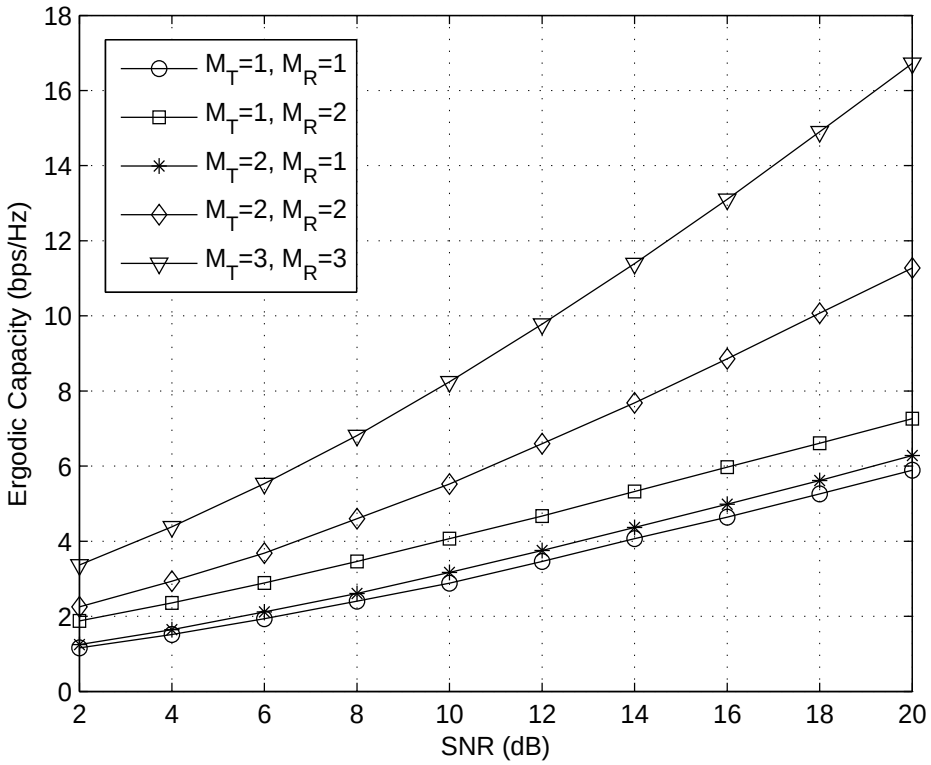

Figure 3.7: Ergodic capacity of different antenna configurations.

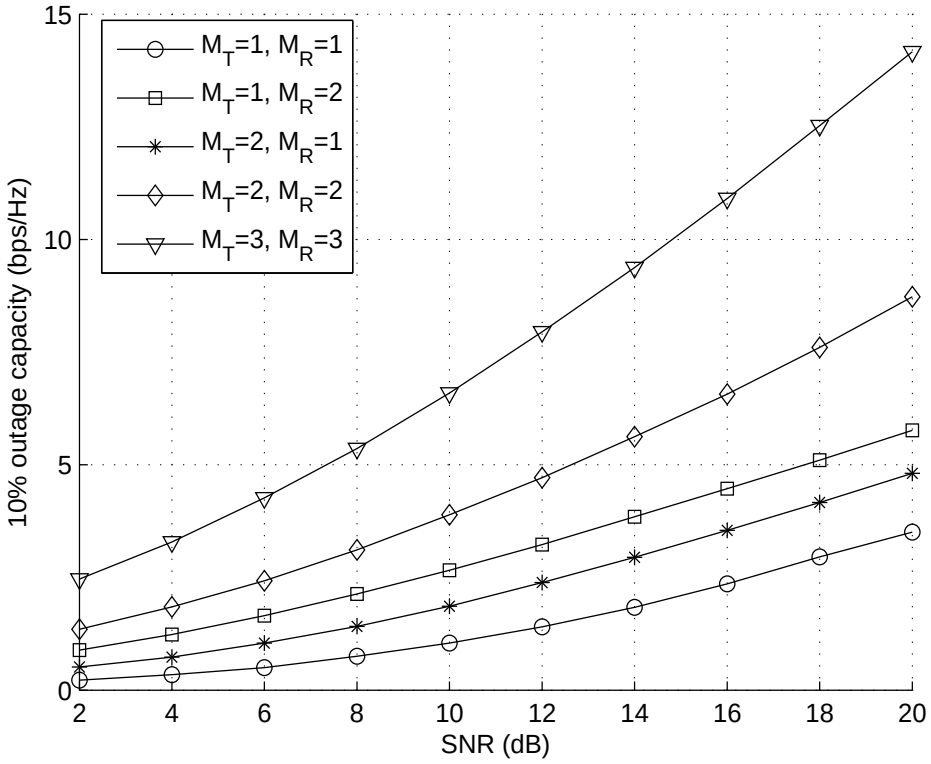

Figure 3.8: 10% outage capacity of different antenna configurations.

3.7 Spatial Multiplexing

Multiple antennas at the transmitter and receiver have emerged as one of the key technologies to increase channel spectral efficiency at no additional bandwidth and power consumption [39, 40]. Fig. 3.9 illustrates the basic principle of spatial multiplexing with three transmit and receive antennas. The concept can be extended to more general MIMO channels.

The high rate bit stream to be transmitted is demultiplexed into M_t independent bit sequences which are then transmitted simultaneously using multiple antennas. The receiver having the knowledge of the channel, can differentiate between the co-channel signals and extract signals, after which demodulation yields the original sub-stream that can now be combined to yield the original bit stream. Thus spatial multiplexing increases the data rate proportionally with the number of transmit-receive antenna pairs. VBLAST is a well known detection technique for spatial multiplexing that detects symbols transmitted at different transmit antennas successively in a certain order.

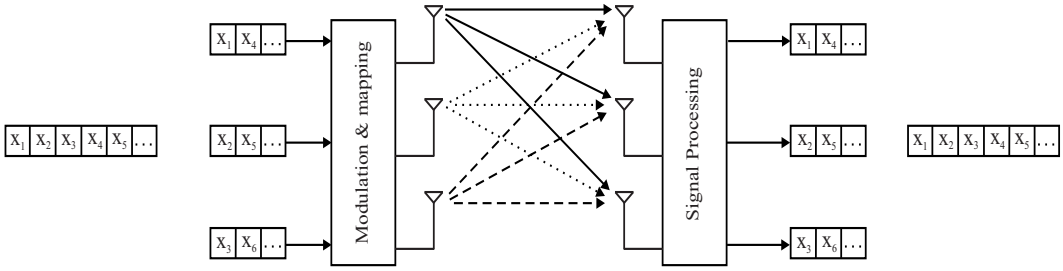

Figure 3.9: Spatial multiplexing system.

3.8 Space-Time Coding (Spatial Diversity)

Coding techniques designed for multiple antennas transmission are called space-time coding (STC) [43]. In STC the signal design extends over both space (via multiple antennas) and time (via multiple symbol times). Due to the joint design,

STC can achieve transmit diversity as well as a coding gain without any additional bandwidth requirement [44]. A MIMO channel with M_t and M_r transmit and receive antennas respectively can achieve the maximum diversity order of $M_t M_r$. Fig. 3.10 shows the block diagram of STC system with M_t transmit antennas and M_r receive antennas.

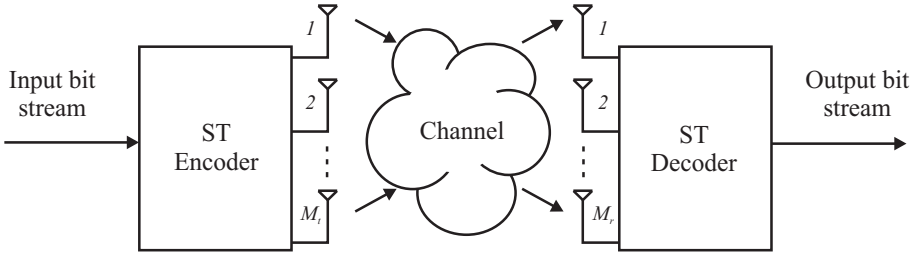

Figure 3.10: Block diagram of STC

STC can be divided into following two types [20].

- Space-Time Trellis Codes (STTC)
- Space-Time Block Codes (STBC)

3.8.1 Space-Time Trellis Codes

In this sub-section, we will discuss the simplest form of STTC - delay diversity [43], as it is related to our work. In this scheme, versions of the same symbol are transmitted through multiple antennas in different times as illustrated in Fig. 3.11. At the receiver, the delays of the second up to the M_t-th transmit antennas introduce a multipath-like distortion for the signal transmitted from the first antenna and creates frequency selective fading at a single receiver. The multipath distortion can be resolved at the receiver by using a MMSE or a MLSE equalizer to obtain diversity gain.

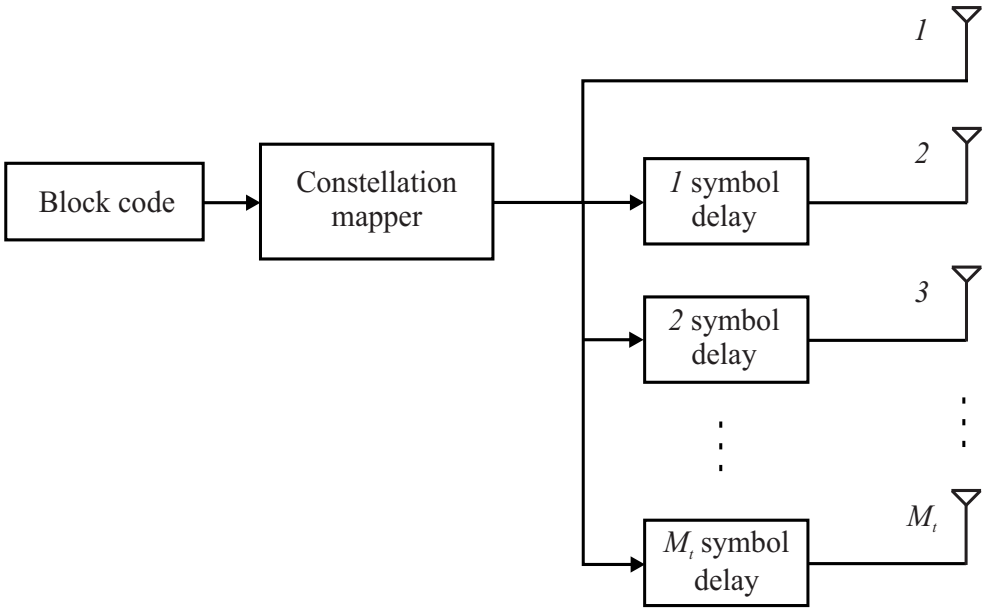

Figure 3.11: Delay Diversity Scheme for M_t transmit antennas.

3.8.2 Space-Time Block Codes

STBC is a simple transmit diversity technique in MIMO systems that was introduced by Alamouti [30]. He proposed a simple scheme for 2 transmit antennas system that achieves full diversity gain. Fig. 3.12 shows the block diagram of

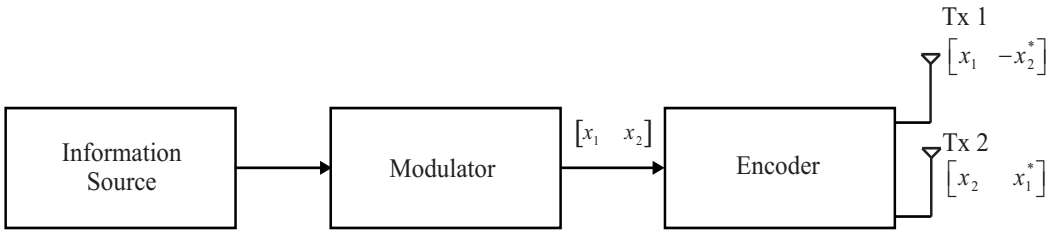

Figure 3.12: Block diagram of the Alamouti space-time encoder.

the Alamouti space-time encoder. Let x_1 and x_2 denote the complex symbols which are to be transmitted over the wireless channel. At the first symbol period t, antenna one will transmit x_1, and simultaneously, antenna two will transmit x_2. In the next symbol period $t+T$, antenna one will transmit $-x_2^*$ and antenna two will transmit x_1^*, where T is the symbol period. This sequence is presented in Table 3.1.

Table 3.1: Space-time coding rules

Time	Antenna 1	Antenna 2
t	x_1	x_2
$t+T$	$-x_2^*$	x_1^*

The two by two space time block code can be written in matrix from as

$$\mathbf{X} = \begin{bmatrix} x_1 & x_2 \\ -x_2^* & x_1^* \end{bmatrix}. \tag{3.25}$$

The key feature of the Alamouti scheme is that the transmit sequence from the two transmit antennas are orthogonal,

$$\begin{aligned} \mathbf{X}\mathbf{X}^H &= \mathbf{X}^H\mathbf{X} \\ &= \begin{bmatrix} x_1^* & -x_2 \\ x_2^* & x_1 \end{bmatrix} \begin{bmatrix} x_1 & x_2 \\ -x_2^* & x_1^* \end{bmatrix} \\ &= \begin{bmatrix} |x_1|^2 + |x_2|^2 & 0 \\ 0 & |x_1|^2 + |x_2|^2 \end{bmatrix} \qquad (3.26) \\ &= \left(|x_1|^2 + |x_2|^2\right) \mathbf{I}_2 \qquad (3.27) \end{aligned}$$

where $\mathbf{I}_2$ is a 2×2 identity matrix.

The block diagram of the receiver for the Alamouti scheme is shown in Fig. 3.13. The channel at time t may be modeled as complex multiplicative distortion $h_1(t)$ for transmit antenna one and $h_2(t)$ for the transmit antenna two. Assuming the channel is flat fading and is constant over two consecutive symbols, we can write

$$h_1(t) = h_1(t+T) = h_1 \tag{3.28}$$

and

$$h_2(t) = h_2(t+T) = h_2. \tag{3.29}$$

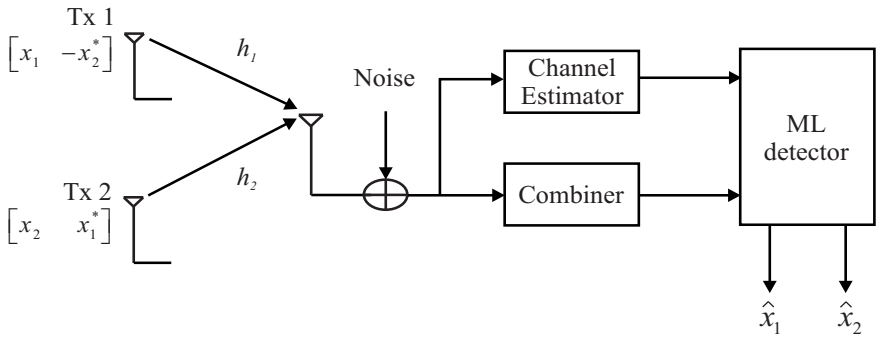

Figure 3.13: Block diagram of the Alamouti space-time receiver.

The received signals can then be given by

$$y(t) = y_1 = h_1 x_1 + h_2 x_2 + n_1 \tag{3.30}$$

$$y(t+T) = y_2 = -h_1 x_2^* + h_2 x_1^* + n_2 \tag{3.31}$$

where y_1 and y_2 are the symbols received at time t and $t+T$, and n_1 and n_2 are complex channel noise. The above two equations can be rewritten in matrix form as

$$\begin{bmatrix} y_1 \\ y_2^* \end{bmatrix} = \underbrace{\begin{bmatrix} h_1 & h_2 \\ h_2^* & -h_1^* \end{bmatrix}}_{\mathbf{H}} \begin{bmatrix} x_1 \\ x_2 \end{bmatrix} + \begin{bmatrix} n_1 \\ n_2^* \end{bmatrix}. \tag{3.32}$$

Now, the combiner will obtain two combined signals by multiplying the received signal at the receiver with the Hermitian transpose of the channel matrix $\mathbf{H}$. We

obtain

$$\begin{bmatrix} r_1 \\ r_2 \end{bmatrix} = \begin{bmatrix} h_1^* & h_2 \\ h_2^* & -h_1 \end{bmatrix} \begin{bmatrix} y_1 \\ y_2^* \end{bmatrix} \tag{3.33}$$

$$= \begin{bmatrix} h_1^* & h_2 \\ h_2^* & -h_1 \end{bmatrix} \begin{bmatrix} h_1 & h_2 \\ h_2^* & -h_1^* \end{bmatrix} \begin{bmatrix} x_1 \\ x_2 \end{bmatrix} + \begin{bmatrix} h_1^* & h_2 \\ h_2^* & -h_1 \end{bmatrix} \begin{bmatrix} n_1 \\ n_2^* \end{bmatrix} \tag{3.34}$$

$$= \left(|h_1|^2 + |h_2|^2\right) \begin{bmatrix} x_1 \\ x_2 \end{bmatrix} + \begin{bmatrix} v_1 \\ v_2 \end{bmatrix} \tag{3.35}$$

where v_1 and v_2 defines the 2×1 vector of additive complex noise contributions in the combiner outputs with variance $N_o\left(|h_1|^2 + |h_2|^2\right)$.

Eq. (3.35) can be generalized into

$$r_k = \left(|h_1|^2 + |h_2|^2\right) x_k + v_k, \qquad k = 1, 2. \tag{3.36}$$

These combined signals are then sent to the maximum likelihood (ML) decoder. Assuming that all the signals in the modulation constellation are equiprobable, a ML decoder chooses a pair of signals $(\hat{x}_1, \hat{x}_2)$ from the signal modulation constellation to minimize the distance metric over all possible values of $\hat{x}_1$ and $\hat{x}_2$. Mathematically, ML decoder can be represented as

$$\hat{x_1} = \arg \min_{\hat{x}_1 \in \mathbf{S}} \left\| r_1(t) - \left(|h_1|^2 + |h_2|^2\right) \hat{x}_1 \right\|^2 \tag{3.37}$$

and

$$\hat{x_2} = \arg \min_{\hat{x}_2 \in \mathbf{S}} \left\| r_2(t) - \left(|h_1|^2 + |h_2|^2\right) \hat{x}_2 \right\|^2 \tag{3.38}$$

where $\mathbf{S}$ is a set of all possible modulated symbols.

Monte-Carlo simulation is carried out to illustrate the BER performance of Alamouti's scheme as a function of SNR in Fig. 3.14. Circular-symmetric complex

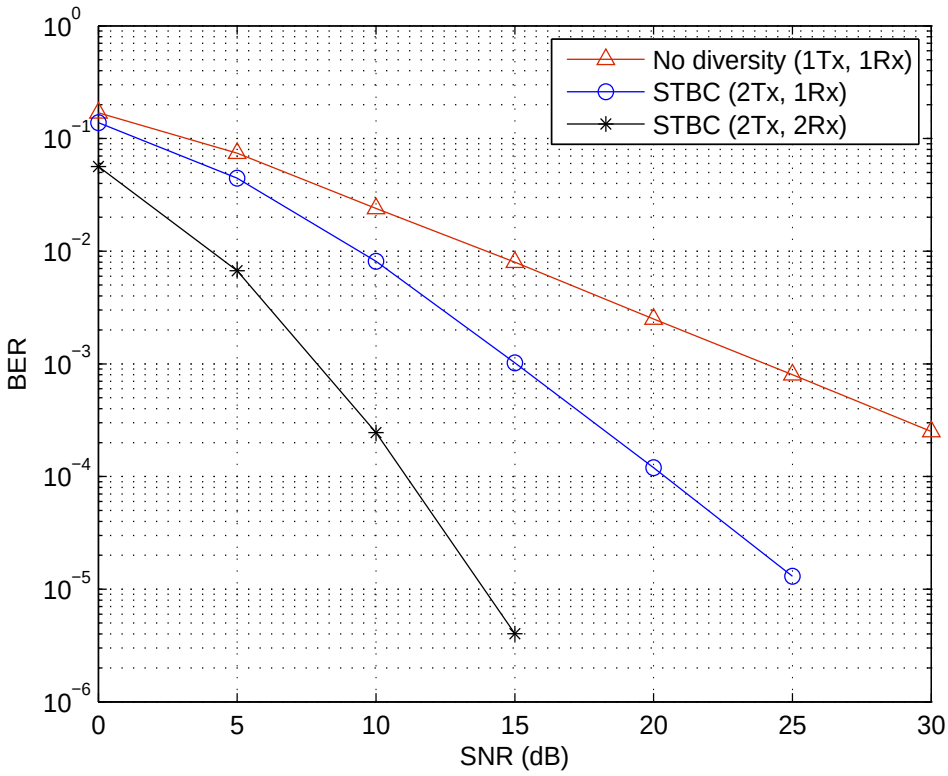

Figure 3.14: BER performance of Alamouti scheme as a function of SNR.

Gaussian noise with zero mean and N_o spectral density is considered. The total transmit power of system is kept constant for a fair comparison between SISO and Alamouti's STBC scheme. The channel is assumed to be quasi-static Rayleigh flat faded. Furthermore, we assume that the receiver has perfect knowledge of the channel.

At BER of 10^{-3}, a gain of 8dB to SISO is observed by employing Alamouti scheme with single receive antenna. This is due to the diversity achieved by STBC. The addition of another antenna at the receiver further improves the performance.

Chapter 4

Cooperative MIMO Communication

4.1 Introduction

The objective of this chapter is to summarize the important references that relates to the problem studied in this work. We will define cooperative communication and also review the key results in section 4.2. Several cooperative signalling techniques that can be implemented at the relay channels are defined in section 4.3. Section 4.4 presents the performance analysis of one of the cooperating protocol that relates to the work presented in the following chapters.

4.2 Cooperative Communication and its History

As discussed in this last chapter, diversity is used in wireless communication to mitigate the effects of fading. Spatial diversity is a common method of creating multiple copies of signals by employing more than one antenna at the transmitter and/or the receiver. Cooperative diversity is an extension of spatial diversity that exploits the broadcast nature of wireless channel [45–51]. Fig. 4.1 illustrates a

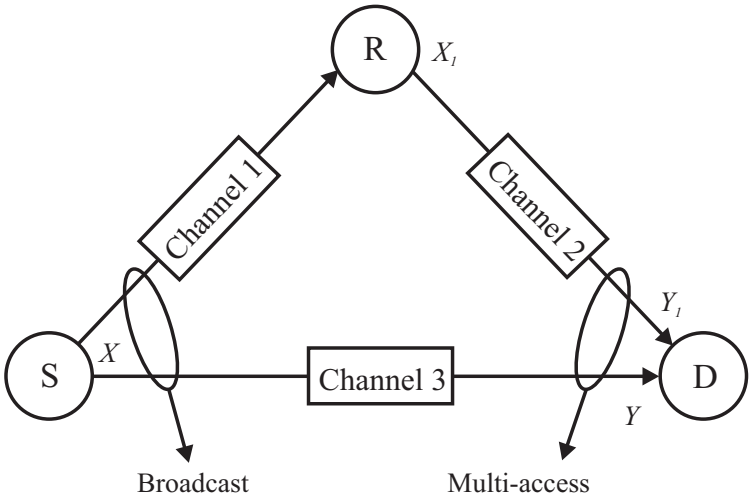

Figure 4.1: The single relay cooperative communication network.

single relay cooperative network. The source (S) node broadcasts data to the relay (R) and destination (D) nodes. The relay node subsequently forwards the received signal to the destination. Both the direct and relayed signals are combined at the destination using diversity combiners [32].

A relay channel model was introduced and studied by van der Meulen in [52] where he considered communication using three terminals. Cover and El Gamal [53] discussed the discrete memory-less and AWGN relay channel and established the capacity of physically degraded relay channels. Laneman *et al.* [7] developed several half duplex cooperative protocols including fixed and adaptive relaying protocols. In fixed relay protocols such as amplify-and-forward (ANF) and decode-and-forward (DNF), the relay always assists by forwarding the information from source to destination node. In the case of ANF, the relay simply amplifies the noisy version of the signal transmitted by the source. In DNF, the relay decodes, re-encodes and re-transmits the signals to the destination node.

Although, fixed relaying is easy to implement, it has a disadvantage of low bandwidth efficiency e.g. there is 50% loss in the spectral efficiency with transmissions in two stages [54]. In addition, fixed DNF relaying suffers from the fact

that the performance is limited by a weakest S-R and R-D links, which could reduce the diversity gains to one. To overcome this issue, adaptive relaying including selection and incremental relaying is introduced in [7]. With selection relaying, the relay only forwards the information signal if the measured channel amplitude of source-relay link lies above a particular threshold. In incremental relaying, limited feedback from the destination is employed to indicate the success or failure of direct transmission. Sendonaris *et al.* [9, 55] examined the detect-and-forward cooperative protocol and gave the theoretical insight of cooperative communication network. They also discussed practical implementation of cooperation for code-division multiple-access (CDMA) systems in which pairs of nodes cooperate with each other and alleviate multiple access interference by using orthogonal spreading codes [9, 55]. Hunter and Nosratinia introduced the coded cooperation, where cooperation is achieved through channel coding [10]. In the following sections, we will discuss some of these cooperative strategies in detail.

4.3 Cooperative Signalling Methods

In this section a review of several major cooperative signalling methods is given. Frame or symbol level synchronization between the terminals is assumed for cooperative diversity to be effective.

4.3.1 Fixed Cooperating Strategies

In fixed cooperative schemes the relay always assists by forwarding the data from the source to the destination node and therefore, the channel resources are divided between the source and the relay. The processing at the relay differs according to the employed protocols. The most common fixed relaying techniques are ANF

and DNF protocols.

Amplify and Forward Cooperation

ANF is the simplest cooperative signalling scheme proposed by Laneman *et al.* [7,8]. A three node cooperative network containing the source (S), relay (R) and destination (D) nodes is shown in the Fig. 4.2. The information will be transmitted from the source node to the destination node directly and also through the relay node. The conventional ANF channel model is characterized by transmitting and receiving in orthogonal frequency bands or time slots [7]. Here we consider the ANF scheme with the relay node transmitting at the same frequency band as the source node, but in subsequent time-slot.

In the first time slot, the source node broadcasts the signal to the destination and the relay node. The received signal at the destination node directly from the source node is

$$y_{sd}(t) \quad = \quad x(t)\ \sqrt{E^s}\ h_{sd} + n_d(t) \tag{4.1}$$

where $x(t)$ is the transmitted signal from the source node at time t with unit energy, E^s is the transmitted signal energy from the source node, h_{sd} is the normalized channel gain from the source to the destination node and is modeled as Rayleigh flat fading channel, and $n_d(t)$ captures the effect of AWGN at the destination.

Similarly, at the same time slot the relay node receives the same signal from the source node, given by

$$y_{sr}(t) \quad = \quad x(t)\ \sqrt{E^s}\ h_{sr} + n_r(t) \tag{4.2}$$

where h_{sr} is the normalized channel gain from the source to the relay node that

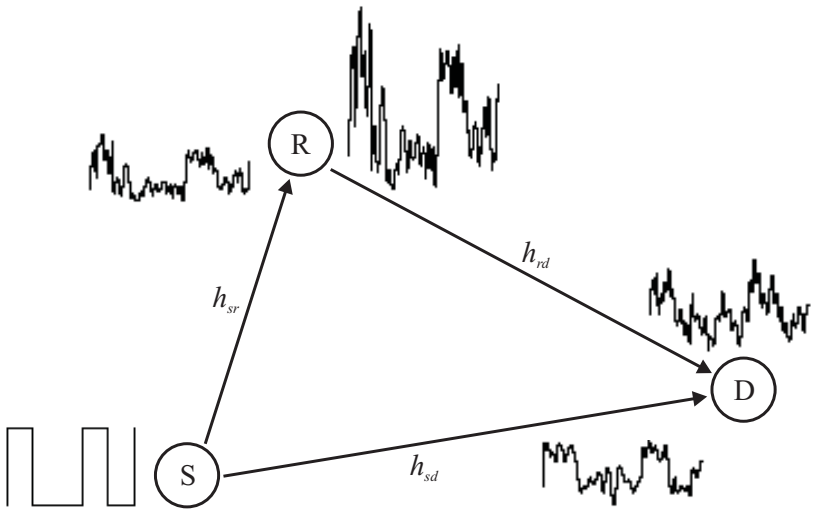

Figure 4.2: Amplify and forward cooperative scheme.

is modeled as Rayleigh flat fading channel, and $n_r(t)$ is the AWGN at the relay node.

In the second time slot, the relay node amplifies the received signal from the source node and forwards it to the destination node

$$y_{rd}(t+T) \quad = \quad k'_r \; y_{sr}(t) \; h_{rd} + n_d(t+T) \tag{4.3}$$

where T is the time slot or frame duration, and k'_r is the amplification factor at the relay, h_{rd} is the normalized channel gain from relay to the destination that is also modeled as Rayleigh flat fading channel, and $n_d(t+T)$ is the AWGN at the destination.

The amplification factor k'_r should be selected such that the SNR is maximized. There are two different strategies for selecting this amplification factor: *regenerative amplification* and *non-regenerative amplification*. In *regenerative amplification*, the signal transmitted by the relay has the same power as the signal transmitted by the source. On the other hand in *non-regenerative amplification*,

the relay uses an amplification factor $k_r' = 1$ in order to minimize the noise amplification [56]. The amplification factor k_r' for regenerative transmission is given by [7]

$$k_r' = \sqrt{\frac{\mathbb{E}\left[|x|^2\right]}{\mathbb{E}\left[|y_{sr}|^2\right]}} = \frac{\sqrt{E^s}}{\sqrt{E^s\,|h_{sr}|^2 + N_o}}. \tag{4.4}$$

Substituting (4.2) and (4.4) in (4.3) we obtain

$$\begin{aligned} y_{rd}(t+T) &= k_r'\; y_{sr}(t)\; h_{rd} + n_d(t+T) \\ &= \sqrt{\frac{E^s}{E^s\,|h_{sr}|^2 + N_o}}\left(\sqrt{E^s}x(t)h_{sr} + n_r(t)\right) h_{rd} + n_d(t+T) \\ &= \sqrt{\frac{E^s}{E^s\,|h_{sr}|^2 + N_o}}\sqrt{E^s}x(t)h_{sr}h_{rd} + n_d'(t) \end{aligned} \tag{4.5}$$

where

$$n_d'(t) = n_d(t+T) + \sqrt{\frac{E^s}{E^s\,|h_{sr}|^2 + N_o}}h_{rd}n_r(t). \tag{4.6}$$

Assuming the noise at relay and destination nodes are independent, the equivalent noise $n_d'(t)$ is zero mean, complex Gaussian random variable with variance

$$N_o' = N_o\left(1 + \frac{E^s\,|h_{rd}|^2}{E^s\,|h_{sr}|^2 + N_o}\right). \tag{4.7}$$

MRC is employed at the destination node to combine the two copies of signal from the direct and relay link. The output of the MRC is given by

$$y = a_1\; y_{sd}(t) + a_2\; y_{rd}(t+T) \tag{4.8}$$

where a_1 and a_2 should be selected such that the combined SNR is maximized.

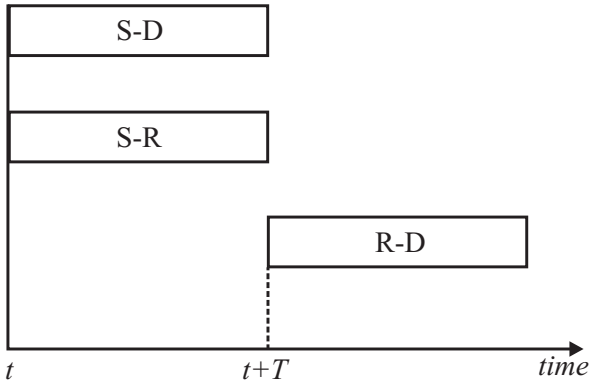

Figure 4.3: Timing diagram of ANF cooperative scheme.

Therefore a_1 and a_2 are taken to be

$$a_1 = \frac{\sqrt{E^s}}{N_o} h_{sd}^* \tag{4.9}$$

and

$$a_2 = \frac{\sqrt{\frac{1}{E^s|h_{sr}|^2+N_o}} E^s h_{sr}^* h_{rd}^*}{N_o\left(1+\frac{E^s|h_{rd}|^2}{E^s|h_{sr}|^2+N_o}\right)}. \tag{4.10}$$

The exact channel state information (CSI) is assumed to be available at the receiver only, and not at the transmitter.

Fig. 4.3 illustrates the timing diagram of ANF cooperative system, where, t is the time when the source node starts transmitting the data to the destination and relay nodes. The relay node will start transmitting after a duration of T. The diversity gain achieved through cooperation can compensate for the additional noise in the relay [7]. Hence, the cooperative diversity schemes achieve better performance than non-cooperative schemes.

Decode and Forward Cooperation

In this type of fixed cooperative protocol, the relay node decodes the signal, re-encodes it, and then retransmits it to the destination node as illustrated in Fig 4.4. The first phase of this scheme is similar to the ANF where the source node broadcasts the information signal to the destination and relay nodes as given by (4.1) and (4.2). In the second phase, assuming the decoded signal at the relay node is denoted by $\hat{x}\,(t)$, the transmitted signal from the relay to the destination is given by

$$y_{rd}(t+T) \;=\; \hat{x}(t)\,\sqrt{E^s}\,h_{rd} + n_d(t+T). \tag{4.11}$$

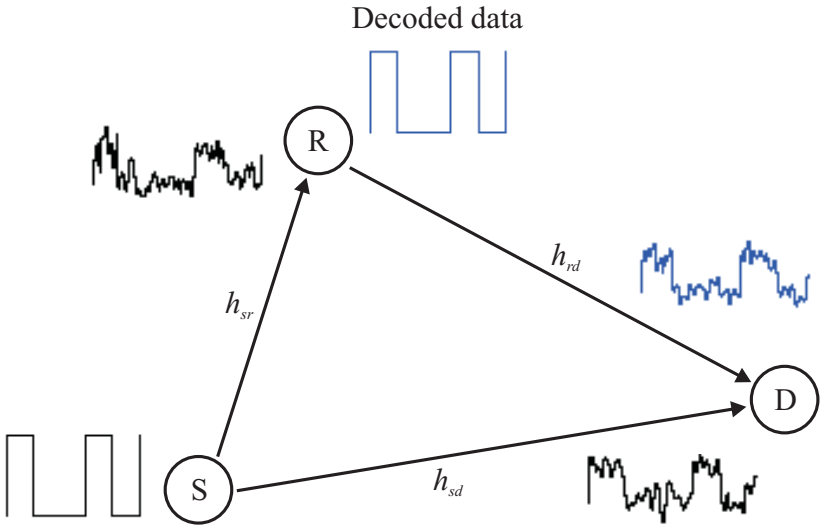

Figure 4.4: Decode and forward cooperative scheme.

4.3.2 Coded Cooperation

In previously discussed cooperative schemes, a relay may either simply forward the analog signal received from the source or retransmit estimates of the received symbols, obtained via hard detection. Coded cooperation is different from these

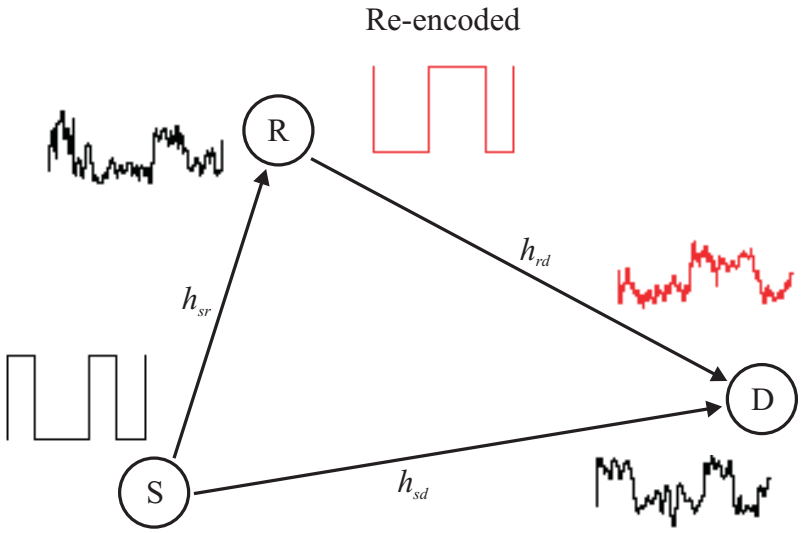

Figure 4.5: Coded cooperative scheme.

previous schemes as it integrates user cooperation with channel coding [10]. Instead of repeating some form of the received signal, the relay decodes the source's transmission and transmits additional parity symbols according to overall coding scheme. The relay employs error checking such as cyclic redundancy check (CRC) code to avoid transmitting erroneous data. Fig. 4.5 illustrates the coded cooperative network.

4.3.3 Adaptive Cooperative Strategies

Fixed relaying suffers from the low bandwidth efficiency as half of the channel resources are allocated to the relay for the transmission. Moreover, fixed DNF relaying suffers from the fact that the performance is limited by the weakest S-R and R-D link which reduces the diversity gain to one [54]. To overcome this problem, adaptive relaying is developed. Here we revisit two strategies: selective relaying and incremental relaying.

Selective relaying

DNF is limited by the direct transmission between the source and relay. As the channel fading coefficient between the source and relay can be measured to high accuracy by the cooperating node, they can adjust their transmission configuration according to the channel fading value of the S-R channel.

In a selective relaying scheme, if the SNR of a signal received at the relay is larger than a certain threshold, the relay decodes the received signal and forwards it to the destination. On the other hand, if the channel between the source and the relay suffers severe fading, the SNR will fall below the threshold and no cooperation will take place.

Incremental relaying

In this type of adaptive relaying, a limited feedback from the destination terminal is employed to determine the success or failure of the received data at destination from the source node. If source transmission in the first phase is positively acknowledge from the destination, there is no second phase and the source transmits a new information data in the second time slot. On the other hand, if the source transmission was not successful, the destination feedback requests the relay to retransmit what it has received from the source. Therefore this protocol makes more efficient use of the degree of freedom of channel as they repeat only rarely.

The incremental relaying protocols can be viewed as extensions of incremental redundancy or hybrid automatic-request-repeat (ARQ) to the relay context [7]. In ARQ, the source re-transmits when negative acknowledgement is received via feedback from the destination terminal, whereas in incremental relaying the relay retransmits in an attempt to exploit the spatial diversity.

This protocol has the best spectral efficiency among fixed ANF, fixed DNF and selective relaying because the relay does not need to transmit all the time.

Hence, the second transmission becomes opportunistic depending on the CSI of the direct link.

4.4 Performance Analysis of ANF Scheme

As the proposed energy efficient cooperative scheme in the following chapters is based on ANF, in this section we present the performance analysis of ANF in terms of BER, capacity and outage analysis. For all simulations, the wireless channels are assumed to be quasi-static Rayleigh flat faded. Zero mean circular-symmetric complex Gaussian noise is considered.

4.4.1 BER Evaluation of ANF

The BER performance results for non-cooperative and ANF schemes are shown in Fig. 4.6. The end-to-end spectral efficiency is kept constant to 1 bps/Hz by using BPSK for non-cooperative scheme and QPSK for ANF cooperative network. The transmit power of the network elements is normalized such that it is equal for all schemes. It can be observed that the non-regenerative transmission outperforms the regenerative transmission. This is because, in case of no amplification ($k'_r = 1$), the relay significantly contributes to the final decision when there is good channel conditions between the source and relay. While for poor channels, the noisy signal will almost be discarded at the relay and hence, cannot lead to a wrong decision at the destination. In the case of regenerative amplification (as in (4.4)), a full channel inversion at the relay will only amplify the relay receiver noise which eventually degrades the system performance. However, comparing with the non-cooperative scheme, both regenerative and non-regenerative ANF schemes have better performance. The improvement in non-regenerative case over regenerative case comes at the cost of high power consumption.

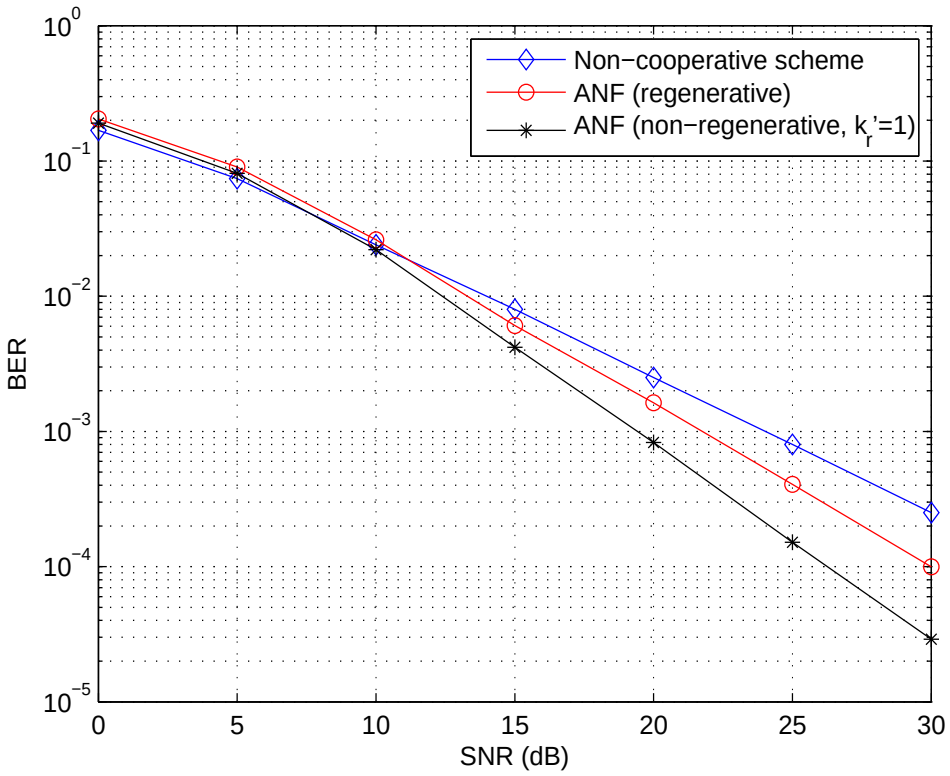

Figure 4.6: Bit error rate performance comparison of non-cooperative and ANF cooperative schemes.

4.4.2 Capacity Analysis of ANF

The capacity of conventional ANF is the maximum mutual information between the source and the destination node as shown in (3.21) and is given by

$$C_{ANF} = \frac{1}{2}\log\left(1 + \Gamma\left|h_{sd}\right|^2 + f(\Gamma\left|h_{sr}\right|^2, \Gamma\left|h_{rd}\right|^2)\right) \tag{4.12}$$

where

$$f(x,y) \triangleq \frac{xy}{1+x+y} \tag{4.13}$$

and

$$\Gamma = \frac{E^s}{N_o}. \tag{4.14}$$

The 1/2 pre-log factor in (4.12) shows that the conventional ANF takes two orthogonal channels for one complete transmission; thus decreases the spectral efficiency of the system.

Fig. 4.7 presents the capacity of the ANF scheme as compared to the non-cooperative scheme. The decrease in the ANF capacity can be observed. It is due to the half duplex nature of the relay node.

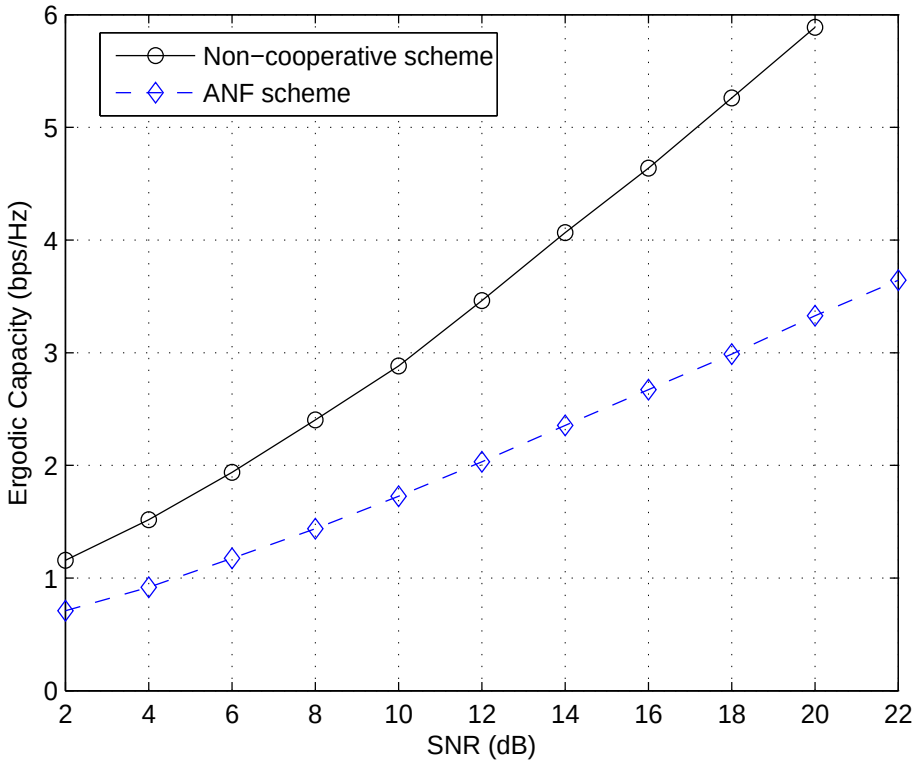

Figure 4.7: Capacity comparison of non-cooperative and ANF schemes.

4.4.3 Outage Behavior of ANF

Outage analysis of the ANF and non-cooperative schemes are presented in Fig. 4.8. The outage event occurs when the mutual information of the channel I falls below a target transmission rate R, i.e., $I < R$. The probability of an outage event, $Pr[I < R]$ is referred to as the outage probability of the channel. As we are using QPSK as the modulation scheme in the proposed scheme to achieve 2bps/Hz data rate, the target rate threshold R is selected to be 2bps. After 17dB, the outage observed by the ANF cooperative scheme becomes less than non-cooperative scheme. The change in the asymptotic slope shows that diversity gain is achieved.

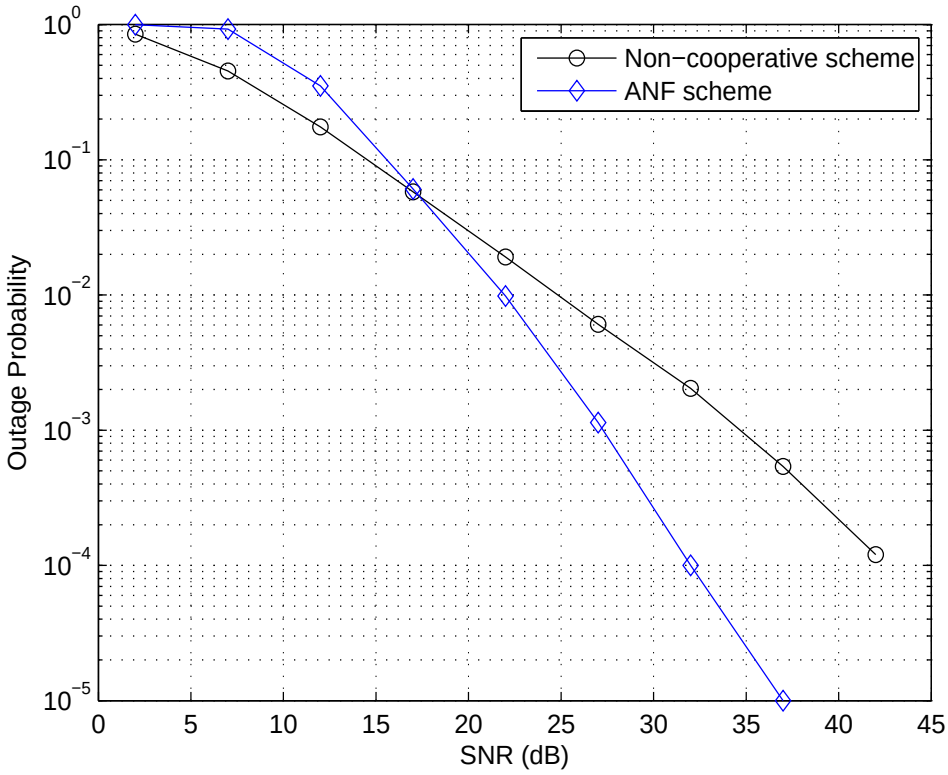

Figure 4.8: The outage probability comparison of ANF scheme.

Chapter 5

Energy Efficient Asynchronous Polarized Cooperative MIMO Protocol

5.1 Introduction

In the last chapter we presented some of the major cooperative communication methods that require frame or symbol level synchronization between the cooperating nodes. If the source and relay nodes lose synchronization, ISI will occur and significantly affects the performance. In [15] and [16], asynchronous cooperative protocols are proposed to tackle this problem. They considered asynchronous cooperation transmission as an equalization problem. The difference between these two schemes is in the relay to destination (R-D) link transmission. In [15] delay diversity transmission in the R-D link is used and spatial diversity is achieved using decision feedback equalizer. On the other hand, [16] employs asynchronous STBC in the R-D link to achieved distributed cooperative diversity. However it

could suffer performance degradation due to diversity loss by random row selection. In addition to that the schemes in the previous chapter including [15, 16] are practically assumed to be half duplex which results in low spectral efficiency. Constellation size has to be increased to maintain the spectral efficiency which then reduces the performance gain over non-cooperative SISO scheme.

In this chapter, we present a novel asynchronous polarized cooperative MIMO communication scheme that also does not require frame or symbol level synchronization at the relay node. The relay node in the proposed scheme employs dual-polarized antennas that enables it to transmit and receive at the same timeslot and frequency band which further increases the transmission data rate and reliability of the system. For practical consideration, path loss is considered in the investigation, which is usually ignored in existing literature.

This chapter begins with the basic system model and assumptions for conventional cooperative systems with path loss in section 5.2. Section 5.3 presents the new asynchronous polarized cooperative scheme. Energy analysis of the proposed scheme is presented in section 5.4, and section 5.5 discusses the capacity analysis of the proposed scheme. Simulation results demonstrating the marked improvement in performance are presented in section 5.6. Section 5.7 summarizes the chapter.

5.2 Conventional Cooperative System Model

In this section we present the conventional ANF scheme with path loss. In a three node cooperative network containing the source, relay, and destination nodes, information will be transmitted from the source node to the destination node directly and also through the relay node. The conventional ANF channel model is characterized by transmitting and receiving in orthogonal frequency bands or timeslots [7]. As in Chapter 4, we assume the relay node transmitting at the same

frequency band as the source node, but in subsequent time-slot. The channel $\tilde{h}_{ij}$ between the i-th transmit and j-th receive antenna is given by

$$\tilde{h}_{ij} = \frac{h_{ij}}{\sqrt{PL_{ij}}} \tag{5.1}$$

where h_{ij} is the normalized channel gain, which is an i.i.d complex Gaussian random variable with zero mean and unit variance. This describes the random fading effect of multipath channels, and is assumed to be quasi-static flat fading. The path loss factor PL_{ij} models the signal attenuation over distance, and is given by [20]

$$PL_{ij} = \frac{G_t G_r \lambda^2}{(4\pi)^2} (d_{ij})^{\alpha} = PL_0 (d_{ij})^{\alpha} \tag{5.2}$$

where PL_0 is the reference path loss factor, d_{ij} is the distance between i-th transmitter and j-th receiver, α is the path loss exponent depending on the propagation environment which is assumed to be the same over all links, λ is the wavelength, and G_t and G_r are the transmitter and receiver antenna gains respectively.

In a typical three node system, single transmission is normally divided into two timeslots [57, 58]. In the first timeslot, the source node broadcasts the signal to the destination and the relay node. The received signal at the destination node directly from the source node is

$$y_{sd}(t) \;=\; x(t) \sqrt{\frac{E^s}{PL_{sd}}}\, h_{sd} + n_d(t) \tag{5.3}$$

where $x(t)$ is the transmitted signal from the source at time t with unit energy, E^s is the transmitted signal energy from the source, h_{sd} is the normalized channel gain from the source to the destination with a corresponding path loss of PL_{sd}, and $n_d(t)$ captures the effect of AWGN at the destination. Similarly, at the same

timeslot the relay node receives the same signal from the source, given by

$$y_{sr}(t) \;=\; x(t)\,\sqrt{\frac{E^s}{PL_{sr}}}\,h_{sr} + n_r(t) \tag{5.4}$$

where h_{sr} is the normalized channel gain from the source to the relay with a corresponding path loss of PL_{sr}, and $n_r(t)$ is the AWGN at the relay.

In the second timeslot the signal received at the relay node is amplified by a factor k'_r and forwarded to the destination given by

$$y_{rd}(t+T) \;=\; \frac{k'_r}{\sqrt{PL_{rd}}}\,y_{sr}(t)\,h_{rd} + n_d(t+T) \tag{5.5}$$

where $T = LT_s$ is the timeslot or frame duration with L being the total number of symbols per frame and T_s the symbol period, h_{rd} is the normalized channel gain from the relay to destination node having a corresponding path loss of PL_{rd}, and $n_d(t+T)$ is the AWGN at the destination node. The transmitter estimates path loss through the reverse link and is assumed to be perfectly estimated. On the other hand, instantaneous channel fading gain is not assumed to be known at the transmitter, as it requires feedback information. Therefore, setting identical received signal energy from the direct and relayed link, the amplification factor k'_r is given by

$$k'_r = \sqrt{\frac{E^s\;\mathbb{E}\left[\left|\tilde{h}_{sd}\right|^2\right]}{E^r\;\mathbb{E}\left[\left|\tilde{h}_{rd}\right|^2\right]}} = \sqrt{\frac{E^s/PL_{sd}}{\left(E^s/PL_{sr}+N_o\right)/PL_{rd}}} \tag{5.6}$$

where E^r is the received signal energy at the relay node. The signal in (5.3) and (5.5) are combined at the destination node using diversity combiners, e.g., MRC. All AWGN noises are modeled as zero mean mutually independent circular symmetric complex Gaussian random sequences with PSD N_o. Exact CSI is

assumed to be available at the receiver only, and not at the transmitter.

The conventional ANF takes two orthogonal channels for one complete transmission, thus decreases the spectral efficiency of the system. Also frame level synchronization is required in conventional ANF, which is not always achievable in multi-node wireless communication.

5.3 Proposed Asynchronous Polarized Cooperative MIMO System

In the previous section, the drawbacks on the conventional ANF have been discussed. To alleviate these problems, a novel asynchronous polarized cooperative protocol and a frequency domain receiver are proposed in this section.

5.3.1 Proposed System Model

Fig. 5.1 illustrates the proposed polarized cooperative system. The relay node and destination node both have dual polarized antennas installed, with separate RF chains for vertical and horizontal polarization. On the other hand, the source node has only a vertical polarized transmit antenna. The solid lines represent transmission and reception on the same polarization, also known as co-polarization. On the other hand, the dotted lines represent transmission in one polarization but reception in the other polarization, also known as cross-polarization.

For a relay to operate in full duplex mode the transmission and reception channels must be orthogonal either in time-domain or in frequency domain, otherwise the transmitted signal will interfere with the received signal. In theory, it is possible for relay to cancel out interferences as it has the knowledge of transmitted signal. In practice, however, the transmitted signal is 100-150dB stronger

than the received signal and any error in the interference cancellation can potentially be disastrous [59]. Due to this reason, the installation of co-polarized antennas at the relay node in place of dual-polarized antennas is not feasible for full duplex relay. However, with dual-polarized antenna the transmitted signal on one polarization is orthogonal to the received signal at another polarization, thereby, enabling the relay to communicate in full duplex mode, not the overall system.

The source node will broadcast using vertical polarization. The vertically polarized received signal at the relay node is the same as (5.4).

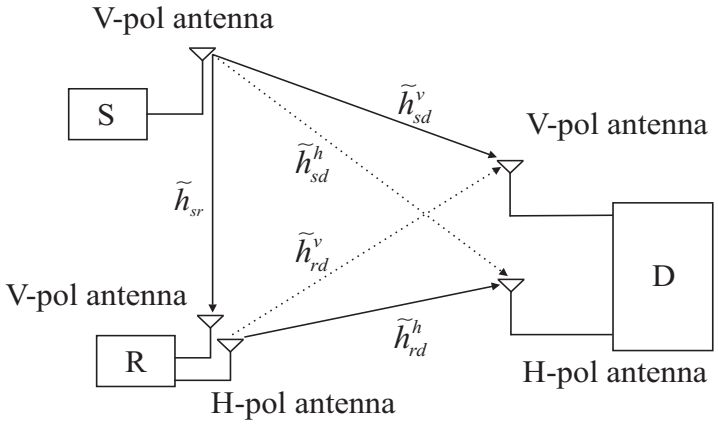

Figure 5.1: Schematic of one relay polarized cooperative MIMO network with cross-polarized channels.

The received signal at the relay node is amplified by a factor k_r, and transmitted immediately to the destination node through horizontal polarization. Radio propagation and signal processing at the relay node will cause some additional time delay τ, which could be a few symbols duration and is much shorter than the frame duration T. It must be noted that the proposed system does not require symbol level synchronization, between the source and relay, and thus τ can be any positive real number. The vertically and horizontally polarized signal received at

the destination, denoted as y_{d_v} and y_{d_h} respectively, are given by

$$y_{d_v}(t) = \sqrt{E^s}\; x(t)\; \tilde{h}^v_{sd} + k_r\; y_{sr}\,(t-\tau)\;\; \tilde{h}^v_{rd} + n_{d_v}(t) \tag{5.7}$$

and

$$y_{d_h}(t) = \sqrt{E^s}\; x(t)\; \tilde{h}^h_{sd} + k_r\; y_{sr}\,(t-\tau)\;\; \tilde{h}^h_{rd} + n_{d_h}(t). \tag{5.8}$$

The received signals of the above equations can therefore be written in matrix form as

$$\underbrace{\begin{bmatrix} y_{d_v}(t) \\ \\ y_{d_h}(t) \end{bmatrix}}_{\mathbf{y}_d} = \underbrace{\begin{bmatrix} \tilde{h}^v_{sd} & \tilde{h}^v_{rd} \\ \\ \tilde{h}^h_{sd} & \tilde{h}^h_{rd} \end{bmatrix}}_{\mathbf{H}} \begin{bmatrix} \sqrt{E^s}x(t) \\ \\ k_r y_{sr}(t-\tau) \end{bmatrix} + \underbrace{\begin{bmatrix} n_{d_v}(t) \\ \\ n_{d_h}(t) \end{bmatrix}}_{\mathbf{n}} \tag{5.9}$$

where $\mathbf{n}$ is the 2×1 i.i.d. zero mean complex AWGN vector with variance $\mathbb{E}\left[\mathbf{n}\,\mathbf{n}^H\right] = N_o\;\mathbf{I}$, and $\mathbf{I}$ is an identity matrix. The diagonal elements of $\mathbf{H}$ correspond to co-polarization, while the off-diagonal elements correspond to cross-polarization. The relay amplification factor k_r is

$$k_r = \sqrt{\frac{E^s\left(\mathbb{E}\left[\left|\tilde{h}^v_{sd}\right|^2\right] + \mathbb{E}\left[\left|\tilde{h}^h_{sd}\right|^2\right]\right)}{E^r\left(\mathbb{E}\left[\left|\tilde{h}^v_{rd}\right|^2\right] + \mathbb{E}\left[\left|\tilde{h}^h_{rd}\right|^2\right]\right)}} \tag{5.10}$$

where E^r is the received signal energy at the relay node given by

$$E^r = E^s\;\mathbb{E}\left[\left|\tilde{h}_{sr}\right|^2\right] + N_o. \tag{5.11}$$

Since the source and relay node are spatially separated apart, we can assume the channel from the source to the destination is not correlated with the channel from the relay to the destination. In other words, the co-polarization elements

of the channel h_{sd}^{v} and h_{rd}^{h} and the cross-polarization elements h_{sd}^{h} and h_{rd}^{v} are assumed to be completely un-correlated. Therefore

$$\mathbb{E}\left[h_{sd}^{v}h_{rd}^{h*}\right] = \mathbb{E}\left[h_{sd}^{h}h_{rd}^{v*}\right] = 0 \tag{5.12}$$

and

$$\mathbb{E}\left[h_{sd}^{v}h_{rd}^{v*}\right] = \mathbb{E}\left[h_{sd}^{h}h_{rd}^{h*}\right] = 0. \tag{5.13}$$

We define the receive correlation coefficient as

$$\rho_r = \frac{\mathbb{E}\left[h_{sd}^{v}h_{sd}^{h*}\right]}{\sqrt{\chi}} = \frac{\mathbb{E}\left[h_{rd}^{v}h_{rd}^{h*}\right]}{\sqrt{\chi}}. \tag{5.14}$$

5.3.2 Proposed Receiver Structure

At the destination node, the vertical and horizontal polarized signals are received at different time due to the signal processing and additional propagation delay τ caused by the relay. Because of cross polarization, the delayed signal from the relay becomes an ISI. Therefore equalization for each polarization is required. As there are two branches from the vertical and horizontal polarization, diversity combiner is needed. Here we propose the frequency domain diversity combiner and equalizer (FDE-MRC) and is shown in Fig. 5.2. Assuming that cyclic prefix (CP) with duration longer than delay τ is inserted before transmission from the source node, and removed at the destination node, the signals received at the destination node from the source and relay nodes are transformed into frequency domain by taking L points discrete Fourier transform (DFT). The resulting signal spectras at the k-th subcarrier from vertical and horizontal polarized branches

are respectively given by

$$Y_{d_v}(k) = \sqrt{E^s}\ X(k)\left[\tilde{h}^v_{sd} + k_r\tilde{h}^v_{rd}\tilde{h}_{sr}e^{-j2\pi\frac{k}{L}\tau}\right] + k_r\tilde{h}^v_{rd}N_r(k)e^{-j2\pi\frac{k}{L}\tau} + N_{d_v}(k)$$
$$\triangleq \sqrt{E^s}X(k)\ H_v(k) + N_v(k) \tag{5.15}$$

and

$$Y_{d_h}(k) = \sqrt{E^s}\ X(k)\left[\tilde{h}^h_{sd} + k_r\tilde{h}^h_{rd}\tilde{h}_{sr}e^{-j2\pi\frac{k}{L}\tau}\right] + k_r\tilde{h}^h_{rd}N_r(k)e^{-j2\pi\frac{k}{L}\tau} + N_{d_h}(k)$$
$$\triangleq \sqrt{E^s}X(k)\ H_h(k) + N_h(k) \tag{5.16}$$

where $k = \{1, 2, \ldots, L\}$, $X(k)$ is the transmitted signal in frequency domain, $N_r(k)$ is the relay noise in frequency domain, and $N_v(k)$ and $N_h(k)$ are the effective noises at the vertical and horizontal antennas respectively at the destination

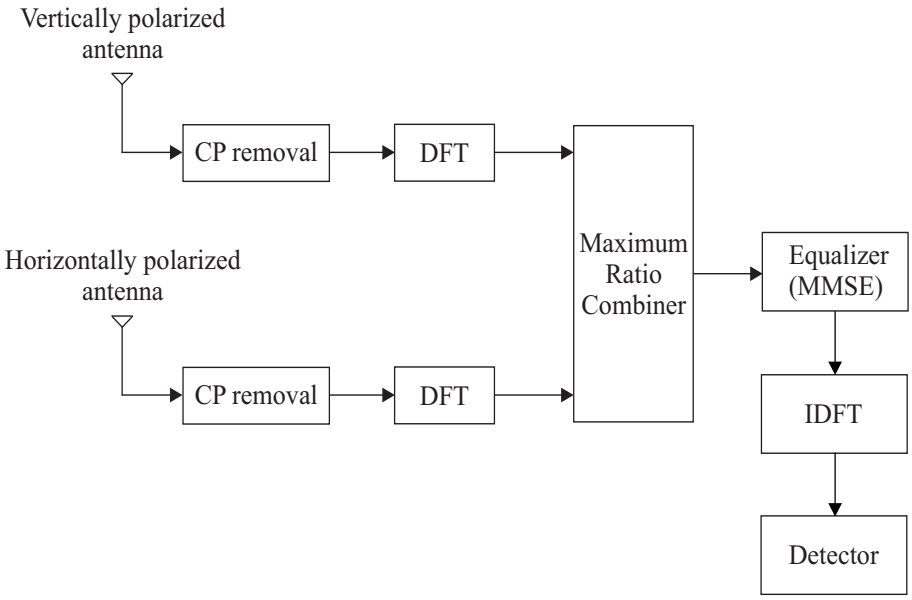

Figure 5.2: Receiver structure of the proposed cooperative MIMO system.

node, $H_v(k)$ and $H_h(k)$ are the effective channels at vertical and horizontal antennas respectively at the destination node given by

$$H_v(k) = \tilde{h}^v_{sd} + k_r \tilde{h}^v_{rd} \tilde{h}_{sr} e^{-j2\pi \frac{k}{L}\tau} \tag{5.17}$$

and

$$H_h(k) = \tilde{h}^h_{sd} + k_r \tilde{h}^h_{rd} \tilde{h}_{sr} e^{-j2\pi \frac{k}{L}\tau}. \tag{5.18}$$

The polarized frequency domain signals $Y_{d_v}(k)$ and $Y_{d_h}(k)$ are combined through MRC at the destination node and the resultant signal spectrum $Y(k)$ is

$$Y(k) = Y_{d_v}(k) H^*_v(k) + Y_{d_h}(k) H^*_h(k). \tag{5.19}$$

The combined signal $Y(k)$ is input to MMSE equalizer given by

$$W(k) = \arg\min_{W} \ \mathbb{E}_h \left[\left| W(k)\ Y(k) - \sqrt{E^s} X(k) \right|^2 \right] \tag{5.20}$$

where $\mathbb{E}_h[.]$ denotes the expectation conditioned on the channel gains. For ease of notation and without loss of generality, we drop the index k in the following derivation. Substituting the value of Y from (5.15), (5.16), and (5.19) into the objective function of (5.20)

$$J = \mathbb{E}_h \left[\left| W \left(\sqrt{E^s} X |H_v|^2 + N_v H^*_v + \sqrt{E^s} X |H_h|^2 + N_h H^*_h \right) - \sqrt{E^s} X \right|^2 \right]$$

$$= \mathbb{E}_h \left[\left| \left(W |H_v|^2 + W |H_h|^2 - 1 \right) \sqrt{E^s} X + W N_v H^*_v + W N_h H^*_h \right|^2 \right]. \tag{5.21}$$

Solving the above equation for minimum value of W, we take the derivate of J w.r.t. W and set it to 0, i.e. $\frac{dJ}{dW} = 0$

$$\begin{aligned}
\Rightarrow & E^s \left(|H_v|^4 W^* + |H_h|^4 W^* + 2 |H_v H_h|^2 W^* - |H_v|^2 - |H_h|^2 \right) \\
& + N_o^v |H_v|^2 W^* + N_o^h |H_h|^2 W^* = 0
\end{aligned}$$

$$\begin{aligned}
\Rightarrow & \left(E^s |H_v|^4 + E^s |H_h|^4 + 2 |H_v H_h|^2 + |H_v|^2 N_o^v + |H_h|^2 N_o^h \right) W^* \\
& = E^s \left(|H_v|^2 + |H_h|^2 \right)
\end{aligned} \tag{5.22}$$

Rearranging (5.22) we obtain,

$$W^* = \frac{E^s \left(|H_v|^2 + |H_h|^2 \right)}{E^s \left(|H_v|^4 + |H_h|^4 + 2 |H_v H_h|^2 \right) + |H_v|^2 N_o^v + |H_h|^2 N_o^h} \tag{5.23}$$

Assuming $H = |H_v|^2 + |H_h|^2$, (5.23) becomes,

$$W^* = \frac{H}{|H|^2 + |H_v|^2 \frac{N_o^v}{E^s} + |H_h|^2 \frac{N_o^h}{E^s}}. \tag{5.24}$$

Taking the conjugate on both side and adding the index k, we obtain the final form

$$W(k) = \frac{H^*(k)}{|H(k)|^2 + |H_v(k)|^2 \frac{N_o^v}{E^s} + |H_h(k)|^2 \frac{N_o^h}{E^s}} \tag{5.25}$$

where

$$H(k) = |H_v(k)|^2 + |H_h(k)|^2 , \tag{5.26}$$

$$\begin{aligned}
N_o^v &= N_o \left(1 + k_r^2 \, \mathbb{E} \left[\left| \tilde{h}_{rd}^v \right|^2 \right] \right) \\
&= N_o \left(1 + \frac{k_r^2 \, \chi}{P L_{rd}^v} \right)
\end{aligned} \tag{5.27}$$

and

$$N_o^h = N_o \left(1 + k_r^2 \, \mathbb{E}\left[\left|\tilde{h}_{rd}^h\right|^2\right]\right) = N_o \left(1 + \frac{k_r^2}{PL_{rd}^h}\right). \tag{5.28}$$

As the dual polarized antennas at the destination node are closely spaced, we can assume the distance for the cross-polarized channels from the same node are the same, i.e., $d_{sd}^v = d_{sd}^h = d_{sd}$ and $d_{rd}^v = d_{rd}^h = d_{rd}$. Therefore (5.27) and (5.28) becomes

$$N_o^v = N_o \left(1 + \frac{k_r^2 \chi}{PL_{rd}}\right) \tag{5.29}$$

and

$$N_o^h = N_o \left(1 + \frac{k_r^2}{PL_{rd}}\right). \tag{5.30}$$

The detected data in frequency domain is then transformed back to time domain by using inverse discrete Fourier transform (IDFT). Due to the full duplex nature of the relay, the transmission time is reduced, which in turn increases the data rate as compared to the conventional ANF protocol. Also no frame or symbol synchronization is required at the relay node because of the use of FDE-MRC at the destination node.

5.4 Energy Analysis

Cooperative communication achieves diversity through spatially separated cooperating nodes. In most potential applications, these nodes are battery powered. Therefore energy consumption must be minimized without compromising the transmission quality. As more RF front ends are used by polarized antennas in the proposed scheme, the total energy requirement to achieve a required quality must be compared to the conventional ANF. In this section we formulate the

transmission energy consumption and total energy consumption of the proposed scheme.

In the following analysis, the energy consumption model developed by Cui *et.al.* [60] is used. For completeness of presentation some of the important equations in [60] are revisited in this thesis. The total energy consumption model that includes both the transmission energy and the circuit energy consumption per bit is given by

$$E_{bt} = \frac{(P_{PA} + P_C)}{R_b} \tag{5.31}$$

where P_C is the power consumption of all circuit blocks, R_b is the bit rate, and P_{PA} is the power consumption of all power amplifiers, which depends on the transmit power P_{out},

$$P_{out} = E_T \ R_b \tag{5.32}$$

where E_T is the sum of transmission energy from both the source and relay nodes. For the proposed scheme E_T can be written as

$$\begin{aligned} E_T &= E^s + k_r^2 \ E^r \\ &= E^s \left(1 + \frac{\mathbb{E}\left[\left|\tilde{h}_{sd}^v\right|^2\right] + \mathbb{E}\left[\left|\tilde{h}_{sd}^h\right|^2\right]}{\mathbb{E}\left[\left|\tilde{h}_{rd}^v\right|^2\right] + \mathbb{E}\left[\left|\tilde{h}_{rd}^h\right|^2\right]} \right) \\ &= E^s \left(1 + \frac{1/PL_{sd} + \chi/PL_{sd}}{\chi/PL_{rd} + 1/PL_{rd}} \right) \\ &= E^s \left(1 + \frac{PL_{rd}}{PL_{sd}} \right) \end{aligned} \tag{5.33}$$

whereas in the case of conventional ANF, E_T is given as

$$\begin{aligned} E_T &= E^s + {k'_r}^2 \, E^r \\ &= E^s \left(1 + \frac{\mathbb{E}\left[\left| \tilde{h}_{sd} \right|^2 \right]}{\mathbb{E}\left[\left| \tilde{h}_{rd} \right|^2 \right]} \right) \\ &= E^s \left(1 + \frac{PL_{rd}}{PL_{sd}} \right). \end{aligned} \tag{5.34}$$

The power consumption of the power amplifier can be approximated as

$$P_{PA} = (1 + \psi) \, P_{out} \tag{5.35}$$

where $\psi = (\xi/\eta) - 1$, with η the drain efficiency of the RF power amplifier and ξ the peak to average ratio, which depends on the modulation scheme and the associated constellation size M [60]

$$\xi = 3 \frac{M - 2\sqrt{M} + 1}{M - 1}. \tag{5.36}$$

The power consumption of all circuit blocks along the signal path is given by

$$\begin{aligned} P_C \approx & M_t \left(P_{DAC} + P_{MIX} + P_{FILT} \right) + 2P_{SYN} \\ & + M_r \left(P_{LNA} + P_{MIX} + P_{IFA} + P_{FILR} + P_{ADC} \right) \end{aligned} \tag{5.37}$$

where P_{DAC}, P_{MIX}, P_{FILT}, P_{SYN}, P_{LNA}, P_{IFA}, P_{FILR}, P_{ADC} are the power consumptions values of the digital-to-analog converter (DAC), the mixer, the active filter at transmitter side, the frequency synthesizer, the low-noise amplifier, the intermediate frequency amplifier, the active filter at receiver side, and the analog-to-digital converter (ADC) respectively. M_t and M_r is the number of RF chains

involved in one complete transmission at transmitter and receiver side respectively. Although the proposed scheme has two extra physical antennas installed as compared to conventional ANF, both the proposed and the conventional ANF effectively use the same number of RF chains for one complete transmission. It is because conventional ANF takes two time-slots for one complete transmission, which uses the RF chains again at the relay and the destination.

Simulation results for energy analysis are shown in section 5.6 under the same throughput and BER requirement. The energy efficiency is also compared over different relay positions and transmission distances.

5.5 Capacity Analysis

In this section, the capacity of the proposed scheme with one relay node will be presented. For fairer comparison, we also present the capacity of ANF cooperative system which employs dual polarized antenna at the destination node, such that polarization diversity is also exploited.

5.5.1 Proposed Scheme

The channel capacity is defined as the mutual information of the channel maximized over all possible input distributions [38]. The symbols and noise are assumed to be statistically independent. Given the channel information at receiver,

the ergodic capacity of the system in (5.15) and (5.16) can be computed as

$$
\begin{aligned}
C &= \max_{p(x)} I(x;\mathbf{y}_d) \\
&= \frac{L}{L+\tau}\,\mathbb{E}\left[\log_2\left(1+\frac{E^s}{G}\left(\mathbb{E}_h\left[\frac{|H_v|^2}{|N_v|^2}+\frac{|H_h|^2}{|N_h|^2}\right]\right)\right)\right] \\
&\cong \mathbb{E}\left[\log_2\left(1+\frac{E^s}{GL}.\mathbb{E}_h\left[\sum_{k=1}^{L}\frac{\left|\tilde{h}^v_{sd}+k_r\tilde{h}^v_{rd}\tilde{h}_{sr}e^{-j2\pi\frac{k}{L}\tau}\right|^2}{\left|k_r\tilde{h}^v_{rd}N_r(k)e^{-j2\pi\frac{k}{L}\tau}+N_{d_v}(k)\right|^2}\right.\right.\right. \\
&\qquad\qquad \left.\left.\left. + \sum_{k=1}^{L}\frac{\left|\tilde{h}^h_{sd}+k_r\tilde{h}^h_{rd}\tilde{h}_{sr}e^{-j2\pi\frac{k}{L}\tau}\right|^2}{\left|k_r\tilde{h}^h_{rd}N_r(k)e^{-j2\pi\frac{k}{L}\tau}+N_{d_h}(k)\right|^2}\right]\right)\right] \\
&= \mathbb{E}\left[\log_2\left(1+\frac{E^s}{GLN_o}\left(\frac{\sum_{k=1}^{L}\left|\tilde{h}^v_{sd}+k_r\tilde{h}^v_{rd}\tilde{h}_{sr}e^{-j2\pi\frac{k}{L}\tau}\right|^2}{1+k_r^2\left|\tilde{h}^v_{rd}\right|^2}\right.\right.\right. \\
&\qquad\qquad \left.\left.\left. + \frac{\sum_{k=1}^{L}\left|\tilde{h}^h_{sd}+k_r\tilde{h}^h_{rd}\tilde{h}_{sr}e^{-j2\pi\frac{k}{L}\tau}\right|^2}{1+k_r^2\left|\tilde{h}^h_{rd}\right|^2}\right)\right)\right]
\end{aligned}
\tag{5.38}
$$

where G is a normalization factor that is used to make sure that the transmission energy of the proposed scheme is the same as that of non-cooperative scheme, which is the multiplicative factor of (5.33)

$$G = 1+\frac{PL_{rd}}{PL_{sd}}. \tag{5.39}$$

Notice that the pre-log factor $\frac{L}{L+\tau}$ can be approximated as one as the frame length L is much larger than the delay τ. Hence the proposed scheme will have a higher capacity than the conventional scheme, which inevitably has the 1/2 pre-log factor.

5.5.2 Polarized ANF

As conventional ANF does not have the cross polarized channels, therefore a polarized ANF system is presented in this subsection for fairer comparison with the proposed scheme. The system model of polarized ANF with vertical polarized source antenna, vertical polarized relay antenna and dual polarized destination is discussed in this subsection.

In the first timeslot, the source node broadcasts the vertically polarized signal to the destination and relay node. The vertically polarized received signal at the relay node is identical to (5.4). The received signals from co-polarized and cross-polarized channels at vertical and horizontal antennas of destination node are given by

$$y_{sd}^{v}(t) = \sqrt{E^s}\ x(t)\ \tilde{h}_{sd}^{v} + n_{d_v}(t) \tag{5.40}$$

and

$$y_{sd}^{h}(t) = \sqrt{E^s}\ x(t)\ \tilde{h}_{sd}^{h} + n_{d_h}(t). \tag{5.41}$$

In the second timeslot, the relay amplifies the received signal by k_r and transmit it to the destination node. The vertically and horizontally polarized signal received at the destination are given by

$$y_{rd}^{v}(t+T) = k_r\ y_{sr}(t)\ \tilde{h}_{rd}^{v} + n_{d_v}(t+T) \tag{5.42}$$

and

$$y_{rd}^{h}(t+T) = k_r\ y_{sr}(t)\ \tilde{h}_{rd}^{h} + n_{d_h}(t+T) \tag{5.43}$$

where all the channels are equivalent to the proposed scheme except $\tilde{h}_{rd}^{v}$ and $\tilde{h}_{rd}^{h}$ are the co-polarized and cross-polarized channels respectively.

The received signals in the above equations can be written in matrix form as

$$\mathbf{y}_{pa} = \mathbf{H}_{pa}\ \sqrt{E^s}\ x(t) + \mathbf{n}_{pa}$$

where $\mathbf{H}_{pa} = \left[\tilde{h}_{sd}^{v}\ \ \tilde{h}_{sd}^{h}\ \ k_r\tilde{h}_{rd}^{v}\tilde{h}_{sr}\ \ k_r\tilde{h}_{rd}^{h}\tilde{h}_{sr}\right]^T$ and

$$\mathbf{n}_{pa} = \underbrace{\begin{bmatrix} 1 & 0 & 0 & 0 & 0 \\ 0 & 1 & 0 & 0 & 0 \\ 0 & 0 & 1 & 0 & k_r\ \tilde{h}_{rd}^{v} \\ 0 & 0 & 0 & 1 & k_r\ \tilde{h}_{rd}^{h} \end{bmatrix}}_{\mathbf{Q}} \begin{bmatrix} n_{d_v}(t) \\ n_{d_h}(t) \\ n_{d_v}(t+T) \\ n_{d_h}(t+T) \\ n_r(t) \end{bmatrix}.$$

The ergodic capacity of the polarized ANF is thus given by

$$C_{pa} = \frac{1}{2}\mathbb{E}\left[\log_2\ \det\left(\mathbf{I} + \frac{E^s}{GN_o}\mathbf{H}_{pa}\mathbf{H}_{pa}^{H}\left(\mathbf{Q}\mathbf{Q}^{\mathbf{H}}\right)^{-1}\right)\right] \tag{5.44}$$

where the normalization factor G is identical to (5.39). It can be noted that the 1/2 pre-log factor in (5.44) shows that polarized ANF also requires two time-slots for one complete transmission.

5.6 Simulation Results and Analysis

Computer based Monte-Carlo simulations are carried out to illustrate the bit error rate (BER) performance, capacity and energy consumption of the proposed system. In order to provide a fair comparison among different schemes, spectral efficiency is kept constant for all protocols and is set to be 2bps/Hz. The SISO and the proposed scheme use QPSK, whereas the ANF protocol uses 16QAM for

one relay network. This is because the SISO and the proposed scheme takes approximately one time-slot for complete transmission of one data frame, whereas conventional ANF protocol takes two time-slots. For both the polarized ANF and the proposed polarized cooperative MIMO scheme, the cross-polarized channel power (χ) and receiver correlation coefficient (ρ_r) are set to be 0.4 and 0.5 respectively. The additional delay τ is assumed to be one symbol period. To obtain reasonable values of received SNR, the transmitted signal from the source node is amplified by $\sqrt{PL_{sd}}$ to compensate for the path loss. The direct link SNR after this normalization is defined as γ_{sd}. For the ANF and proposed scheme, normalization factor G in (5.39) is used to ensure the same total transmission power as the SISO. Hence the normalization SNR γ_{sd} can be used as a reference for all schemes in capacity, outage and BER analysis. Table 5.1 summarizes the system parameters for all simulations, which are mostly based on [60–62]. The parameter B is the bandwidth, f_c is the carrier frequency, $\bar{P}_b$ is the average probability of error for energy consumption analysis, and M_L is the link margin compensating the hardware process variations and other background interference and noise. The number of transmit antennas M_t and receive antennas M_r involved in one complete transmission are respectively 2 and 3 for conventional and polarized ANF as well as the proposed schemes, whereas they are both one for SISO scheme.

Table 5.1: System Parameters

$P_{DAC} = 15.4$mW	$G_t G_r = 5$dBi
$P_{MIX} = 30.3$W	$\alpha = 3$
$P_{FILT} = 2.5$mW	$f_c = 2.5$GHz
$P_{FILR} = 2.5$mW	$\eta = 0.35$
$P_{SYN} = 50$mW	$\bar{P}_b = 10^{-4}$
$P_{LNA} = 20$mW	$M_L = 40$dB
$P_{IFA} = 3$mW	$B = 10$KHz
$P_{ADC} = 6.7$mW	

For outage probability, capacity and BER analysis, the source to destination

node distance d_{sd} is set to be $200m$. The relay node is set at the midpoint between the source and destination node, i.e, $d_{sr} = d_{rd} = 100m$. For energy analysis, various positions of the relay node are considered.

5.6.1 Capacity Results

The increase in capacity of the proposed scheme as compared to the conventional ANF scheme is demonstrated in Fig. 5.3. The capacity of the proposed scheme significantly outperforms the conventional ANF protocols due to the relay's full duplex capability. For polarized ANF, the use of dual polarized antenna at the destination node provides a marginal increase in capacity. Therefore, the proposed scheme has a significant capacity advantage over the ANF scheme, even if polarized antennas are also used. The new scheme without cross-polarization has slightly less capacity than the new system with cross-polarization but still it is higher than the ANF systems.

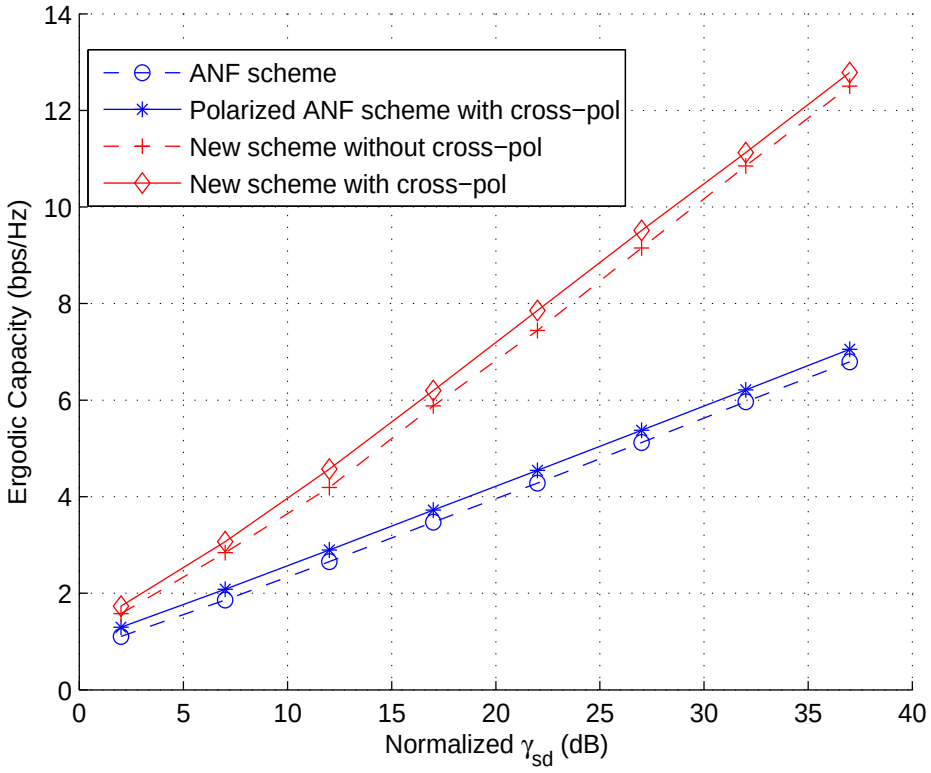

Figure 5.3: Capacity comparison of one relay proposed scheme.

5.6.2 Outage Probability Results

Fig. 5.4 shows the outage probabilities for the various protocols as a function of normalized γ_{sd}. The target rate threshold R is selected to be 2bps/Hz. The effect of cross polarization is also evaluated. The outage observed by the proposed polarized cooperative scheme is much lower than the non-cooperative scheme. Compared to the ANF scheme, the proposed scheme without cross polarization achieves a SNR gain of 4dB. The performance of the proposed scheme improves in the presence of cross polarized channels. The change in asymptotic slope shows that diversity gain increases when cross polarization exists. This improvement is similarly observed for the polarized ANF scheme. Comparing to the non-cooperative scheme, the proposed scheme in cross-polarized channels has a significantly better performance.

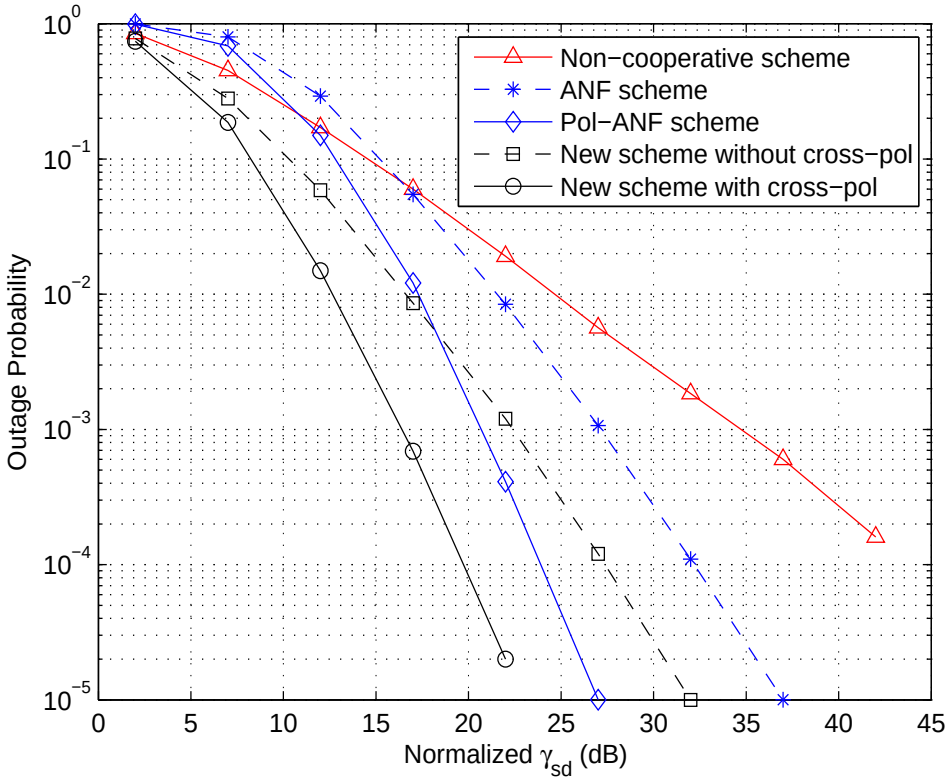

Figure 5.4: The outage probability comparison of proposed polarized cooperative scheme.

5.6.3 BER Results

The BER performance comparison among the SISO, ANF protocol, and the proposed system is presented in Fig. 5.5. The proposed system without cross-polarization has a gain of about 6dB over the conventional ANF protocol at BER 10^{-4}. Thus the cost of using dual polarized antennas and separate RF chains at the relay node is justified by the significantly lowered BER. With the presence of cross-polarization, the performance further improves because polarization diversity can be achieved. The polarized ANF also has a marked improvement, but is approximately 3-4dB worse than the proposed scheme. Another observation is the differences in the asymptotic slope of SISO to the proposed scheme. It verifies that diversity is achieved for cooperative schemes with and without

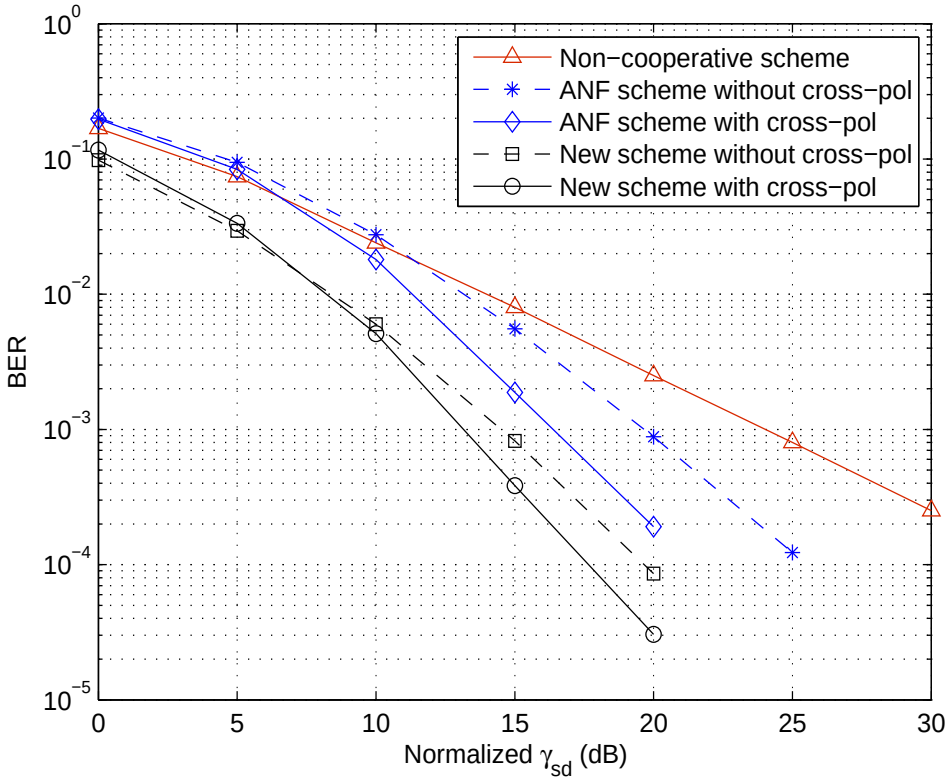

Figure 5.5: BER performance of proposed cooperative MIMO system as a function of received SNR.

cross-polarization.

The effect of receive correlation coefficient ρ_r and XPD χ on BER performance is shown in Fig. 5.6. The SNR is set at 13dB. It can be observed from the figure that BER decreases with increasing χ, and is lowest when χ equals to 1. This is because as χ increases the cross-polarized channels energy increases which then increase the diversity gain. Moreover, we can see the degradation in BER with decreasing receiver correlation coefficient, which effectively shows that the less the channels are correlated, the better is the performance.

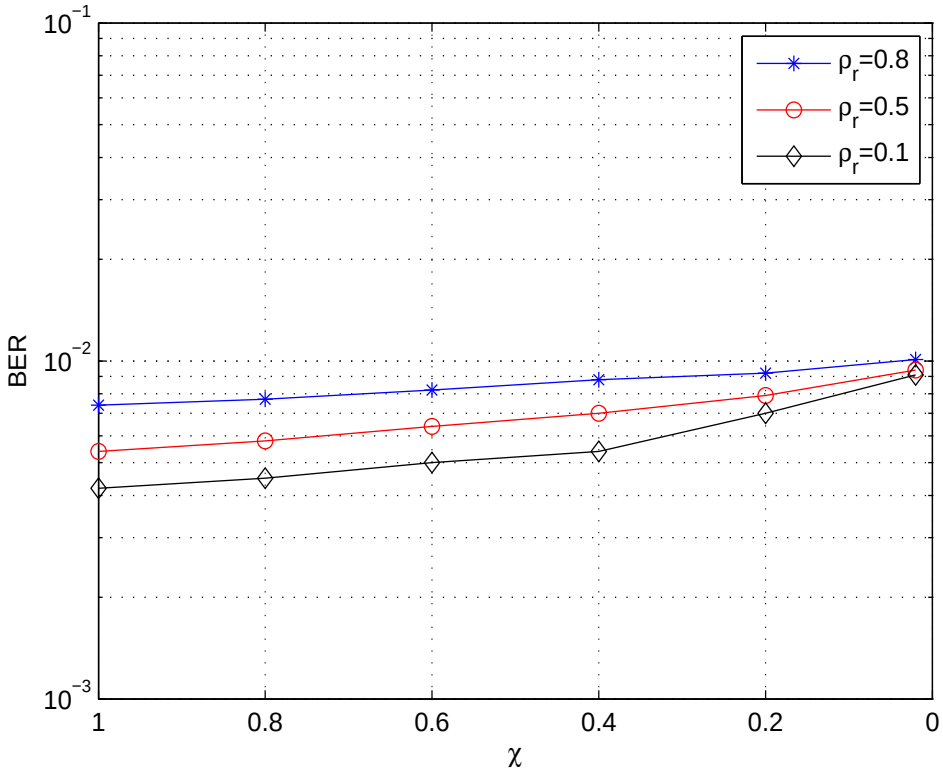

Figure 5.6: BER for proposed scheme as a function of χ for varying receive correlation.

5.6.4 Energy Consumption

Fig. 5.7 plots the transmission energy consumption per bit against the direct link distance d_{sd} when relay node is positioned midway between the source and the destination node. All the channels are assumed to be Rayleigh faded. The results show that the proposed scheme requires less transmission energy than conventional ANF and SISO schemes to achieve the same throughput and BER. This is due to the high diversity gain achieved by the proposed scheme. Therefore by employing the proposed scheme, energy consumption is minimized without compromising the transmission quality. Thus the network life-time can be considerably increased.

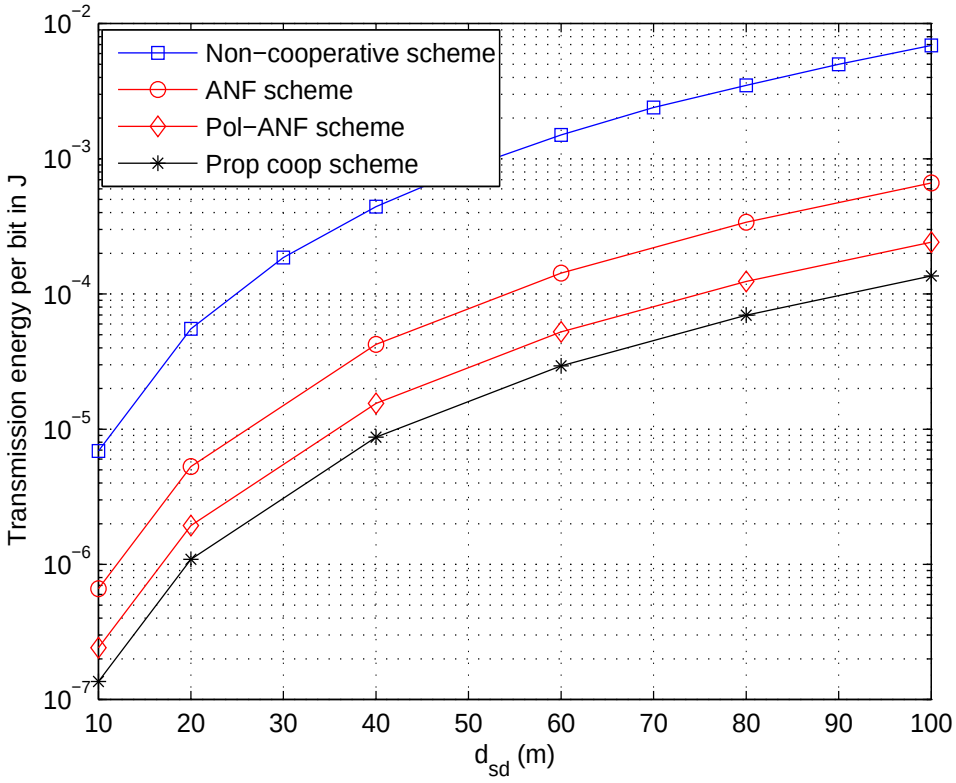

Figure 5.7: Transmission energy consumption per bit over d_{sd} when relay node is located midway between source and destination nodes.

As more RF front ends are installed in the proposed scheme, the total energy

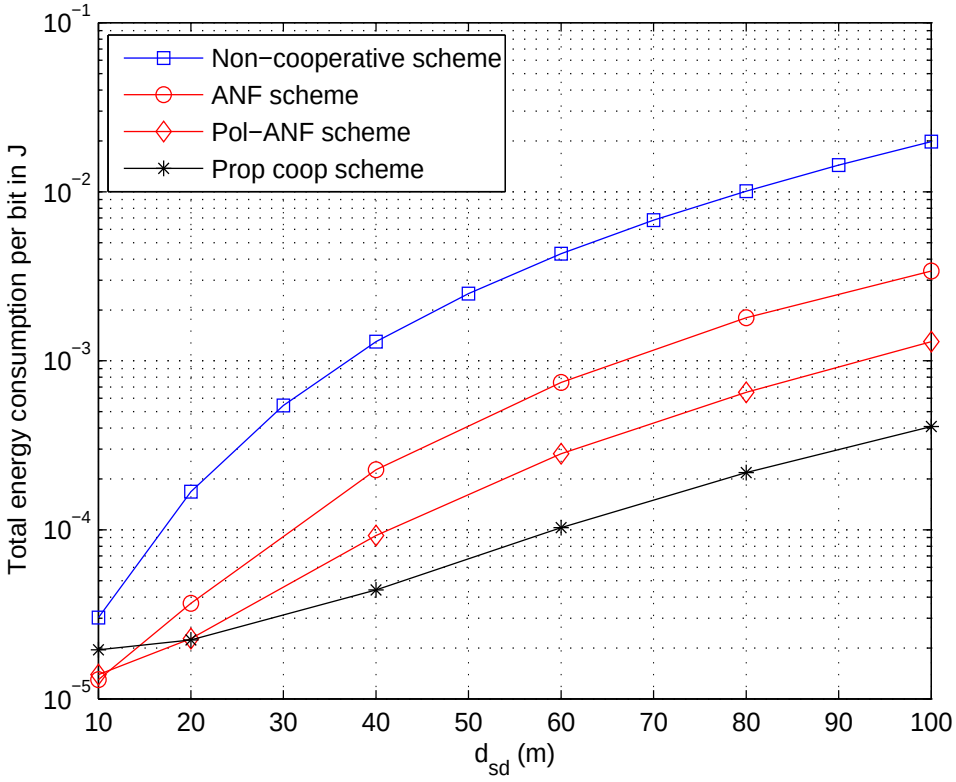

Figure 5.8: Total energy consumption per bit over d_{sd} when relay node is located midway between source and destination nodes.

required to achieve a particular quality is compared with the conventional ANF and SISO schemes in Fig. 5.8. The total energy consumption is calculated using (5.33), where E^s is obtained using the direct link SNR γ_{sd} observed at BER=10^{-4}, where $\gamma_{sd} = E^s/N_o$. The direct link SNR is obtained by evaluating the BER over 10,000 randomly generated channel samples at each transmission distance. Again the relay is located midway between the source and destination nodes. It can be observed that the proposed scheme becomes more energy-efficient than both the ANF and SISO protocols when $d_{sd} \geq 20m$. The crossover point indicates the distance where the transmission energy saving exceeds the extra circuit energy consumption in the proposed scheme comparing to the SISO and ANF scheme.

The special case where the relay is very near the source node is also investigated. The distances d_{sd} and d_{rd} are assumed equal, i.e., $d_{sd} = d_{rd}$. The distance d_{sr} is taken to be 1m, and the channel h_{sr} is assumed to be Rician faded with Rician factor $K = 6dB$. The other channels h^v_{sd}, h^h_{sd}, h^v_{rd} and h^h_{rd} are all considered to possess Rayleigh fading. The transmission energy consumption and total transmission energy over distance are shown in Fig. 5.9 and 5.10 respectively. We observe that the proposed scheme requires less transmission energy than the

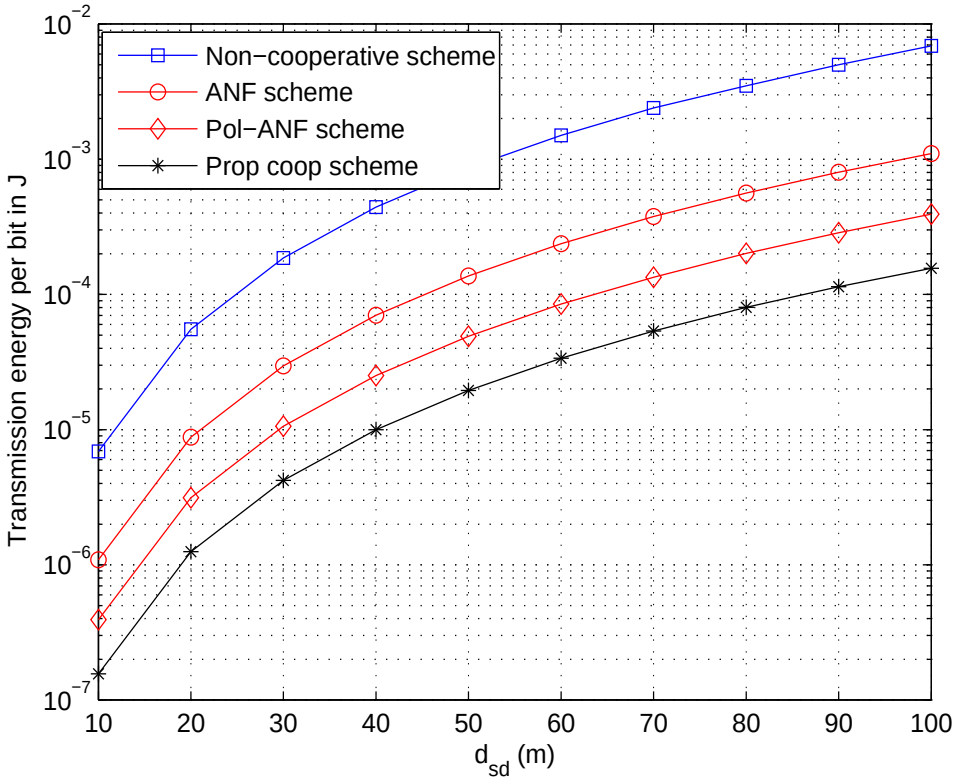

Figure 5.9: Transmission energy consumption per bit over d_{sd} when relay node is located near source node.

conventional ANF and SISO schemes due to the diversity gain achieved by employing extra antennas at relay and destination node. Comparing the total energy consumption, the proposed scheme outperforms the conventional ANF and SISO schemes when $d_1 \geq 19m$ as shown in Fig. 5.10. The energy consumption is also

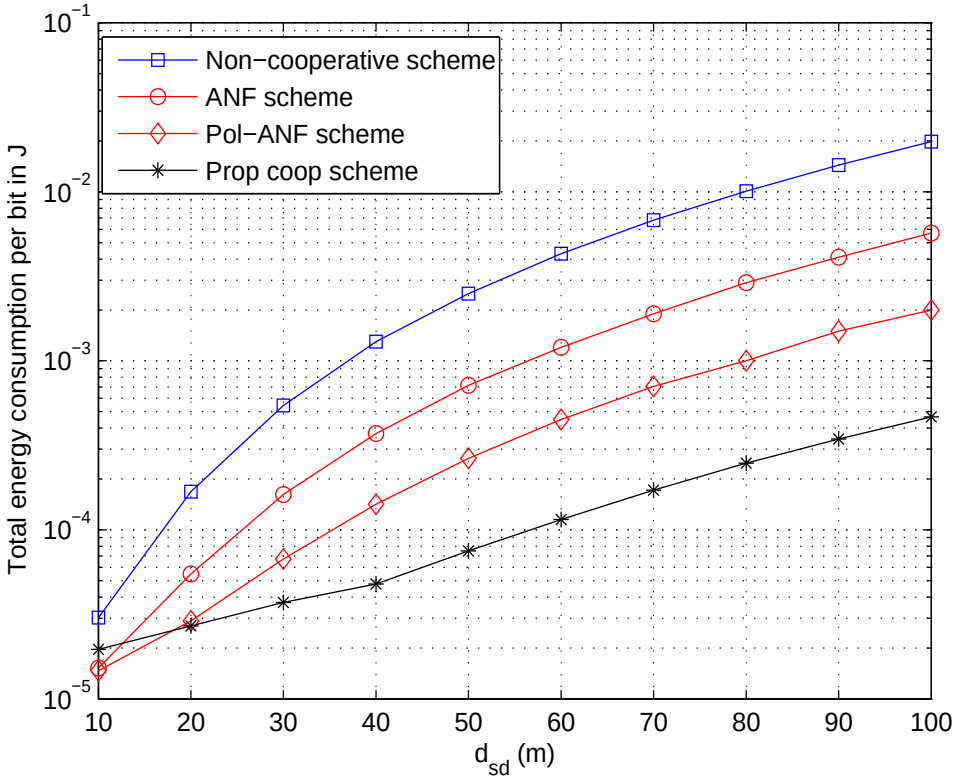

Figure 5.10: Total energy consumption per bit over d_{sd} when relay node is located near source node.

evaluated when the relay node is located near the destination node, but omitted in the presentation as the results have similar trend.

To identify the optimal position for the relay node, the energy consumption analysis is performed by varying its distance between the source and destination nodes. All the channels between the nodes are assumed to be Rayleigh faded. The sum of distance from source to relay d_{sr} and relay to destination node d_{rd} is equal to the distance from source to destination node d_{sd}, which is $200m$. The total energy consumption for this scenario is plotted in Fig. 5.11. It can be seen that the proposed scheme has higher energy consumption if the relay is placed near to the source. The energy consumption starts decreasing when the relay moves away from the source node. Optimal performance is achieved when the

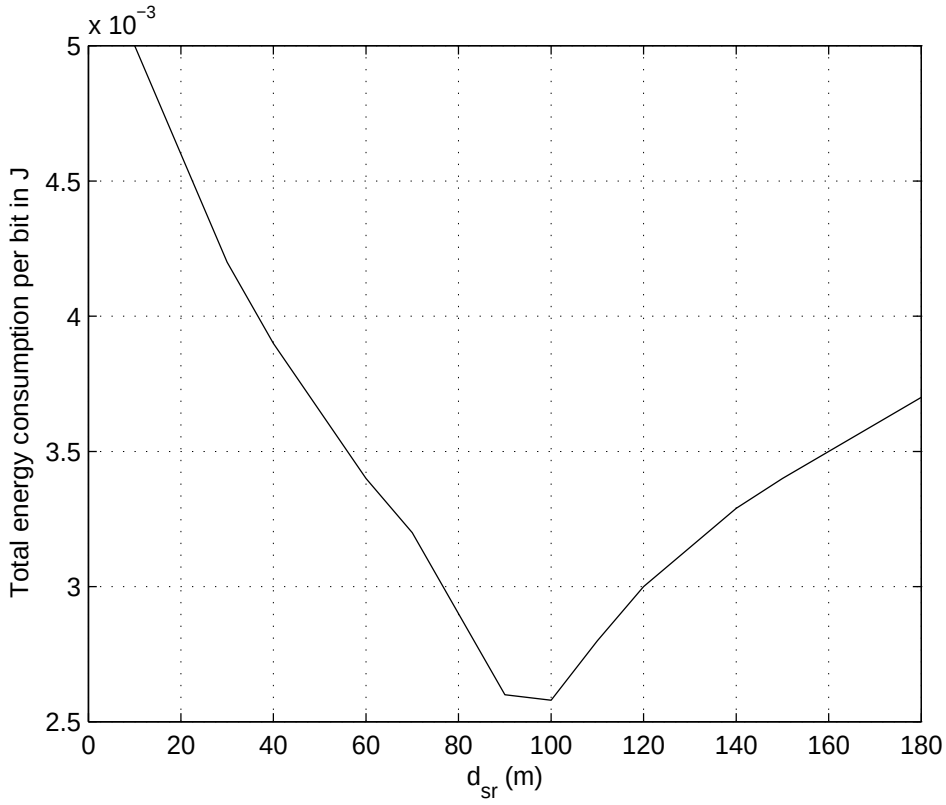

Figure 5.11: Total energy consumption per bit over d_{sr} when relay node is moving between source and destination nodes.

relay is positioned approximately in the middle of the source and destination nodes. The energy consumption again increases as the relay moves away from the middle point towards the destination node. Another observation is the higher energy consumption when the relay is placed nearer to the source than when it is closer to the destination node. This can be explained using (5.33).When the relay is located very close to the source node, PL_{rd}/PL_{sd} approaches unity implying E_T approaches $2E^s$. On the other hand, when the relay is located nearer to the destination node, PL_{rd}/PL_{sd} becomes very small and therefore E_T approaches E^s. Although the value of E^s is different depending on the location of the relay node, this difference is much less than the multiplicative factor 2 that increases the E_T when relay is positioned close to source node. Hence the total transmit

energy required to achieve the same BER is higher when the relay is closer to the source than when it is closer to the destination.

5.7 Summary

In this chapter we have presented a novel asynchronous cooperative communication scheme that does not require frame or symbol level synchronization at the relay node. Co-polarized multiple antennas are installed at the relay node which enables it to transmit and receive at the same timeslot and frequency band, which increases the transmission rate and spectral efficiency. The capacity, outage, BER and energy analysis are used to demonstrate the performance improvement over the conventional ANF protocol.

Chapter 6

Power Allocation for Efficient Multiple Relay Cooperative Communication

6.1 Introduction

Nodes in most cooperative networks are powered by batteries and some of which are even non-rechargeable. Therefore, power allocation schemes must be developed to save the transmit power and improve the life-time of the system [18, 63]. In [60, 64] it was shown that the total energy consumption for data transmission can be reduced by using cooperative communication. In [7, 8], equal distribution of signal energy between direct and relayed links was used for cooperative communication which is generally not an optimal power allocation. In [19], symbol error rate is minimized for optimal power allocation. However, these contributions ignore the channel path loss, which is necessary for any practical implementation of cooperative communication system.

In this chapter we present a novel power allocation technique for conventional

ANF cooperative communication. This scheme aims to minimize the total transmission energy without affecting the transmission quality which is obtained by optimally allocating power to the direct and relayed link(s).

The chapter starts with the power allocation for efficient cooperative communication protocol in Section 6.2. Section 6.3 provides the generalized analytical solution to find the optimal power ratio between direct and relayed links that minimizes the total transmitted energy consumption. Single and two relay are then discussed as special cases. The simulation results demonstrating the marked energy saving in single and two relays case are presented in Section 6.4. Capacity analysis is discussed in Section 6.5. Section 6.6 summarizes the chapter.

6.2 Multiple Relay Cooperative Communication with Power Allocation

Fig. 6.1 illustrates the M-relay cooperative network. The source node (S) transmits information to the destination node (D) directly and also through the relay nodes (R_m).

In conventional ANF, the transmission power is equally distributed between the direct and the relayed link which can lead to high energy consumption to achieve particular performance. By varying the energy ratio between the direct and relayed link, a considerable amount of energy can be saved without affecting the quality of transmission. Thus, the network life-time can be considerably increased.

In this section, we analyze the optimum power allocation for efficient cooperative communication protocol in wireless network with ANF cooperative protocol. We define the power distribution factor Ω_m as the ratio of received energy at destination node from the source node through the m-th relay link to the energy

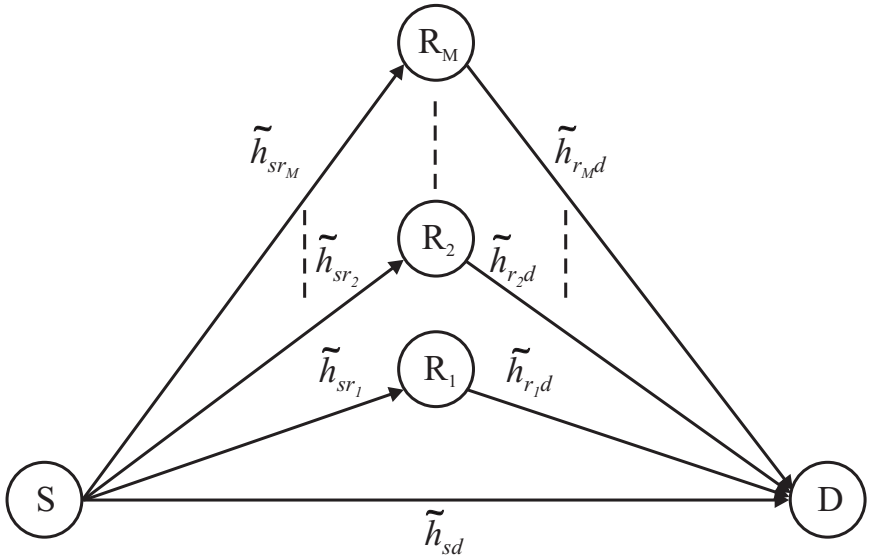

Figure 6.1: Multi relay cooperative system.

received at destination through the direct link. Mathematically, it can be written as

$$\begin{aligned}
\Omega_m &= \frac{Rx\ Signal\ Energy\,(S - R_m - D)}{Rx\ Signal\ Energy\,(S - D)} \\
&= \frac{(k_m\ E^{r_m})\,/PL_{r_md}}{E^s/PL_{sd}} \\
&= \frac{(k_m/PL_{r_md})\,(E^s/PL_{sr_m} + N_o)}{E^s/PL_{sd}} \\
&= \frac{k_m}{E^s}\left(\frac{d_{sd}}{d_{r_md}}\right)^{\alpha}\left(\frac{E^s}{PL_{sr_m}} + N_o\right) \qquad (6.1)
\end{aligned}$$

where E^{r_m} is the transmitted signal energy from the m-th relay node. For realistic bit error rates, the required SNR will have E^s/PL_{sr_m} much larger than N_o. Thus, neglecting N_o in (6.1), Ω_m can be simplified to

$$\Omega_m = \frac{k_m}{PL_o}\left(\frac{d_{sd}}{d_{sr_m}\ d_{r_md}}\right)^{\alpha}. \qquad (6.2)$$

If Ω_m is small, most of the signal energy will flow directly to the destination from the source node. In other words, higher transmission power is allocated to the source node than the relay node(s). On the other hand, when Ω_m is high, a large amount of energy flows to destination through the relay link than the direct one. The mathematical expressions for the multi-relay communication are the same as single relay expressions as in (5.3), (5.4) and (5.5) with the addition of subscript m to r and k representing m-th relay (r_m) and its corresponding amplification factor (k_m). Substituting $y_{sr_m}(t)$ in (5.4) and k_m in (6.2) into (5.5), we get

$$\begin{aligned} y_{r_m d}(t+T) &= \sqrt{\frac{k_m}{PL_{r_m d}}}\, y_{sr_m}(t)\; h_{r_m d} \;+\; n_{d_m}(t) \\ &= \sqrt{\frac{k_m\; E^s}{PL_{sr_m} PL_{r_m d}}} x(t) h_{sr_m} h_{r_m d} + \sqrt{\frac{k_m}{PL_{r_m d}}}\; h_{r_m d}\; n_{r_m}(t) \;+\; n_{d_m}(t) \\ &= \sqrt{\frac{\Omega_m}{PL_{sd}}\; E^s}\; x(t)\; h_{sr_m}\; h_{r_m d} + n'_m \end{aligned} \tag{6.3}$$

where

$$n'_m = \sqrt{\Omega_m \left(\frac{d_{sr_m}}{d_{sd}}\right)^{\alpha}}\; h_{r_m d}\; n_{r_m}(t) + n_{d_m}(t)\,. \tag{6.4}$$

MRC is employed at the destination node where two received signals, directly from the source node and through m-relay nodes are combined. The received SNR of the direct link from the source node at destination is given as

$$\gamma_{sd} \;=\; \frac{E^s}{PL_{sd}\, N_o}. \tag{6.5}$$

The received SNR at the mth-relay from the source node is

$$\gamma_{sr_m} \;=\; \frac{E^s}{PL_{sr_m}\, N_o} \tag{6.6}$$

and the received SNR of the mth-relay to the destination link becomes

$$\gamma_{r_m d} = \frac{E^s}{PL_{sd}\, N_o}\left(\frac{\Omega_m}{1+\Omega_m\left(\frac{d_{sr_m}}{d_{sd}}\right)^{\alpha}}\right). \tag{6.7}$$

The total received SNR at the destination node after MRC is given by

$$\gamma_{total} = \gamma_{sd} + \gamma_{r_m d} \tag{6.8}$$

$$= \frac{E^s}{PL_{sd}\, N_o}\left(1+\sum_{m=1}^{M}\frac{\Omega_m}{1+\Omega_m\left(\frac{d_{sr_m}}{d_{sd}}\right)^{\alpha}}\right). \tag{6.9}$$

The total transmitted signal energy (E_T) is defined as the sum of transmitted energy from the source and relay nodes and is given by

$$\begin{aligned} E_T &= E^s + E^{r_1} + E^{r_2} + \ldots + E^{r_M} \\ &= E^s + \sum_{m=1}^{M} E^{r_m} \\ &= E^s + E^s \sum_{m=1}^{M} \frac{k_m}{PL_{sr_m}} \\ &= E^s\left(1+\sum_{m=1}^{M}\frac{k_m}{PL_{sr_m}}\right) \\ &= E^s\left(1+\sum_{m=1}^{M}\Omega_m\left(\frac{d_{r_m d}}{d_{sd}}\right)^{\alpha}\right). \end{aligned} \tag{6.10}$$

6.3 Optimal Power Allocation Factor Ω_m

In the previous section, we presented the signal model for cooperative communication with power allocation. In this section, the value of energy distribution factor Ω_m that achieves best performance with least total transmitted energy consumption will be determined analytically. Assuming the magnitude of channels

h_{ij} to be Rayleigh faded, the probability of error at high SNR region averaged over channel statistics is given by [65]

$$P_e \approx W(M) \frac{1}{\gamma_{sd}} \prod_{m=1}^{M} \left(\frac{1}{\gamma_{sr_m}} + \frac{1}{\gamma_{r_m d}} \right). \tag{6.11}$$

where

$$W(M) = \frac{(2)^{M+1} \prod_{j=1}^{M+1} (2j-1)}{2\,(M+1)!\; j^{(2M+2)}} \tag{6.12}$$

where j depends upon the type of modulation (2 for phase shift keying (PSK)). It clearly shows that using M-relays in the cooperative network, a diversity order of $M+1$ is achieved. Substituting the values of γ_{sd}, γ_{sr_m} and $\gamma_{r_m d}$ from (6.5), (6.6) and (6.7) respectively into (6.11),

$$\begin{aligned} P_e &= W(M) \left(\frac{PL_{sd}\, N_o}{E^s} \right) \prod_{m=1}^{M} \left(\frac{PL_{sr_m} N_o}{E^s} + \frac{PL_{sd} N_o}{E^s} \left(\frac{1 + \Omega_m \left(d_{sr_m}/d_{sd} \right)^{\alpha}}{\Omega_m} \right) \right) \\ &= W(M) \left(\frac{PL_{sd}\, N_o}{E^s} \right)^{M+1} \prod_{m=1}^{M} \left(\left(\frac{d_{sr_m}}{d_{sd}} \right)^{\alpha} + \frac{1 + \Omega_m \left(d_{sr_m}/d_{sd} \right)^{\alpha}}{\Omega_m} \right) \\ &= W(M) \left(\frac{PL_{sd}\, N_o}{E^s} \right)^{M+1} \prod_{m=1}^{M} \left(\frac{1}{\Omega_m} + 2 \left(\frac{d_{sr_m}}{d_{sd}} \right)^{\alpha} \right). \end{aligned} \tag{6.13}$$

Rearranging (6.13), E^s becomes

$$E^s = PL_{sd}\, N_o \left[\frac{W(M)}{P_e} \prod_{m=1}^{M} \left(\frac{1}{\Omega_m} + 2 \left(\frac{d_{sr_m}}{d_{sd}} \right)^{\alpha} \right) \right]^{1/(M+1)}. \tag{6.14}$$

Substituting the value of E^s into (6.10), we obtain the total transmitted energy to be

$$E_T = PL_{sd}\, N_o \left(1 + \sum_{m=1}^{M} \Omega_m \left(\frac{d_{r_m d}}{d_{sd}}\right)^{\alpha}\right) \left[\frac{W(M)}{P_e} \prod_{m=1}^{M} \left(\frac{1}{\Omega_m} + 2\left(\frac{d_{sr_m}}{d_{sd}}\right)^{\alpha}\right)\right]^{1/(M+1)}. \tag{6.15}$$

To minimize E_T w.r.t. Ω_m, we take the derivative of (6.15) w.r.t. Ω_m and set it to zero

$$\frac{dE_T}{d\Omega_m} = 0. \tag{6.16}$$

Solving (6.16), we get

$$\left(\prod_{m=1}^{M} \left(2\left(\frac{d_{sr_m}}{d_{sd}}\right)^{\alpha} + \frac{1}{\Omega_m}\right)\right)^{1/(M+1)} \frac{d}{d\Omega_m} \left(\sum_{m=1}^{M} \Omega_m \left(\frac{d_{r_m d}}{d_{sd}}\right)^{\alpha}\right) +$$

$$\frac{d}{d\Omega_m} \left(\prod_{m=1}^{M} \left(2\left(\frac{d_{sr_m}}{d_{sd}}\right)^{\alpha} + \frac{1}{\Omega_m}\right)\right) \frac{1}{(M+1)} \left(\prod_{m=1}^{M} \left(2\left(\frac{d_{sr_m}}{d_{sd}}\right)^{\alpha} + \frac{1}{\Omega_m}\right)\right)^{-M/(M+1)}$$

$$\left(1 + \sum_{m=1}^{M} \left(\frac{d_{r_m d}}{d_{sd}}\right)^{\alpha} \Omega_m\right) = 0. \tag{6.17}$$

Thus, using (6.17), the optimal values of Ω_m for any number of relay nodes can be calculated. In the following sub-sections we present the calculations for one and two relay nodes only.

6.3.1 Solving for one relay node

For one relay i.e. $m = 1$, (6.17) becomes (6.18). For the ease of notation we have dropped subscript 1 from the Ω in the following equations.

$$-\frac{1}{2\,\Omega^2}\left(\frac{1}{\Omega}+2\left(\frac{d_{sr}}{d_{sd}}\right)^{\alpha}\right)^{-1/2}\left(1+\Omega\left(\frac{d_{rd}}{d_{sd}}\right)^{\alpha}\right)+\left(\frac{d_{rd}}{d_{sd}}\right)^{\alpha}\sqrt{\frac{1}{\Omega}+2\left(\frac{d_{sr}}{d_{sd}}\right)^{\alpha}}=0. \tag{6.18}$$

Equation (6.18) can be simplified to

$$4\left(\frac{d_{sr}}{d_{sd}}\right)^{\alpha}\Omega^2+\Omega-\left(\frac{d_{sd}}{d_{rd}}\right)^{\alpha}=0. \tag{6.19}$$

Solving (6.19), we have

$$\Omega=\frac{1}{8}\left(\frac{d_{sr}}{d_{sd}}\right)^{-\alpha}\left(-1+\left(\frac{d_{rd}}{d_{sd}}\right)^{-\alpha/2}\sqrt{\left(\frac{d_{rd}}{d_{sd}}\right)^{\alpha}+16\left(\frac{d_{sr}}{d_{sd}}\right)^{\alpha}}\right). \tag{6.20}$$

The above expression can be used to find the optimal Ω that gives the best performance with minimum total transmitted energy consumption from the separation between the source, relay and destination nodes.

6.3.2 Solving for two relay nodes

In this subsection, we calculate the optimal power allocation for two relays cooperative communication network. For $M = 2$, solving (6.17) with $m = \{1, 2\}$ we obtain

$$\left(\frac{d_{r_1d}}{d_{sd}}\right)^{\alpha}\left(2\left(\frac{d_{sr_1}}{d_{sd}}\right)^{\alpha}+\frac{1}{\Omega_1}\right)-\frac{1}{3\Omega_1^2}\left(1+\left(\frac{d_{r_1d}}{d_{sd}}\right)^{\alpha}\Omega_1+\left(\frac{d_{r_2d}}{d_{sd}}\right)^{\alpha}\Omega_2\right)=0 \tag{6.21}$$

and

$$\left(\frac{d_{r_2d}}{d_{sd}}\right)^{\alpha}\left(2\left(\frac{d_{sr_2}}{d_{sd}}\right)^{\alpha}+\frac{1}{\Omega_2}\right)-\frac{1}{3\Omega_2^2}\left(1+\left(\frac{d_{r_1d}}{d_{sd}}\right)^{\alpha}\Omega_1+\left(\frac{d_{r_2d}}{d_{sd}}\right)^{\alpha}\Omega_2\right)=0. \tag{6.22}$$

Equation (6.21) and (6.22) can be simplified to quadratic form

$$2\left(\frac{d_{sr_1}}{d_{sd}}\right)^{\alpha}\left(\frac{d_{r_1d}}{d_{sd}}\right)^{\alpha}\Omega_1^2+\frac{2}{3}\left(\frac{d_{r_1d}}{d_{sd}}\right)^{\alpha}\Omega_1-\frac{1}{3}\left(1+\left(\frac{d_{r_2d}}{d_{sd}}\right)^{\alpha}\Omega_2\right)=0 \tag{6.23}$$

and

$$2\left(\frac{d_{sr_2}}{d_{sd}}\right)^{\alpha}\left(\frac{d_{r_2d}}{d_{sd}}\right)^{\alpha}\Omega_2^2+\frac{2}{3}\left(\frac{d_{r_2d}}{d_{sd}}\right)^{\alpha}\Omega_2-\frac{1}{3}\left(1+\left(\frac{d_{r_1d}}{d_{sd}}\right)^{\alpha}\Omega_1\right)=0. \tag{6.24}$$

Now solving the (6.23) for Ω_1 and (6.24) for Ω_2, we have

$$\Omega_1=\frac{1}{6}\left(\frac{d_{sr_1}}{d_{sd}}\right)^{-\alpha}\left(\frac{d_{r_1d}}{d_{sd}}\right)^{-\alpha}\left[-\left(\frac{d_{r_1d}}{d_{sd}}\right)^{\alpha}+\sqrt{\left(\frac{d_{r_1d}}{d_{sd}}\right)^{\alpha}\left(6\left(\frac{d_{sr_1}}{d_{sd}}\right)^{\alpha}+\left(\frac{d_{r_1d}}{d_{sd}}\right)^{\alpha}+6\left(\frac{d_{sr_1}}{d_{sd}}\right)^{\alpha}\left(\frac{d_{r_2d}}{d_{sd}}\right)^{\alpha}\Omega_2\right)}\right] \tag{6.25}$$

and

$$\Omega_2=\frac{1}{6}\left(\frac{d_{sr_2}}{d_{sd}}\right)^{-\alpha}\left(\frac{d_{r_2d}}{d_{sd}}\right)^{-\alpha}\left[-\left(\frac{d_{r_2d}}{d_{sd}}\right)^{\alpha}+\sqrt{\left(\frac{d_{r_2d}}{d_{sd}}\right)^{\alpha}\left(6\left(\frac{d_{sr_2}}{d_{sd}}\right)^{\alpha}+\left(\frac{d_{r_2d}}{d_{sd}}\right)^{\alpha}+6\left(\frac{d_{sr_2}}{d_{sd}}\right)^{\alpha}\left(\frac{d_{r_1d}}{d_{sd}}\right)^{\alpha}\Omega_1\right)}\right]. \tag{6.26}$$

The above expressions can be used to calculate the optimal distribution ratios Ω_1 and Ω_2 with minimum total energy consumption from the separation between the source, relays and destination nodes.

6.4 Simulation Results and Analysis

In this section, we present the analytical results we derived in Section 6.3, and validate it using simulation results. QPSK modulation scheme is used in the analysis and simulation. To obtain reasonable values of SNR, the transmitted signal from source node is amplified by $\sqrt{PL_{sd}}$ to compensate for the path loss. The carrier frequency f_c is set to be 2.5GHz. The path loss exponent is taken to be 3.5. The G_tG_r and $N_o/2$ is set to be 5dBi and -174dBm/Hz respectively. For all simulation results the sum of the distance from source to m-th relay and m-th relay to destination is kept constant and is equal to the distance from the source to the destination node i.e. $d_{sr_m} + d_{r_m d} = d_{sd} = 200m$.

6.4.1 Single Relay Scenario

In this subsection, the simulation results obtained from the single relay cooperative network are discussed. Unless and until stated, the relay is always assumed to be located midway between the source and the destination. Solving (6.20), the value of Ω is found to be approximately 4.4.

Fig. 6.2 shows the simulated BER as a function of Ω at $E_T = -72$dB Joules. A high BER is observed when $\Omega = 0$. This is because only the direct link between the source and destination node is active and there is no transmission through the relay link. It can also be observed that BER decreases as Ω increases until a minimum is achieved, after which it starts to increase. The Ω at which the minimum BER is achieved in our simulation is approximately $4.3 - 5$, as seen in the Fig. 6.2.

The simulated and analytical results of the total transmitted energy as a function of Ω at BER $= 10^{-3}$ are presented in Fig. 6.3. We compare the two results and show that the two sets of values fit well. Analytically, we obtain a minimum E_T at $\Omega = 4.4$, whereas it is approximately 6 in the simulated results.

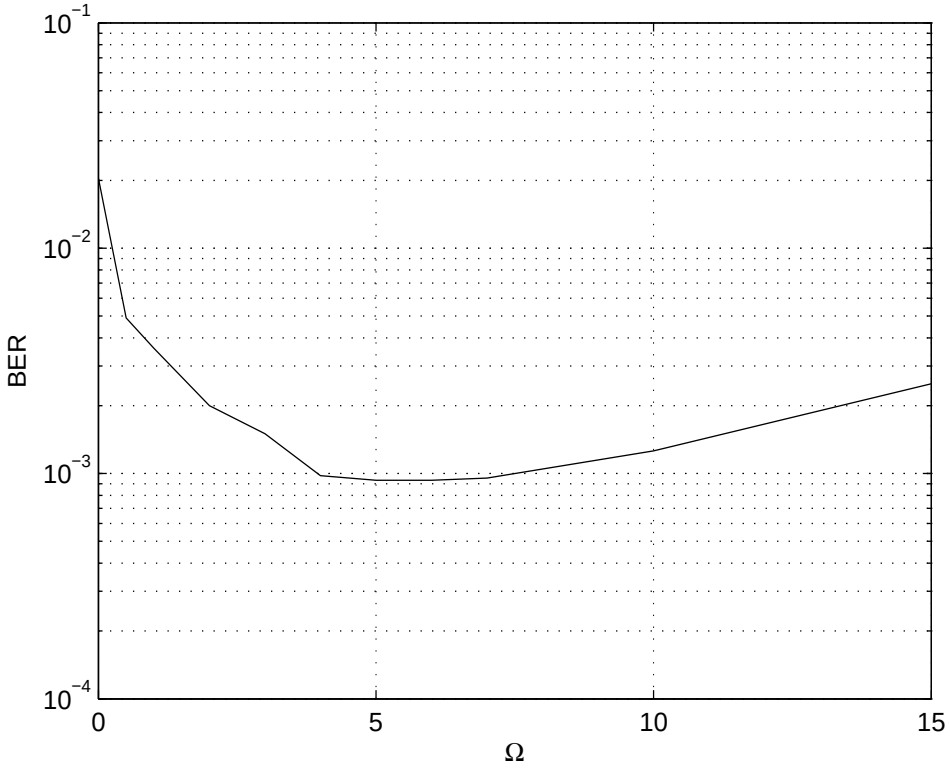

Figure 6.2: Simulated BER as a function of Ω at $E_T = -72$dB Joules.

The difference between them could be due to the assumptions that are made in deriving the probability of error for the single relay cooperative network [65]. Nonetheless, the total transmitted energy is close to the empirical result with only 3.3% difference at $\Omega = 4.4$.

Fig 6.4 shows the total transmission energy consumption for different relay positions. The results shows that the proposed power allocation scheme is more energy efficient than the equal power allocation. It can be observed that the proposed scheme has high energy consumption if the relay is placed near the source and decreases as the relay moves away from it. The minimum total transmitted energy is observed when the relay is approximately 125m away from the source node, and after which the total energy consumption again increases as the relay moves towards the destination node. The minimum energy consumption is

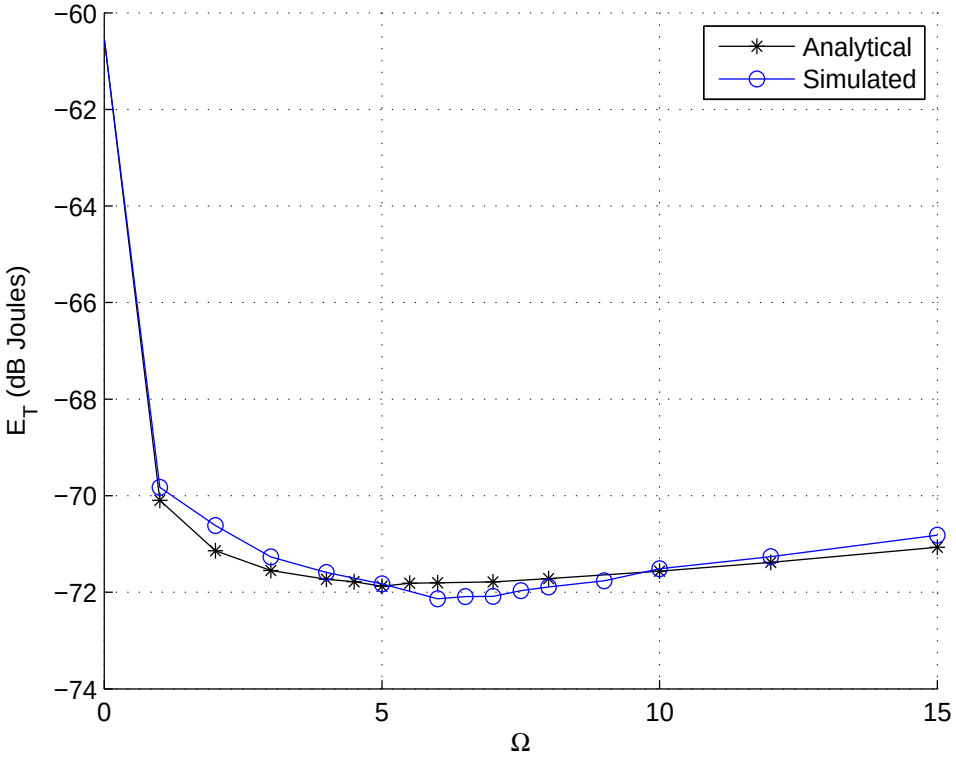

Figure 6.3: Simulated and analytically calculated E_T as a function of Ω at BER $= 10^{-3}$.

not obtained exactly at the middle. This can be explained using (6.10). The minimum simulated E^s is achieved when relay is located at the midpoint between source and destination nodes, but the multiplicative factor $(1 + d_{rd}/d_{sd})$ decreases as the relay moves away from the source node and therefore it shifts the minimum E_T away from the center. Another observation is the higher energy consumption when the relay is positioned nearer the source than when it is closer to the destination. Again (6.10) can be used to explain this trend. When the relay moves nearer the destination, d_{rd}/d_{sd} decreases and E_T tends to E^s. On the contrary, when the relay is located near the source, d_{rd}/d_{sd} becomes unity meaning E_T approaches $2E^s$. Although the value of E^s is different in both cases, the difference is much less than the multiplicative factor 2 that actually increase

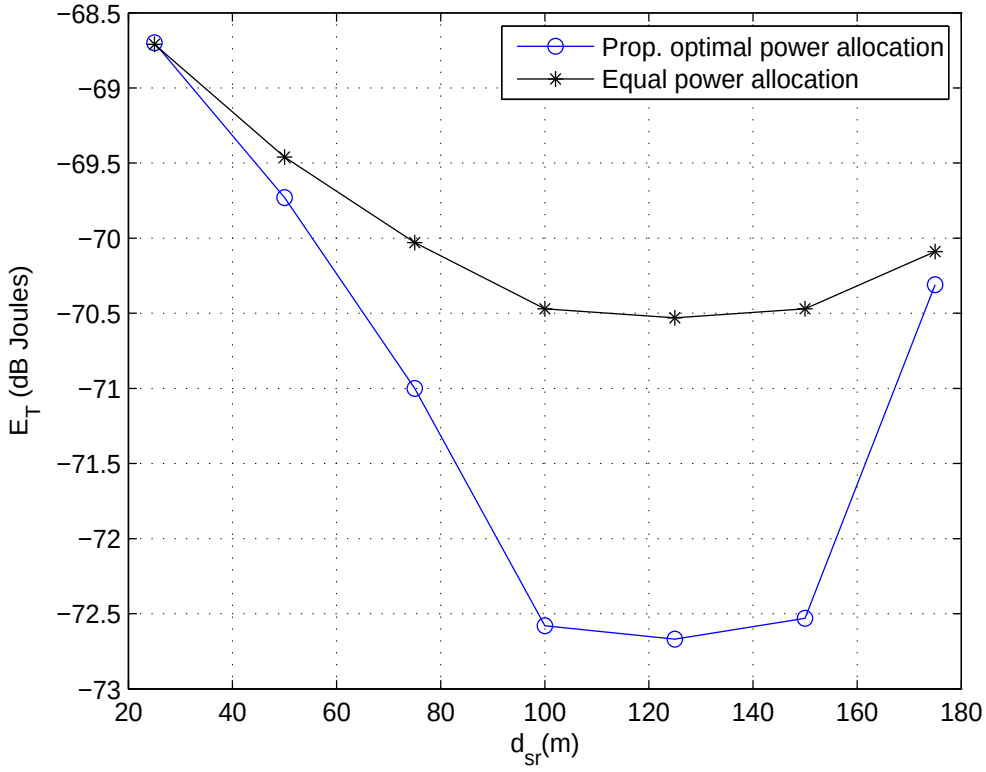

Figure 6.4: Total transmission energy consumption for different relay positions.

the E_T when the relay is located near the source.

6.4.2 Two Relays Scenario

In this section, the two relays cooperative network results are discussed for different relays locations.

The two relays total energy consumption comparison between the proposed optimal and equal power allocation is shown in Fig.6.5, for the case when both the relays are at the same distance from the source i.e. $d_{sr_1} = d_{sr_2}$. The proposed power allocation scheme is more efficient than the conventional equal power allocation. Like single relay case in Fig. 6.4, the total energy consumption begins to decrease as the relay moves away from the source and is minimum at approximately $d_{sr_1} = d_{sr_2} = 125m$. It starts increasing as the relay moves away from this

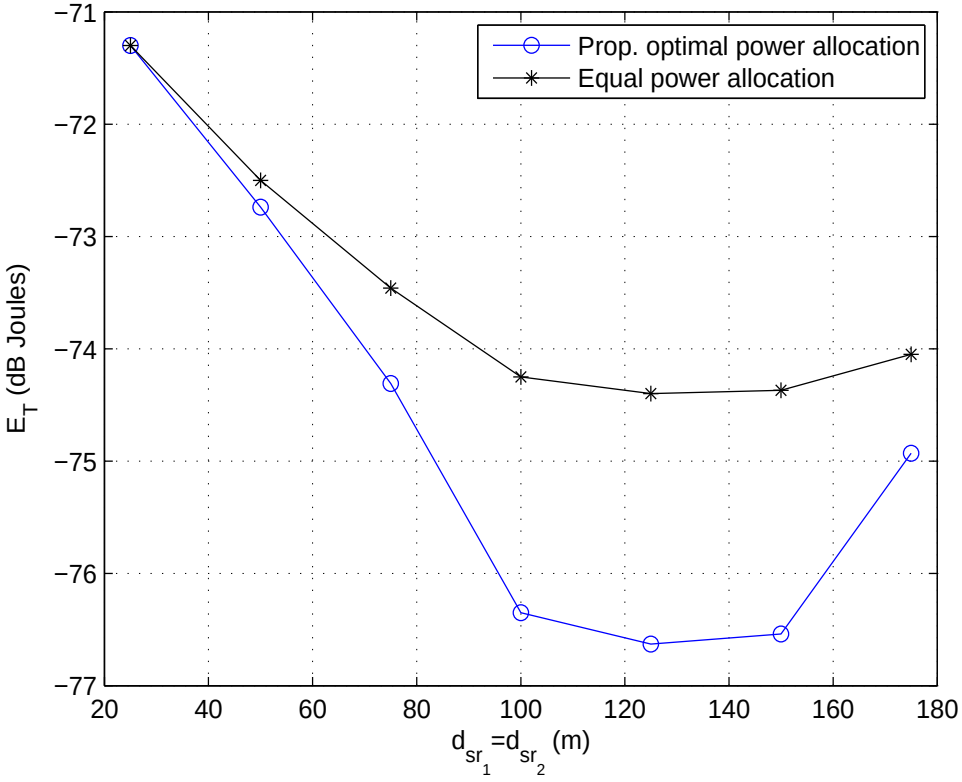

Figure 6.5: E_T as a function of $d_{sr_1} = d_{sr_2}$ at $BER = 10^{-3}$.

point towards the destination. In addition to that, the energy consumption is higher when the relay is placed nearer the source than the case when it is located nearer the destination. The reasons for all these observations are same as for single relay case as depicted in Fig. 6.4.

Fig. 6.6 illustrates the total energy consumption comparison between optimal and equal power allocation for the two relays cooperative network where $d_{sr_1} = d_{r_2d}$. The performance of the proposed scheme degrades as one of the relay nodes get close to the source or destination. The optimal performance is achieved when the relays move to the center between source and destination.

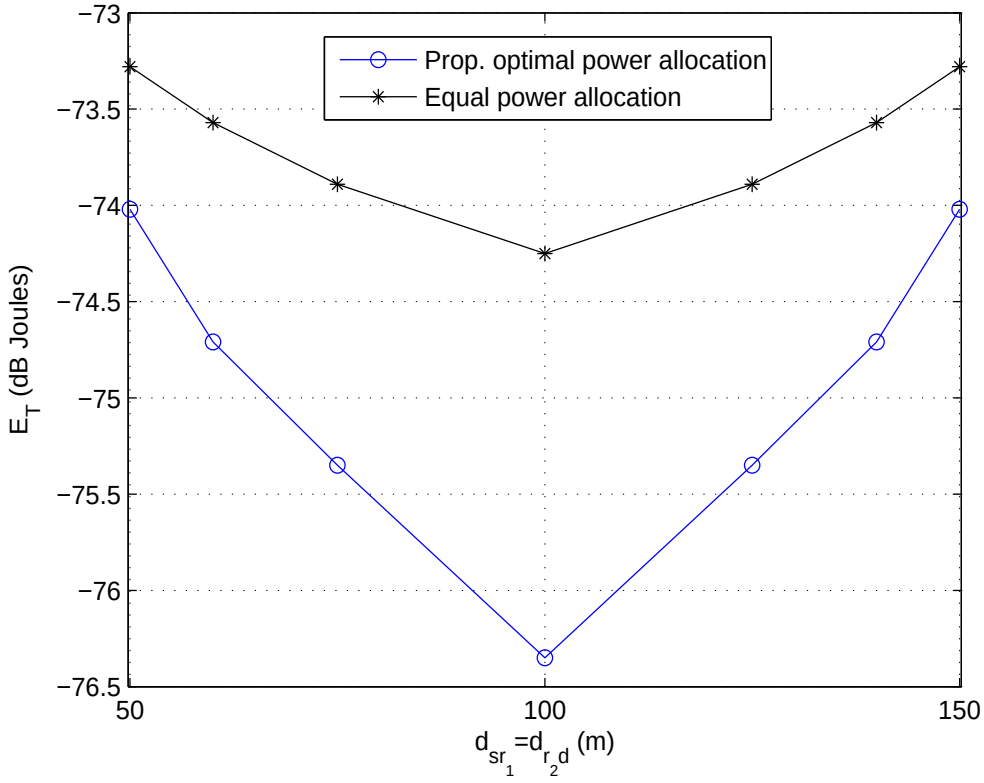

Figure 6.6: E_T as a function of $d_{sr_1} = d_{r_2d}$ at $BER = 10^{-3}$.

6.5 Capacity Analysis

In this section, the capacity of the proposed power allocation cooperative communication scheme for M relay nodes is presented and is compared with conventional equal power allocation scheme. Given the channel information at the receiver, the channel capacity of the proposed system with M relays can be calculated as [7]

$$C = \frac{1}{2}\log_2\left(1 + \gamma_{sd} + \gamma_{sr_md}\right) \tag{6.27}$$

where

$$\gamma_{sr_md} = \sum_{m=1}^{M}\left(\frac{|k_m h_{sr_m} h_{r_md}|^2}{N_o\left(1 + |k_m h_{r_md}|^2\right)}\right). \tag{6.28}$$

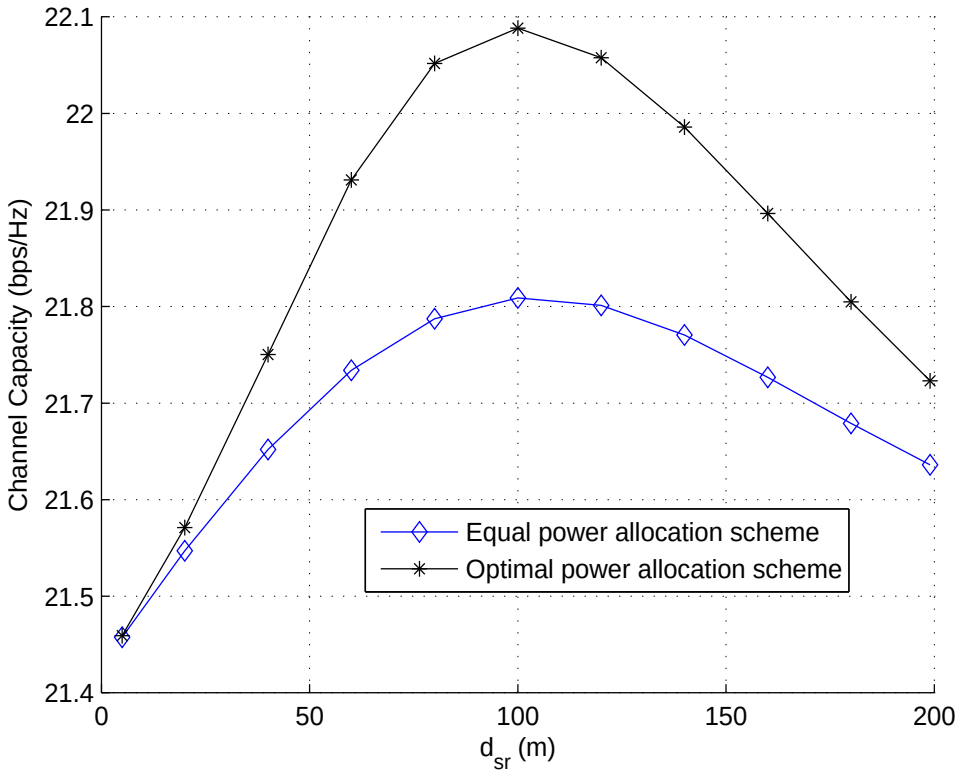

Figure 6.7: Single relay capacity comparison with different power allocation schemes at $E_T = -72$dB Joules.

Fig. 6.7 shows the single relay channel capacity of the proposed power allocation and the conventional equal power allocation schemes as a function of S-R distance at $E_T = -72$dB Joules. It can be observed that the proposed power allocation scheme has the highest capacity.

The channel ergodic capacity for two relays network at $E_T = -72$dB Joules is illustrated in Fig. 6.8. The source to relays distance is kept constant, i.e. $d_{sr_1} = d_{sr_2}$. It can be observed that the proposed power allocation scheme provides better capacity than conventional equal power scheme. The maximum capacity is achieved when the relay is positioned approximately in the centre.

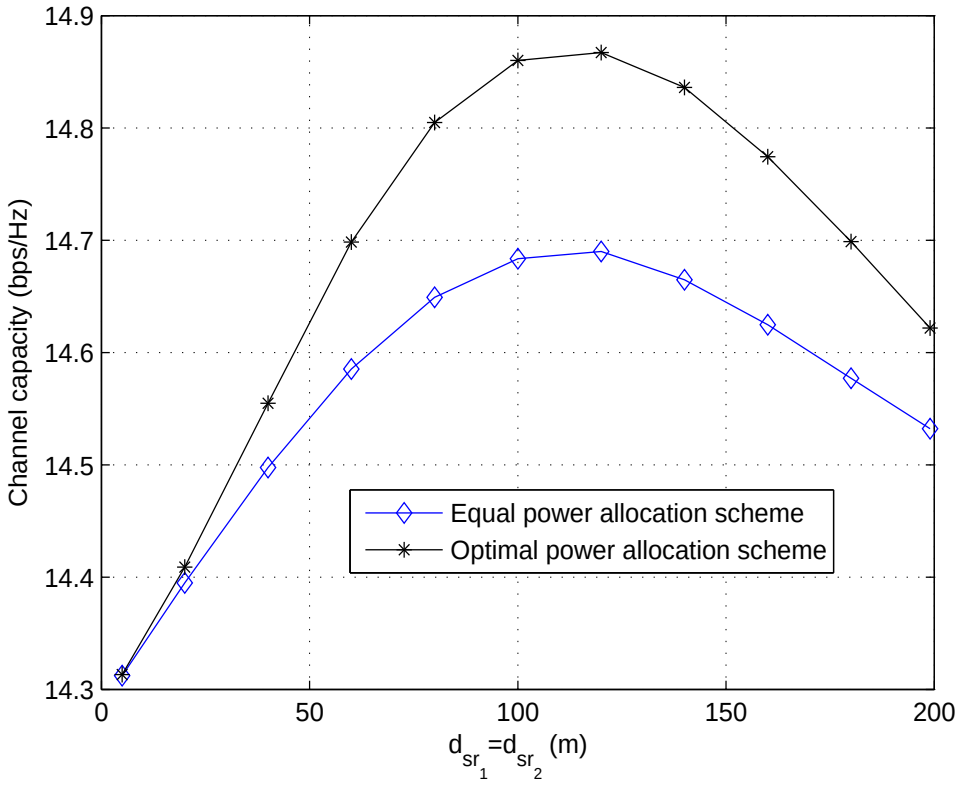

Figure 6.8: Two relays capacity comparison with different power allocation schemes at $E_T = -72$dB Joules.

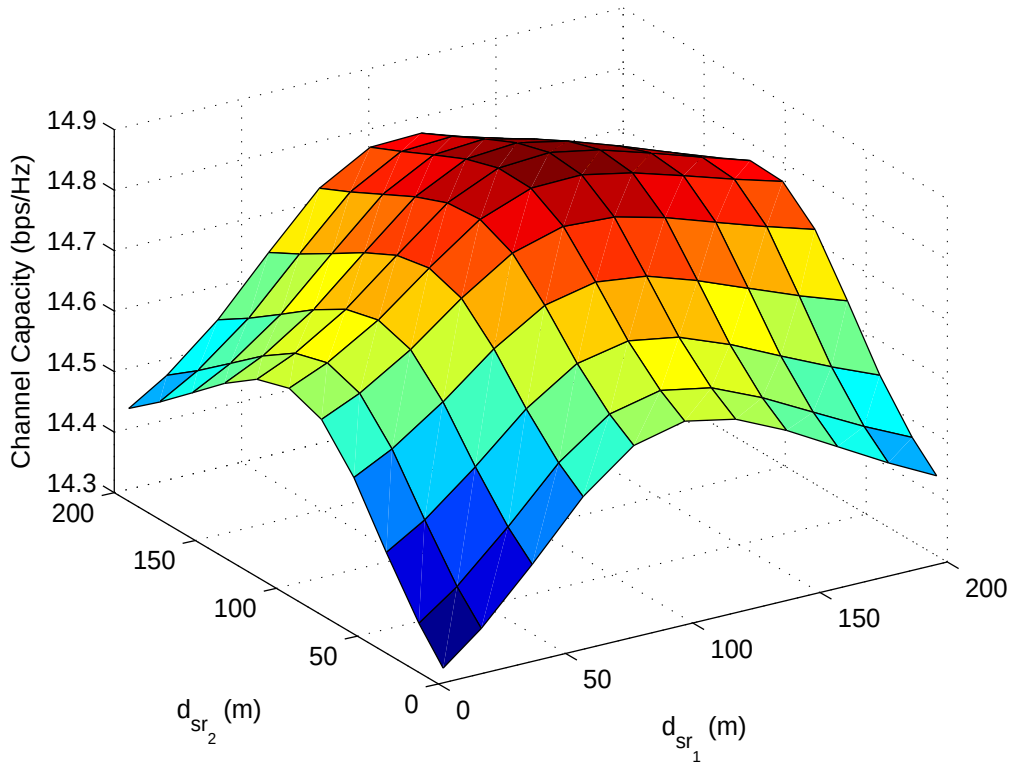

Figure 6.9: Two relays capacity at different relay positions at $E_T = -72$dB Joules.

Fig. 6.9 shows the channel capacity for different relay positions with optimal power allocation scheme. The maximum capacity is achieved when the relays are midway between the source and destination. It is observed that the capacity is fairly sensitive to the relative position of the relay nodes and thus we can determine the relays position where capacity is maximized.

6.6 Summary

In this chapter we have presented a novel optimal power allocation scheme that minimizes the total transmission energy consumption without affecting the reliability of the system. A general solution is derived for arbitrary number of relay nodes. The special cases with single and two nodes are considered. The power

ratio is calculated analytically and is compared with the computer generated simulation results. The BER, total energy consumption and capacity analysis confirm the performance improvement over conventional equal power allocation.

Chapter 7

Conclusions and Future Work

7.1 Conclusions

In this thesis, cooperative wireless communication protocols have been extensively studied. Many cooperative schemes have been proposed in the literature, but most of the schemes assume synchronous communication, which is rather difficult to achieve in practice. The lack of synchronization results in ISI and degrades system performance. Furthermore, the relay nodes are assumed to be half duplex which in turn reduces the spectral efficiency. We investigate these issues and present a novel asynchronous cooperative communication protocol that exploits polarization diversity, and does not require synchronization at relay node. Dual polarized antennas are employed at the relay node to achieve full duplex ANF communication. Hence the transmission duration is reduced which results in an increased throughput rate. Capacity analysis of the proposed scheme ascertains a high data rate as compared to conventional ANF. Simulation results for BER also show that the proposed scheme significantly outperforms both the non-cooperative SISO and the conventional ANF schemes. Considering the path loss, the proposed scheme consumes less total transmission energy as compared to ANF and non-cooperative scheme in more practical distance range. Thus

the proposed scheme is suitable for high rate and energy efficient relay-enabled communication.

Finally, we have also proposed a novel power allocation scheme for multi-relay conventional ANF protocol that aims to minimize the total transmission energy without affecting the BER. Considering channel path loss, the total transmission energy is distributed between the source and the relay nodes. The energy distribution ratio between the relay and direct link is optimized such that the quality of received signal is maintained with minimum total transmission energy consumption. The proposed solution allows fast computation on the required transmission energy in the source and relay node. With the new power allocation scheme, the system also obtains an increased channel capacity as compared to cooperative scheme with conventional equal power allocation. Optimal relay positioning with proposed energy allocation scheme is also explored to maximize the capacity. The analytical analysis performed on the energy distribution ratio is backed through computer simulation verifying the proposed theoretical model.

7.2 Future Work

The following is a list of several possible research directions in the area of asynchronous polarized cooperative communication.

- **Power allocation for proposed asynchronous polarized cooperative scheme**

  Power allocation in the cooperative network is of vital importance as the nodes have limited battery energy. The proposed asynchronous polarized cooperative scheme assumes that the users transmit with equal power. It may be possible to improve performance even further by varying transmit power for each user based on the inter-user channels.

- **Modeling the dual-polarized channel**

  Channels in the simulations of proposed asynchronous polarized scheme are assumed to be Rayleigh faded with a fixed XPD and correlation coefficient. It would be interesting to model the dual-polarized channel with cross polarization and receive correlation as this will give further insights into the proposed asynchronous cooperative scheme.

- **Relay selection for proposed asynchronous polarized cooperative scheme**

  The relay node selection in multi-user network is imperative as it can affect the overall system performance. Therefore, relay node selection algorithms must be devised for the proposed asynchronous polarized cooperative scheme to maximize the system performance with minimum algorithm complexity.

- **Multi-relay proposed asynchronous polarized cooperative scheme**

  The proposed asynchronous polarized cooperative scheme can be further extended to allow a user to have multiple partners. The challenge in this case is to develop a scheme that does not require significant additional systems resource, and treats all users fairly.

References

[1] S. M. Redl, M. K. Weber, and M. W. Oliphant, *An Introduction to GSM*. Artech House, 1995.

[2] C. Smith, *3G Wireless Networks*. McGraw-Hill Osborne, 2006.

[3] S. Parkvall, E. Dahlman, A. Furuskar, Y. Jading, M. Olsson, S. Wanstedt, and K. Zangi, "LTE-advanced - evolving LTE towards IMT-advanced," in *IEEE Vehicular Technology Conference*, pp. 1–5, 2008.

[4] Y. Fan and J. Thompson, "MIMO configurations for relay channels: Theory and practice," *IEEE Transactions on Wireless Communications*, vol. 6, no. 5, pp. 1774–1786, May 2007.

[5] A. Paulraj, D. Gore, R. Nabar, and H. Bölcskei, "An overview of MIMO communications - a key to gigabit wireless," *Proceedings of the IEEE*, vol. 92, pp. 198–218, February 2004.

[6] A. Paulraj, R. Nabar, and D. Gore, *Introduction to Space-Time Wireless Communications*. Cambridge University Press, 2003.

[7] J. Laneman, D. Tse, and G. Wornell, "Cooperative diversity in wireless networks: Efficient protocols and outage behavior," *IEEE Transactions on Information Theory*, vol. 50, no. 12, pp. 3062–3080, Dec. 2004.

[8] J. Laneman and G. Wornell, "Distributed space-time-coded protocols for exploiting cooperative diversity in wireless networks," *IEEE Transactions on Information Theory*, vol. 49, no. 10, pp. 2415–2425, Oct. 2003.

[9] A. Sendonaris, E. Erkip, and B. Aazhang, "User cooperation diversity, Part I: System description," *IEEE Transactions on Communications*, vol. 51, no. 11, pp. 1927–1938, Nov. 2003.

[10] T. Hunter and A. Nosratinia, "Diversity through coded cooperation," *IEEE Transactions on Wireless Communications*, vol. 5, no. 2, pp. 283–289, Feb. 2006.

[11] A. Nosratinia, T. Hunter, and A. Hedayat, "Cooperative communication in wireless networks," *IEEE Communications Magazine*, vol. 42, pp. 74–80, Oct. 2004.

[12] Y.-W. Hong, W.-J. Huang, F.-H. Chiu, and C.-C. Kuo, "Cooperative communications in resource-constrained wireless networks," *IEEE Signal Processing Magazine*, vol. 24, pp. 47 –57, May 2007.

[13] C.-X. Wang, X. Hong, X. Ge, X. Cheng, G. Zhang, and J. Thompson, "Cooperative MIMO channel models: A survey," *IEEE Communications Magazine*, vol. 48, pp. 80 –87, February 2010.

[14] A. Stefanov and E. Erkip, "Cooperative coding for wireless networks," *IEEE Transactions on Communications*, vol. 52, no. 9, pp. 1470–1476, Sept. 2004.

[15] S. Wei, D. L. Goeckel, and M. Valenti, "Asynchronous cooperative diversity," *IEEE Transactions on Wireless Communications*, vol. 5, pp. 1547 – 1557, June 2006.

[16] D. Wang and S. Fu, "Asynchronous cooperative communications with STBC

coded single carrier block transmission," in *Proc. IEEE Global Telecommunications Conference*, pp. 2987 –2991, Nov. 2007.

[17] I. Akyildiz, W. Su, Y. Sankarasubramaniam, and E. Cayirci, "A survey on sensor networks," *IEEE Communications Magazine*, vol. 40, pp. 102–114, Aug 2002.

[18] Z. Jingmei, Z. Qi, S. Chunju, W. Ying, Z. Ping, and Z. Zhang, "Adaptive optimal transmit power allocation for two-hop non-regenerative wireless relaying system," *Proc. IEEE Vehicular Technology Conference*, vol. 2, pp. 1213–1217 Vol.2, May 2004.

[19] W. Su, A. K. Sadek, and K. J. R. Liu, "Cooperative communication protocols in wireless networks: Performance analysis and optimum power allocation," *Wireless Personal Communications*, vol. 44, pp. 181–217, January 2008.

[20] S. Haykin and M. Moher, *Modern Wireless Communications*. Prentice Hall, 2004.

[21] T. S. Rappaport, *Wireless Communications: Principles and Practice*. Prentice Hall, 2002.

[22] D. Tse and P. Viswanath, *Fundamentals of Wireless Communication*. Cambridge University Press, 2005.

[23] J. G. Proakis, *Digital Communications*. McGraw-Hill, 2000.

[24] S. Qureshi, "Adaptive equalization," *Proceedings of the IEEE*, vol. 73, pp. 1349 – 1387, September 1985.

[25] A. F. Molisch, *Wireless Communications*. Wiley Blackwell, 2005.

[26] J. Proakis, "Adaptive equalization for TDMA digital mobile radio," *IEEE Transactions on Vehicular Technology*, vol. 40, pp. 333 –341, May 1991.

[27] D. Gesbert, M. Shafi, S. Da-shan, P. Smith, and A. Naguib, "From theory to practice: an overview of MIMO space-time coded wireless systems," *IEEE Journal on Selected Areas in Communications*, vol. 21, pp. 281–302, April 2003.

[28] B. Vucetic and J. Yuan, *Space-Time Coding*. Wiley Publisher, 2003.

[29] J. Lemieux, M. El-Tanany, and H. Hafez, "Experimental evaluation of space/frequency/polarization diversity in the indoor wireless channel," *IEEE Transactions on Vehicular Technology*, vol. 40, pp. 569 –574, August 1991.

[30] S. M. Alamouti, "A simple transmit diversity technique for wireless communications," *IEEE Journal on Select Areas in Communications*, vol. 16, pp. 1451 – 1458, October 1998.

[31] M. Jankiraman, *Space-Time Codes and MIMO Systems*. Artech House Publisher, 2005.

[32] D. Brennan, "Linear diversity combining techniques," *Proceedings of the IEEE*, vol. 91, no. 2, pp. 331–356, Feb 2003.

[33] D. K. Cheng, *Field and Wave Electromagnetics*. Prentice Hall, 1989.

[34] R. Nabar, H. Bolcskei, V. Erceg, D. Gesbert, and A. Paulraj, "Performance of multiantenna signaling techniques in the presence of polarization diversity," *IEEE Transactions on Signal Processing*, vol. 50, pp. 2553–2562, Oct. 2002.

[35] R. Vaughan, "Polarization diversity in mobile communications," *IEEE Transactions on Vehicular Technology*, vol. 39, pp. 177–186, Aug 1990.

[36] D. Baum, D. Gore, R. Nabar, S. Panchanathan, K. Hari, V. Erceg, and A. Paulraj, "Measurement and characterization of broadband MIMO fixed

wireless channels at 2.5 GHz," *Proc. IEEE International Conference on Personal Wireless Communications*, pp. 203–206, 2000.

[37] E. Biglieri, R. Calderbank, A. Constantinides, A. Goldsmith, A. Paulraj, and H. V. Poor, *MIMO Wireless Communications*. Cambridge University Press, 2007.

[38] T. M. Cover and J. A. Thomas, *Elements of Information Theory*. John Wiley & Sons, 2006.

[39] G. J. Foschini, "Layered space-time architecture for wireless communication in a fading environment when using multielement antennas," *Bell Labs Technical Journal*, vol. 1, no. 2, pp. 41–59, 1996.

[40] E. Telatar, "Capacity of multi-antenna gaussian channels," *European Transactions on Telecommunications*, vol. 10, pp. 585–595, November/December 1999.

[41] W. H. Tranter, K. S. Shanmugan, T. S. Rappaport, and K. L. Kosbar, *Principles of Communication Systems Simulation with Wireless Applications*. Prentice Hall PTR, 2002.

[42] G. J. Foschini and M. J. Gans, "On limits of wireless communications in a fading environment when using multiple antennas," *Wireless Personal Communications*, p. 311335, 1998.

[43] V. Tarokh, N. Seshadri, and A. Calderbank, "Space-time codes for high data rate wireless communication: Performance criterion and code construction," *IEEE Transactions on Information Theory*, vol. 44, pp. 744–765, March 1998.

[44] V. Tarokh, H. Jafarkhani, and A. Calderbank, "Space-time block codes from

orthogonal designs," *IEEE Transactions on Information Theory*, vol. 45, pp. 1456 –1467, July 1999.

[45] J. Laneman, G. Wornell, and D. Tse, "An efficient protocol for realizing cooperative diversity in wireless networks," in *Proc. IEEE International Symposium on Information Theory*, pp. 294–, 2001.

[46] S. Ikki and M. Ahmed, "Performance analysis of generalized selection combining for amplify-and-forward cooperative-diversity networks," in *Proc. IEEE International Conference on Communications*, June 2009.

[47] M. Yuksel and E. Erkip, "Diversity in relaying protocols with amplify and forward," in *Proc. IEEE Global Telecommunications Conference*, vol. 4, pp. 2025 – 2029 vol.4, December. 2003.

[48] P. Herhold, E. Zimmermann, and G. Fettweis, "Cooperative multi-hop transmission in wireless networks," *The International Journal of Computer and Telecommunications Networking*, vol. 49, pp. 299–324, October 2005.

[49] A. K. Sadek, W. Su, and K. J. R. Liu, "Multinode cooperative communications in wireless networks," *IEEE Transactions on Signal Processing*, vol. 55, pp. 341 –355, January 2007.

[50] D. B. da Costa and S. Aissa, "Performance of cooperative diversity networks: Analysis of amplify-and-forward relaying under equal-gain and maximal-ratio combining," in *Proc. IEEE International Conference on Communications*, June 2009.

[51] Y.-W. Hong, W.-J. Huang, F.-H. Chiu, and C.-C. Kuo, "Cooperative communications in resource-constrained wireless networks," *IEEE Signal Processing Magazine*, vol. 24, pp. 47 –57, May 2007.

[52] E. C. van der Meulen, "Three-terminal communication channels," *Advances in Applied Probability*, vol. 3, no. 1, pp. 120–154, 1971.

[53] T. Cover and A. Gamal, "Capacity theorems for the relay channel," *IEEE Transactions on Information Theory*, vol. 25, no. 5, pp. 572–584, Sep 1979.

[54] K. J. R. Liu, A. K. Sadek, W. Su, and A. Kwasinski, *Cooperative Communications and Networking*. Cambridge University Press, 2009.

[55] A. Sendonaris, E. Erkip, and B. Aazhang, "User cooperation diversity, Part II: Implementation aspects and performance analysis," *IEEE Transactions on Communications*, vol. 51, no. 11, pp. 1939–1948, Nov. 2003.

[56] E. Zimmermann, P. Herhold, and G. Fettweis, "On the performance of cooperative diversity protocols in practical wireless systems," *Proc. IEEE Vehicular Technology Conference*, vol. 4, pp. 2212–2216 Vol.4, October. 2003.

[57] X. Tang and Y. Hua, "Optimal design of non-regenerative MIMO wireless relays," *IEEE Transactions on Wireless Communications*, vol. 6, pp. 1398 –1407, April 2007.

[58] S. Peters and R. W. Heath, "Nonregenerative MIMO relaying with optimal transmit antenna selection," *IEEE Signal Processing Letters*, vol. 15, pp. 421 –424, 2008.

[59] F. Fitzek and M. Katz, *Cooperation in Wireless Networks: Principles and Applications*. Springers, 2006.

[60] S. Cui, A. Goldsmith, and A. Bahai, "Energy-efficiency of MIMO and cooperative MIMO techniques in sensor networks," *IEEE Journal on Selected Areas in Communications*, vol. 22, pp. 1089–1098, Aug. 2004.

[61] S. Cui, A. Goldsmith, and A. Bahai, "Energy-constrained modulation optimization," *IEEE Transactions on Wireless Communications*, vol. 4, pp. 2349 – 2360, September 2005.

[62] S. Cui, A. Goldsmith, and A. Bahai, "Energy-constrained modulation optimization for coded systems," in *Proc. IEEE Global Telecommunications Conference*, pp. 372–3761, December 2003.

[63] Y. Chen, G. Yu, P. Qiu, and Z. Zhang, "Power-aware cooperative relay selection strategies in wireless ad hoc networks," in *IEEE International Symposium on Personal, Indoor and Mobile Radio Communications*, 2006.

[64] Z. Chen and C. Yang, "Energy efficiency of cooperative diversity at PHY layer in wireless sensor networks," *Proc. International Conference on Signal Processing*, vol. 4, pp. –, 16-20 2006.

[65] A. Ribeiro, X. Cai, and G. Giannakis, "Symbol error probabilities for general cooperative links," *IEEE Transactions on Wireless Communications*, vol. 4, pp. 1264–1273, May 2005.